

11. Results and Discussion

The purpose of this section is to discuss the data presented in chapter 9, and to examine the relationship between chassis data and engine data with a view to presenting a predictive correlation for future use.

11.1 Correlation of Chassis and Engine Data

The data for the Navistar engine and chassis, for the Cummins engine and single axle (S/A) mode chassis, and the Cummins engine and tandem chassis will be presented separately in many cases below. In each plot, except where designated, each data point represents the average of the several hot engine and chassis runs. Data have also been presented for the combined data base including all three cases. The discussion will center on data for oxides of nitrogen (NO_x) and particulate matter (PM) due to their special significance in heavy duty mobile source concerns. Data for hydrocarbons (HC) and carbon monoxide (CO) will be deemphasized.

The data, in their most basic form, were available in grams per cycle, that is, the total mass quantity of emissions measured over the whole test cycle. Figures 11.1, 11.2 and 11.3 present data in this form for chassis tests versus engine tests for NO_x , while figures 11.4, 11.5 and 11.6 present similar data for PM. (*note: Figures for this section are located after the section text*) In cases where more than one data point is evident at a particular engine emissions rate, the values correspond to sets of chassis runs in different gears. As described in Chapter 3, Test Plan, the Cummins powered vehicle was tested in 7th, 8th, and 9th gears. Data have not been separated out by gear in these plots. For the Navistar engine, the NO_x correlation shown in Figure 11.1 is good, but the PM correlation is less conclusive. It is difficult to comment on correlation of the Cummins data since NO_x levels did not vary widely and since PM was scattered.

It is customary in heavy duty engine testing to express data in the form of mass emissions per unit of energy delivered, in units of grams/bhp-hr. In the case of chassis testing, brake power was not documented, so that the chosen power was the value integrated at the rear axle, neglecting values of negative torque. Units for chassis emissions were therefore taken as grams per axle-horsepower hour, or grams/ahp-hr. Figures 11.7, 11.8 and 11.9 present NO_x data as plots of chassis emissions in g/ahp-hr. versus engine emissions in g/bhp-hr. It is evident that there is a sound correlation for these data. Figure 11.10 provides the data combined in one plot. It is expected that the gathering of data associated with varying drivetrain configurations will weaken the correlation between chassis and engine emissions. Figures 11.11, 11.12 and 11.13 show the PM chassis data in g/ahp-hr. versus the PM engine data in g/bhp-hr, and Figure 11.14 combines the data. Once again, for both the Navistar and the combined plots, the NO_x data are good, but the PM data correlation is poorer.

Figures 11.10 and 11.14 offer one scheme for the correlation of chassis and engine results. However, additional correlations were explored in seeking alternative or superior approaches. Firstly, mass emissions were rendered non-dimensional with respect to emissions of carbon dioxide (CO_2) for purposes of comparison. From a simplistic standpoint, one may argue that CO_2 emissions represent engine energy production so that this method would yield rates that were

independent of accuracy of torque measurements. However, CO₂ levels correspond more closely to indicated power levels, not to brake power levels. In other words CO₂ emissions include the generation of engine frictional horsepower and are finite under idle conditions, even when brake power output is zero. Figures 11.15, 11.16 and 11.17 present NO_x/CO₂ values for chassis tests versus engine tests and Figure 11.18 summarizes the combined data. Figures 11.19, 11.20 and 11.21 show the PM/CO₂ values for chassis data versus engine data and Figure 11.22 summarizes the combined data. The Navistar NO_x/CO₂ data correlate in an outstanding fashion, but the PM/CO₂ data show poorer correlation than with mass or mass/work correlations.

A second alternative correlation was attempted in the following way. Models were developed in Appendix D to describe the efficiency of the drivetrain. Using these models it was possible to take the continuous rear axle torque and engine speed data from a chassis test and project what the engine power output was during the chassis test. Let us term this projected brake horsepower, or pbhp. The procedure for finding the total projected engine energy during a test, in pbhp-hr. involved processing the continuous data set of axle torque and speed on a second-by-second basis to yield pbhp. The term ahp-hr./pbhp-hr. for a test is a measure of overall average drivetrain efficiency during a test. These values for overall drivetrain efficiency are far lower than the 80 to 90% values commonly touted, so that one suspects that the common values are typically given for full power operation. Of course, the drivetrain efficiencies presented in this document include tire losses on the rolls, and those cited anecdotally may not. Calculations were performed on one chassis run (Cummins, stock engine mode, single axle) in this manner, and the resulting NO_x data in g/pbhp-hr. were found not to correspond to the engine average. The engine, while in the chassis, was predicted to perform considerably more work than it did when on the engine test stand. However, under chassis testing, the engine performs work at modest power levels during the idle portions, when little NO_x is emitted, and this will prevent good correlation. In addition, the drivetrain efficiency equation is based on insufficient data to be applied with great confidence.

11.2 Developing a Predictive Tool

The ultimate objective of this program was to develop a tool that might predict certification engine emissions levels from chassis emissions data. In a more limited sense, the ability to predict whether the engine would fail or pass the certification test would meet the objective.

The first step in developing such a predictive tool is to determine the levels that would constitute failure of the engine if it were actually subjected to certification engine testing. Each engine, when originally certified by family, would have precise certification emissions values and degradation factors. This value should not be used directly as an engine pass/fail criterion, because variation of emissions levels between laboratories is well documented. In other words, the original engine manufacturer may have certified an engine in good faith, and that engine, once in use, may continue to emit at or below certification levels, if it were tested by the manufacturer. However, another laboratory might find higher, or lower, levels of emissions. The regression criteria for transient certification tests provide some latitude in the actual torque and speed commands sent to an engine and can affect the resulting emissions. In Round Robin testing of a Navistar 466 engine by a range of certification laboratories the coefficients of variance for

emissions between laboratories were as follows: NO_x: 5.5%, CO: 18%, HC: 10%, PM: 8.5%. The coefficient of variance of a set, often expressed as a percentage, is the standard deviation of the data in that set divided by the average of the values in the set. To remain within a 95% confidence level, the test data might deviate by up to twice the value of coefficient of variance from the measured value. If the concern is with errors of commission, then the engine failure criterion should be set at a value of twice the coefficient of variance above the original certification value. If errors of omission are the concern, then the criterion should be set by that much below, and if there is a desire to match errors of omission and commission, then the original certification value itself should be chosen. Noting the cost of emissions testing, and the difficulty of proving that an engine is emitting at above the certification level, a value of twice the coefficient of variance above the original certification value is recommended. In other words, for an engine originally certified by family to 5 grams/bhp-hr. NO_x, the conservative failure criterion for one engine in a subsequent set of tests on the engine stand might be

$$5(1 + 2(0.055)) = 5.55 \text{ g/bhp-hr.}$$

Certification levels were known and supplied with the Navistar test engine used. Cummins certification levels were obtained from the 1995 EPA website. No degradation factors are included in these values given below.

Navistar	HC: 0.39,	CO: 2.14,	NO _x : 5.21,	PM: 0.139	(g/bhp-hr)
Cummins	HC: 0.40,	CO: 0.80,	NO _x : 4.40,	PM: 0.060	(g/bhp-hr)

For comparison, the stock engine test values found by West Virginia University were as given below.

Navistar	HC: 0.34,	CO: 1.07,	NO _x : 4.98,	PM: 0.08	(g/bhp-hr)
Cummins	HC: 0.18,	CO: 0.98,	NO _x : 5.14,	PM: 0.07	(g/bhp-hr)

There is added concern about the effects of fuel composition on emission. If in-use fuel is employed in the chassis testing, this may cause deviation from certification conditions. The extent of this effect is not well documented but the Engine Manufacturers Association Round Robin data suggests a 10% difference in NO_x results between a certification fuel and a Phillips S-10 (low aromatic) fuel, in the favor of the S-10. A 10% allowance for fuel variation was made. The engine emissions failure criteria, based upon twice the coefficient of variance above the certification values, plus allowance for fuel variation with no degradation factors, for the two engines tested in this program are therefore 21% higher than the certification values and are as follows:

Navistar	HC: 0.47,	CO: 2.59,	NO _x : 6.30,	PM: 0.168	(g/bhp-hr)
Cummins	HC: 0.48,	CO: 0.97,	NO _x : 5.32,	PM: 0.073	(g/bhp-hr)

In this case, for NO_x, the Navistar would pass an engine test in the stock, AS and 15K modes, but would fail in 39K and 83K. The Cummins would pass in stock mode and DM modes but fail in 2V mode.

For PM, the Navistar would pass in all modes while the Cummins would pass in stock mode and fail in the DM and 2V modes.

Next it was necessary to develop a method for predicting engine emissions levels from chassis emissions levels. From figures 11.10 and 11.18 it is evident that one may predict engine NO_x levels from chassis NO_x levels either from a correlation between values in ahp-hr. and bhp-hr. or by ratios with CO₂ emissions, as shown below.

$$\text{Engine NO}_x \text{ (g/bhp-hr.)} = 0.7750 \{ \text{Chassis NO}_x \text{ (g/ahp-hr)} \}$$

$$\text{Engine NO}_x / \text{CO}_2 = 0.9763 \{ \text{Chassis NO}_x / \text{CO}_2 \}$$

It is interesting to note that the NO_x /CO₂ ratio is essentially the same for chassis and engine tests.

However, these two simple models should not be applied directly to the engine failure criteria without first considering the errors that may be inherent in the chassis measurements. One must also consider the number of chassis tests that will be performed in obtaining the chassis emissions data. Two scenarios will be considered, the use of one chassis test and the use of the average of three chassis tests.

Regressions were also performed on the whole databank for HC and CO emissions. While no correlation between engine and chassis HC existed, a reasonable correlation of CO was found.

$$\text{Engine CO (g/bhp-hr.)} = 0.802 \{ \text{Chassis CO (g/ahp-hr)} \} (R^2 = 0.64)$$

There was considerably more data scatter in the CO and HC plots than the NO_x plots. However, CO and HC levels for modern diesel engine are customarily so far below both certification standards and gasoline engine levels that correlation of CO and HC is a moot point.

Examination of the PM data from all chassis tests revealed that only the chassis tests performed on the Navistar with the 82kΩ resistors installed failed to meet certification levels. Additional data including that from gross PM emitters must be collected to ascertain more accurate chassis pass/fail criterion.

When test-to-test variations were considered for groups of tests under the same operating mode, the average coefficient of variance for NO_x in g/ahp-hr. was 2.88% . For a repeat of three tests, the coefficient of variance for the average of the three was therefore 1.66%. The average coefficient of variance for values of NO_x/CO₂ was 2.75%, so that the coefficient of variance for the averages of three tests would be 1.57% (COV for a group of tests will change by the square root of the number of tests in the group). These values can be used in considering the likelihood

of wrongful determination in developing a predictive model, but the coefficients of variance are void of bias errors and contain only random errors. In addition, these coefficients of variance do account also for real variations in truck emissions from test to test in addition to the vagaries of the test equipment. Kittelson and Johnson (1991) have highlighted the way in which differences between laboratories can affect emissions.

Presuming that it is desired to avoid false failing of engines, the chassis test data should be adjusted by twice the coefficient of variance. If Chassis NO_x (in g/ahp-hr.) is less than $(1+0.21+2.88\%)(1/0.775)$ Certification Level (in g/bhp-hr.), then the engine is unlikely to be worthy of removal and dynamometer testing, else it merits engine testing.

If Chassis NO_x/CO_2 is less than $(1+0.21+2.75\%)(1/0.775)$ times the ratio of certification NO_x to certification CO_2 , then the engine is unlikely to be worthy of removal and dynamometer testing, else it merits engine testing.

These two approaches are very conservative and err in the direction of not pursuing engines out of compliance. They identify only those chassis tests which, with 95% confidence, infer that there is a 95% confidence level in failing an engine test.

If it is acceptable that there are as many wrong failures as wrong passes (errors of commission and omission), then one would simply apply the correlation equations directly to the engine certification data to yield fail/pass criteria at the certification level (CL), or directly to the (certification level plus twice the coefficient of variance, "CLplus"), according to the confidence in, and enforcibility of, engine test data.

Consider the conservative failure criteria applied to the NO_x data that were generated in this program. In this case, failure of a single chassis test would occur at 8.33 g/ahp-hr for the Navistar Chassis and 7.03 g/ahp-hr for the Cummins. Failure of an average of three chassis tests would occur at 8.25 g/ahp-hr for the Navistar and 6.96 g/ahp-hr for the Cummins.

Another method that can be used to represent the use of the data bank generated by this program is to plot, on an axis of varying failure criterion, the four curves for fraction passing, fraction failing, fraction passing wrongly (errors of omission) and fraction failing wrongly (errors of commission). Let us propose that the failure criterion for NO_x becomes

$$\text{Chassis } \text{NO}_x \text{ (g/ahp-hr)} \geq k \text{ (Engine certification level in g/bhp-hr)}$$

Where k is a constant. Figure 11.23 shows the NO_x based fractions passing and failing as a function of k for the Navistar when single chassis tests are considered while Figure 11.24 shows the fraction passing and failing wrongly. Figures 11.25 shows the NO_x based number failing and passing as a function of k for individual Cummins chassis test runs while Figure 11.26 shows the number failing wrongly and passing wrongly.

Figures 11.27 shows the number passing and failing as a function of k for all chassis testing performed while 11.28 shows the number failing wrongly and passing wrongly. Consider the plot

in Figure 11.28. There are seventy one chassis tests. Let us assume that the objective would be to minimize the sum of both the number of tests failing wrongly and the number of tests passing wrongly. For a value of $k=1.6$, no vehicles would fail wrongly, 15 or 16 would pass wrongly and 55 or 56 would pass or fail correctly. For this plot, if the passing criterion is made more severe by reducing the value of k , an increasing number of vehicles fail wrongly, but the number passing wrongly is not reduced to the same degree. Of those vehicles that the engine tests showed should actually fail, 11 did fail and 20 passed wrongly. The criterion $k = 1.6$ is therefore recommended as a conservative criterion for establishing a vehicle that is likely to have high engine emissions.

Figure 11.1 - Comparison of Navistar Engine and Chassis NO_x Mass Emissions

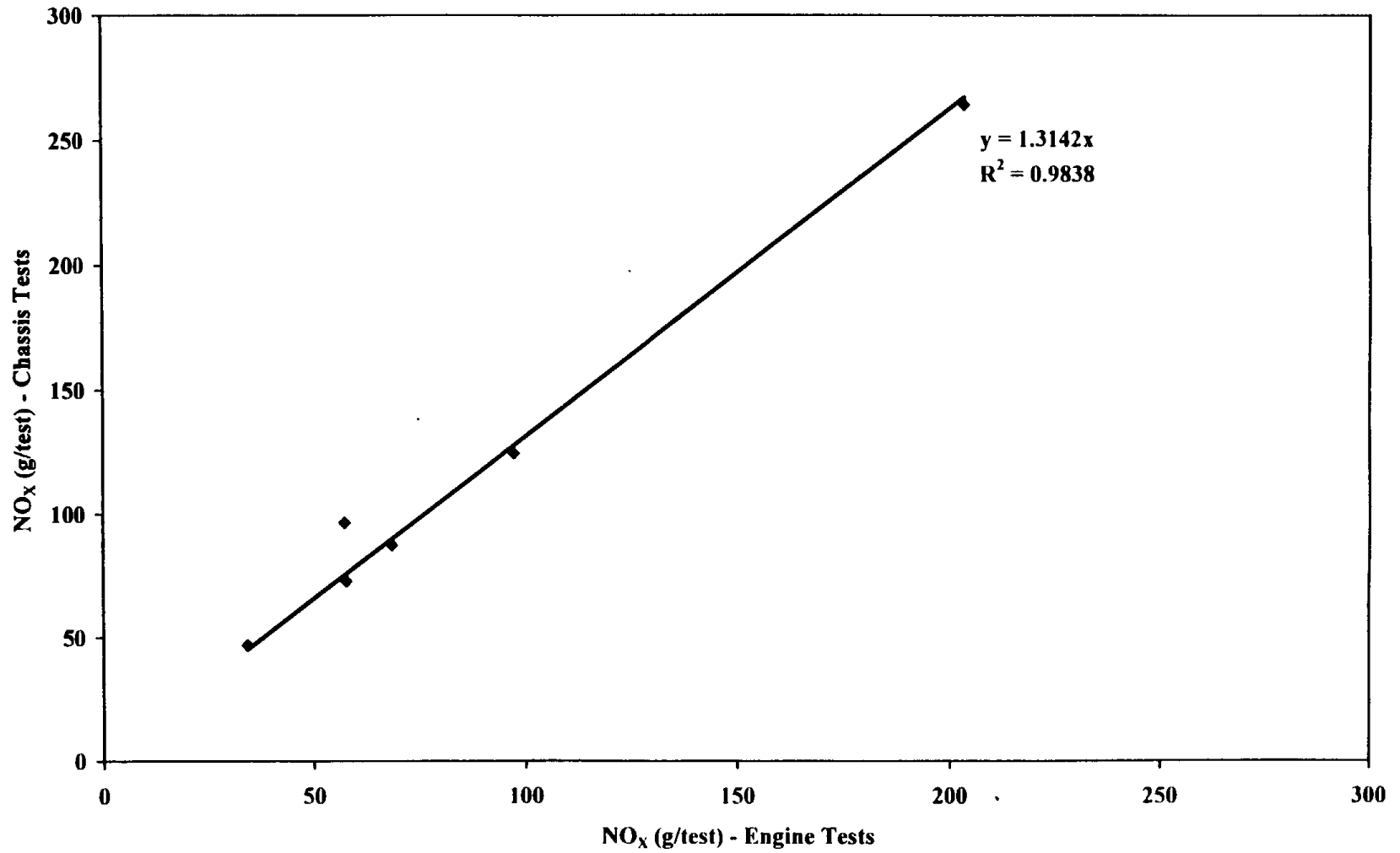


Figure 11.2 - Comparison of Cummins Engine and Chassis NOx Mass Emissions (Single Axle)

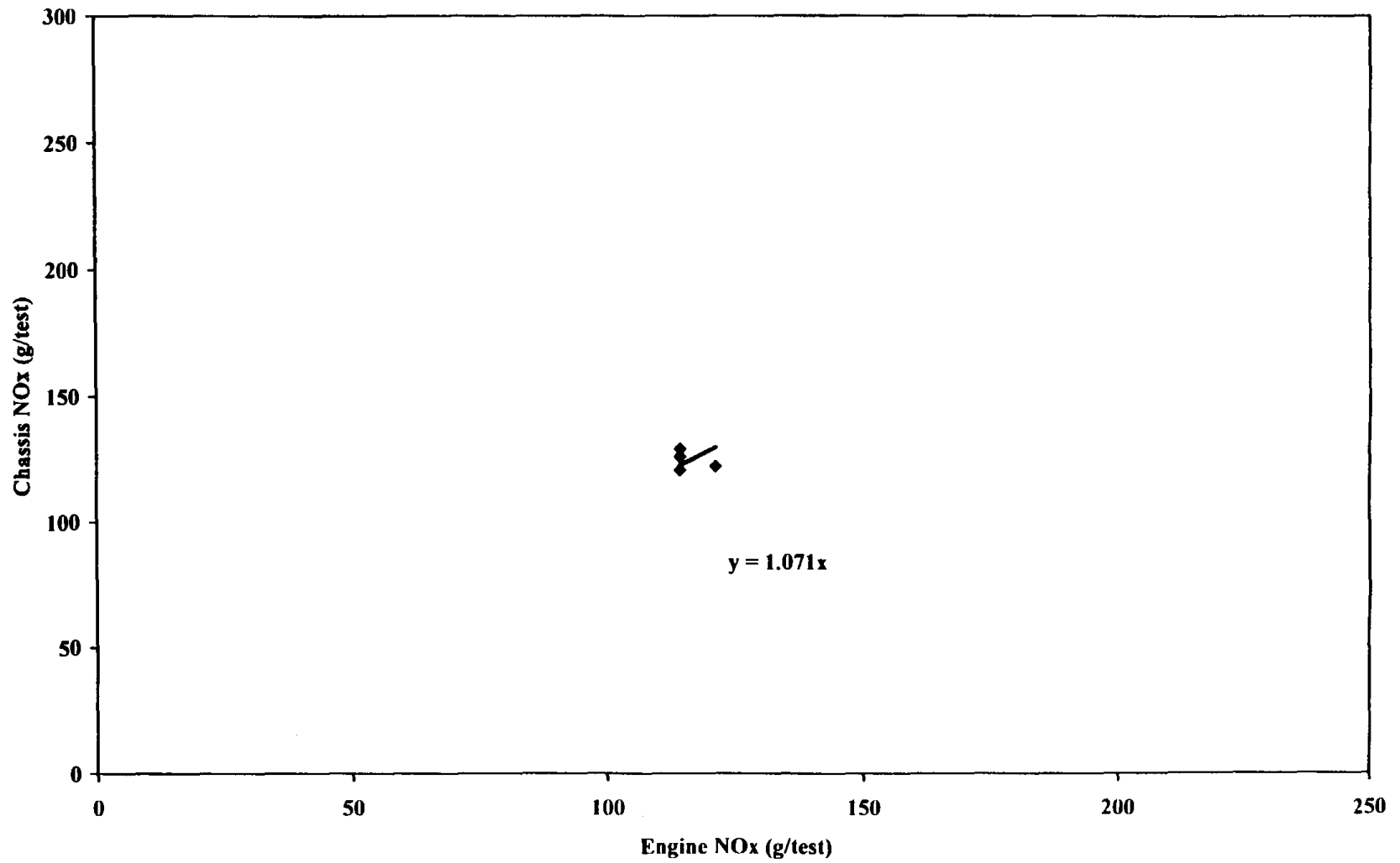


Figure 11.3 - Comparison of Cummins Engine and Chassis NOx Mass Emissions (Tandem Axle)

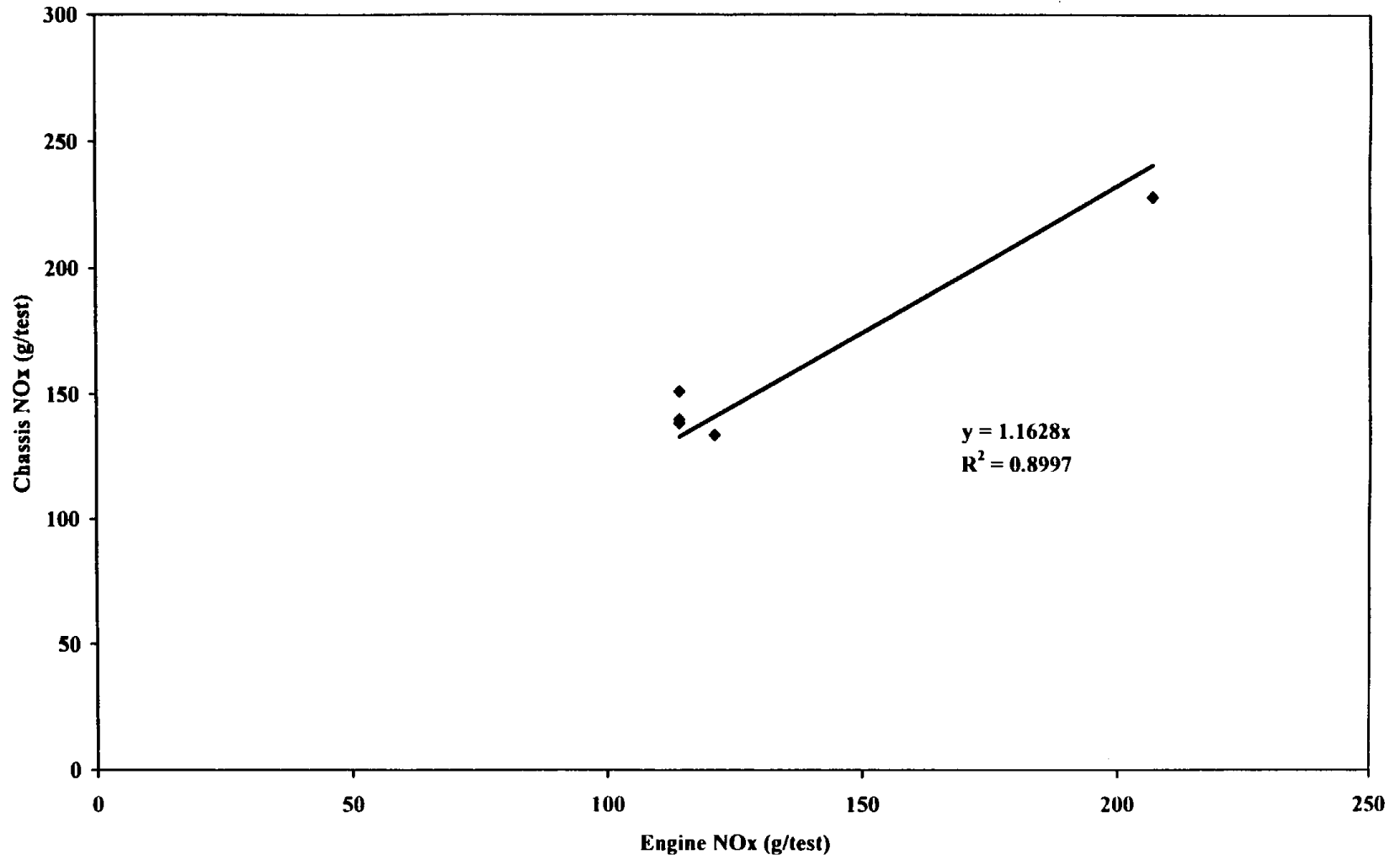


Figure 11.5 - Comparison of Cummins Engine and Chassis PM Mass Emissions (Single Axle)

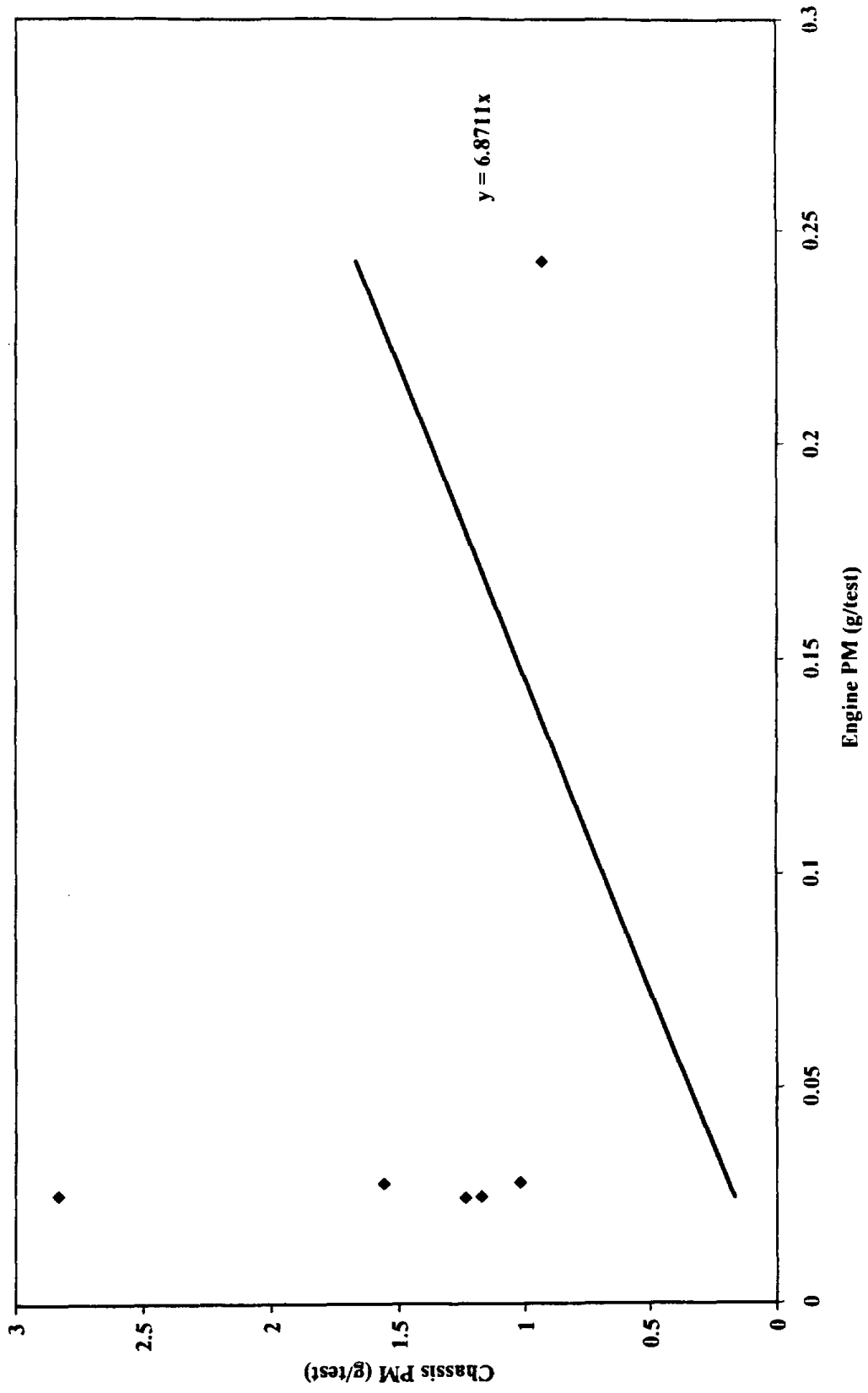


Figure 11.5 - Comparison of Cummins Engine and Chassis PM Mass Emissions (Single Axle)

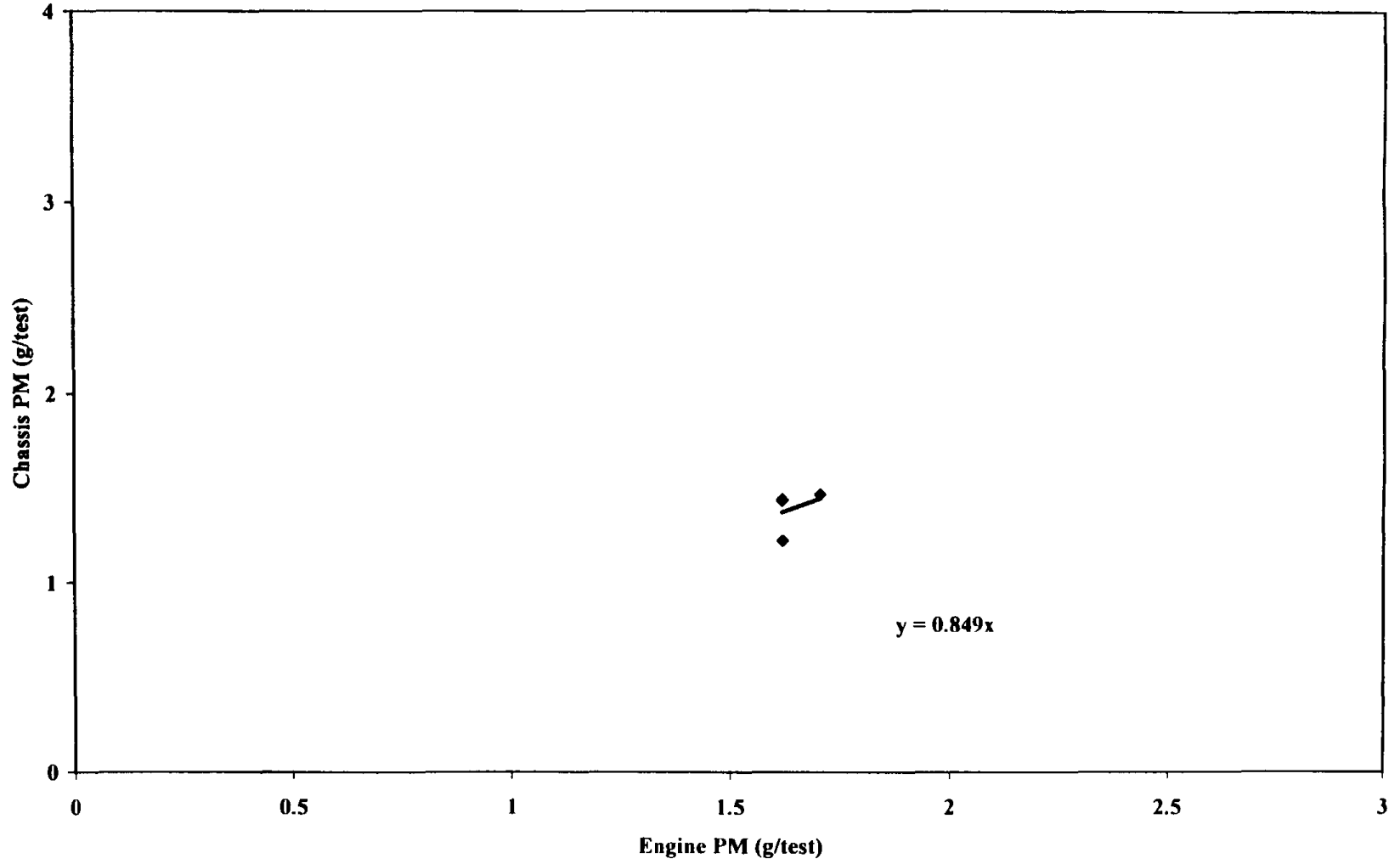


Figure 11.6 - Comparison of Cummins Engine and Chassis PM Mass Emissions (Tandem Axle)

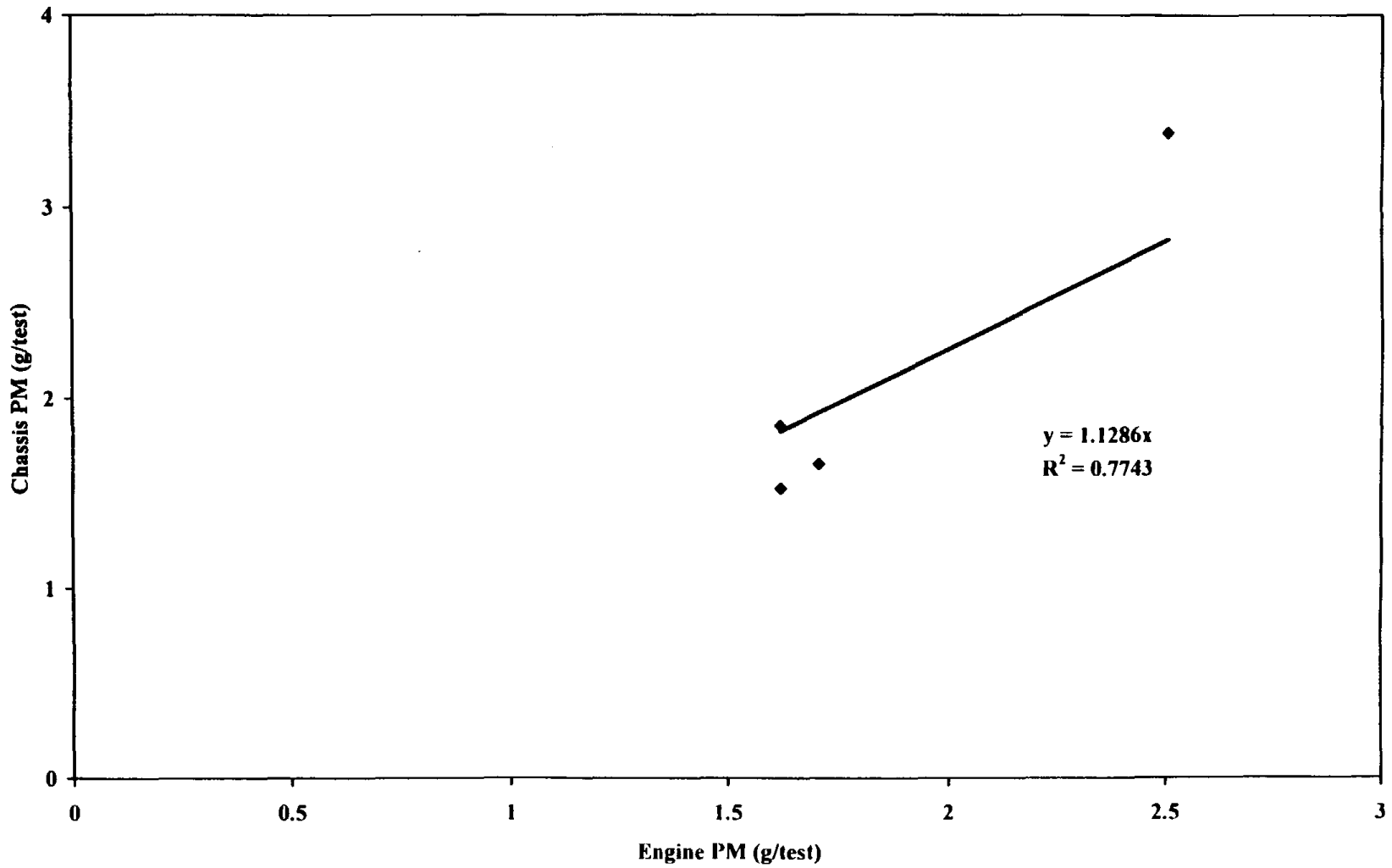


Figure 11.7 - Comparison of all Navistar Chassis and Engine NOx Mass/Work Emissions

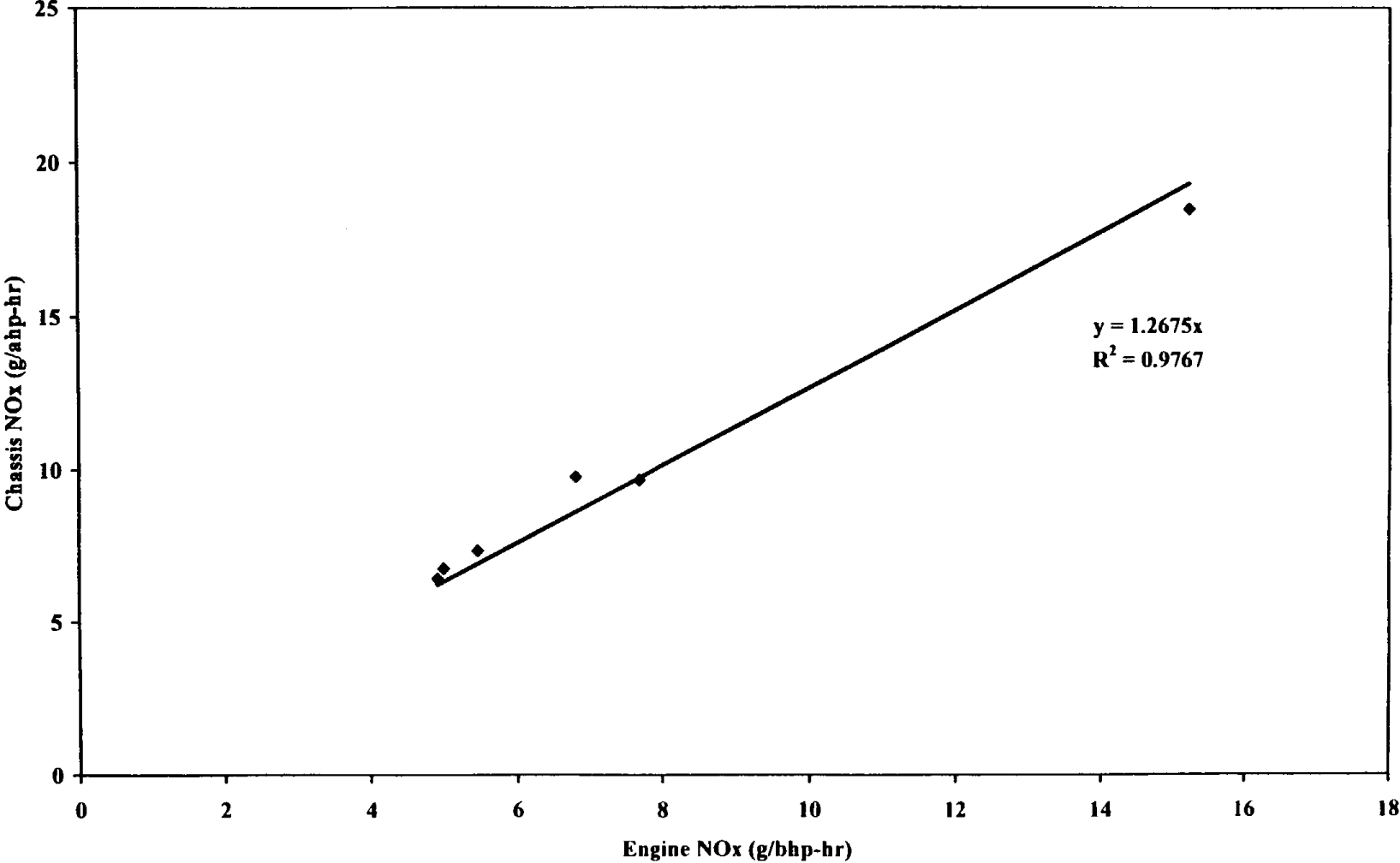


Figure 11.8 - Comparison of Cummins Chassis and Engine NOx Mass/Work Emissions (Single Axle)

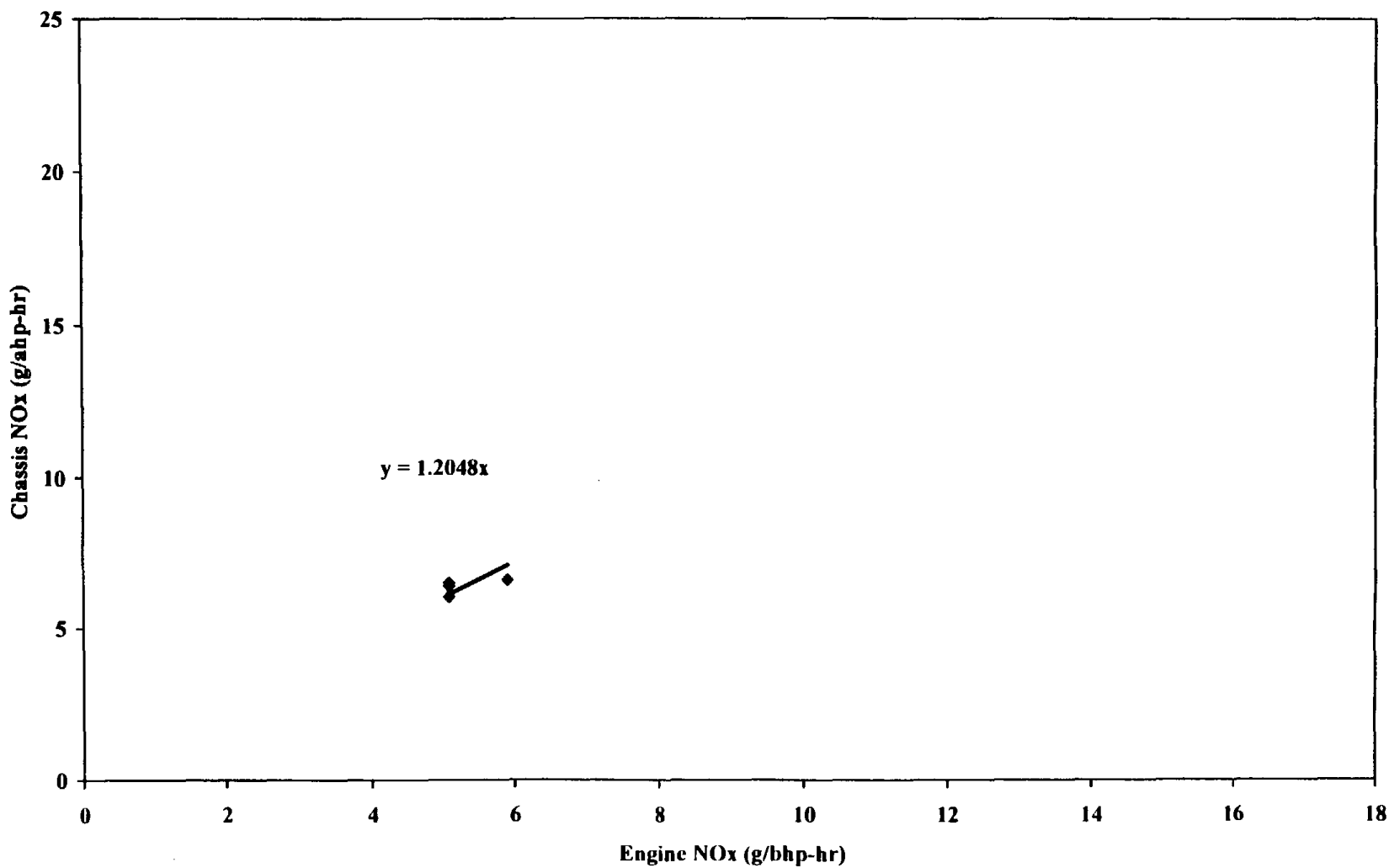


Figure 11.9 - Comparison of Cummins Engine and Chassis NOx Mass/Work Emissions (Tandem Axle)

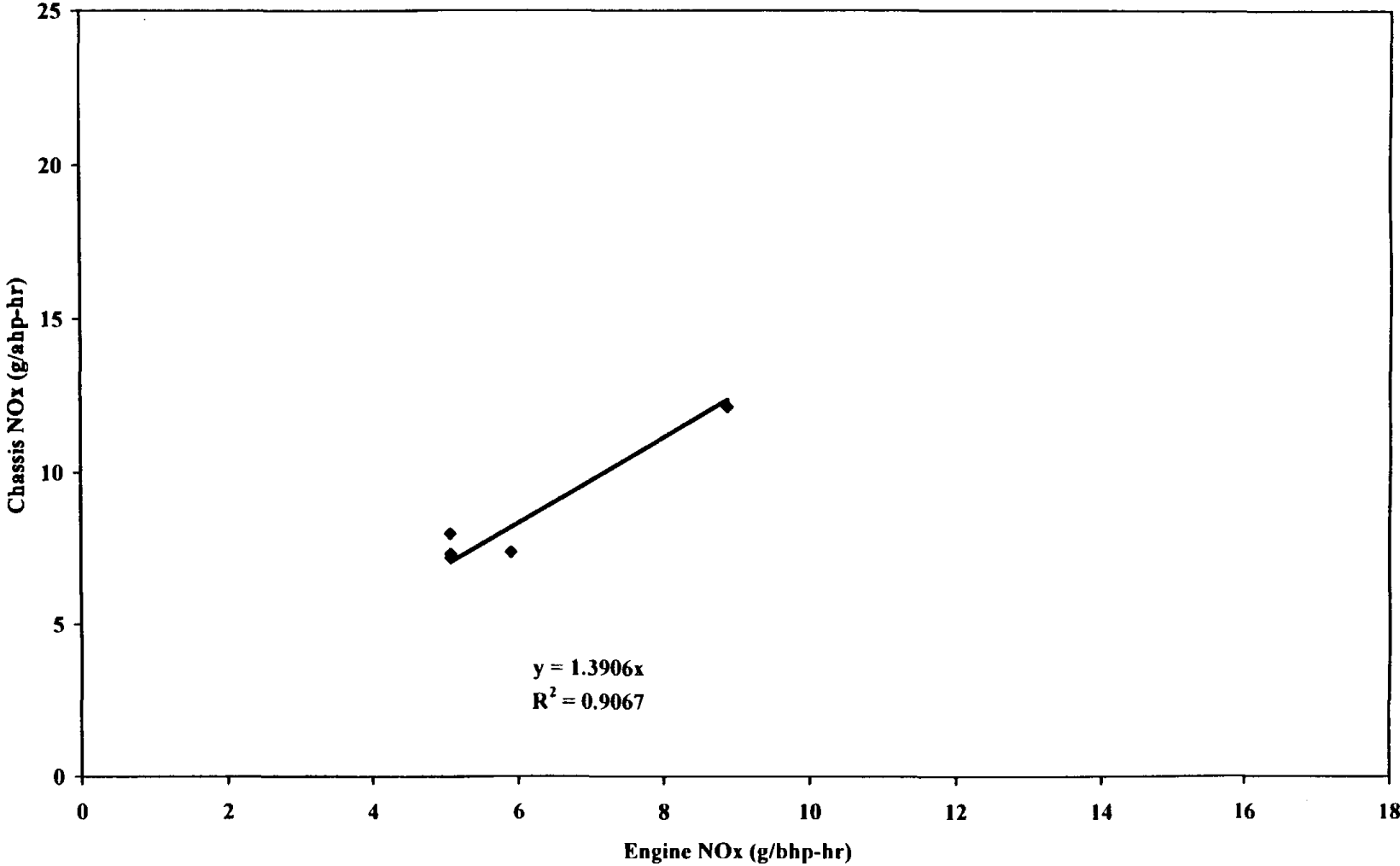


Figure 11.10 - Comparison of all Navistar and Cummins Chassis and Engine NOx Mass/Work Emissions (Single and Tandem Axle)

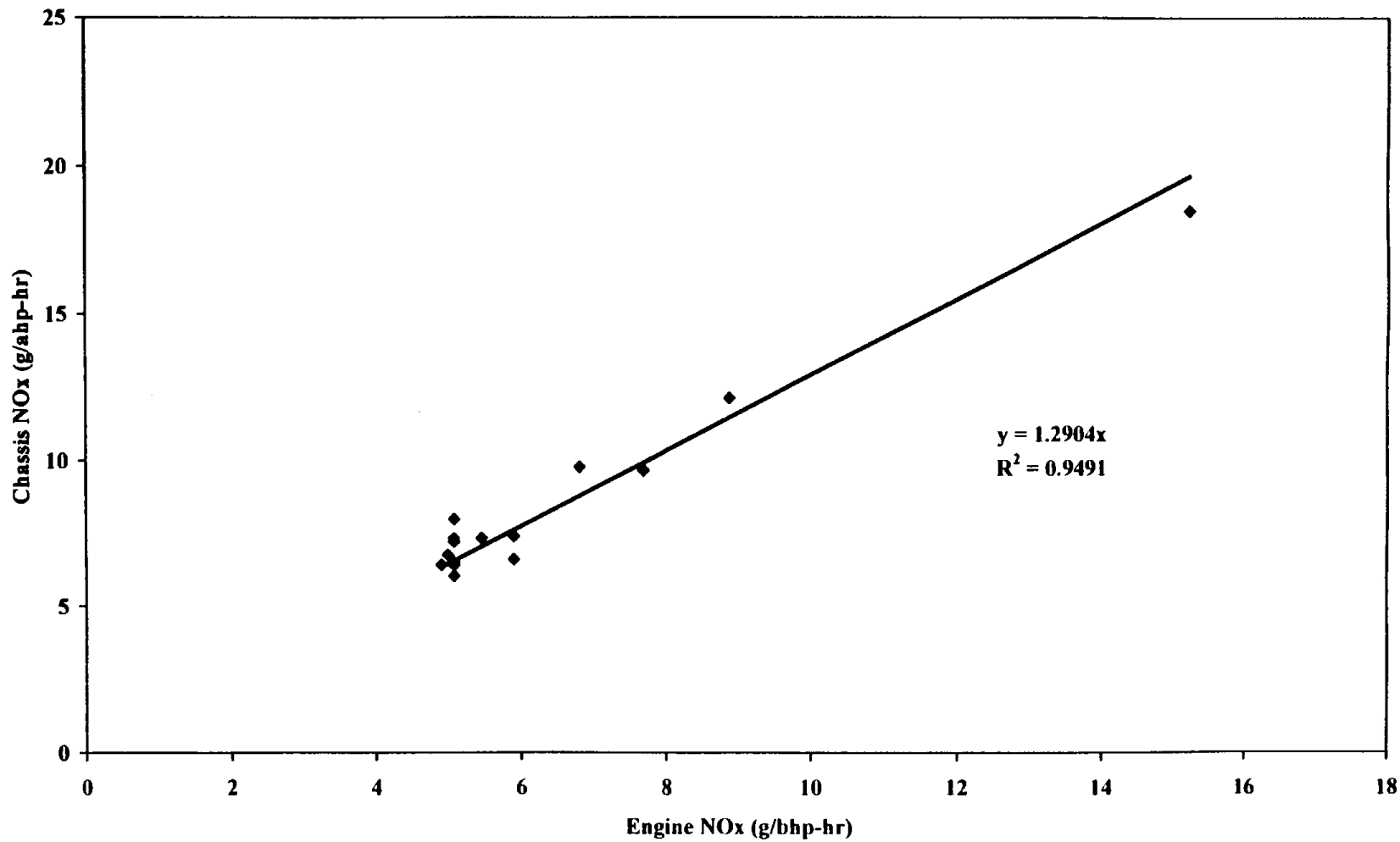


Figure 11.11 - Comparison of Navistar Engine and Chassis PM Mass/Work Emissions

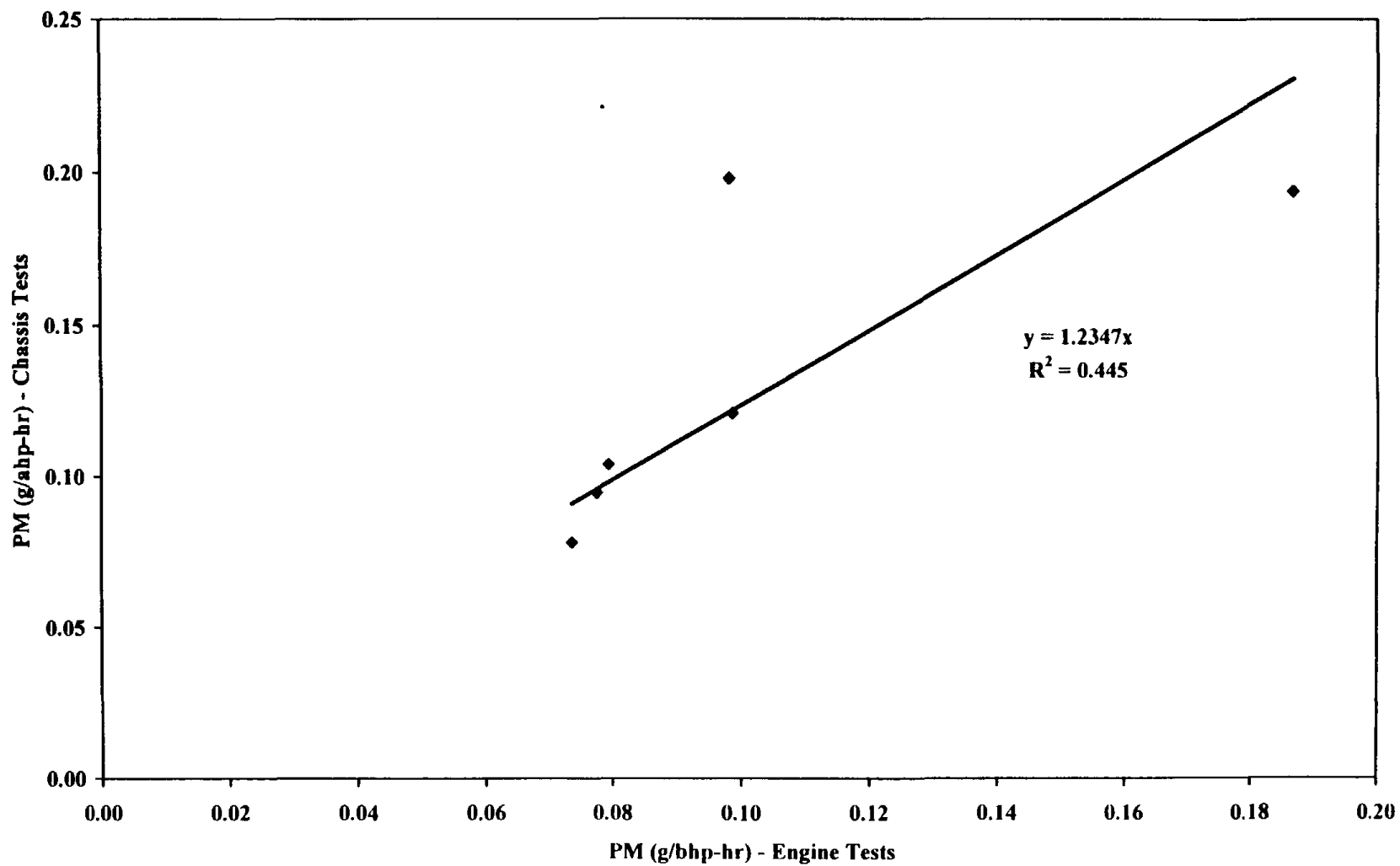


Figure 11.12 - Comparison of Cummins Engine and Chassis PM Mass/Work Emissions (Single Axle)

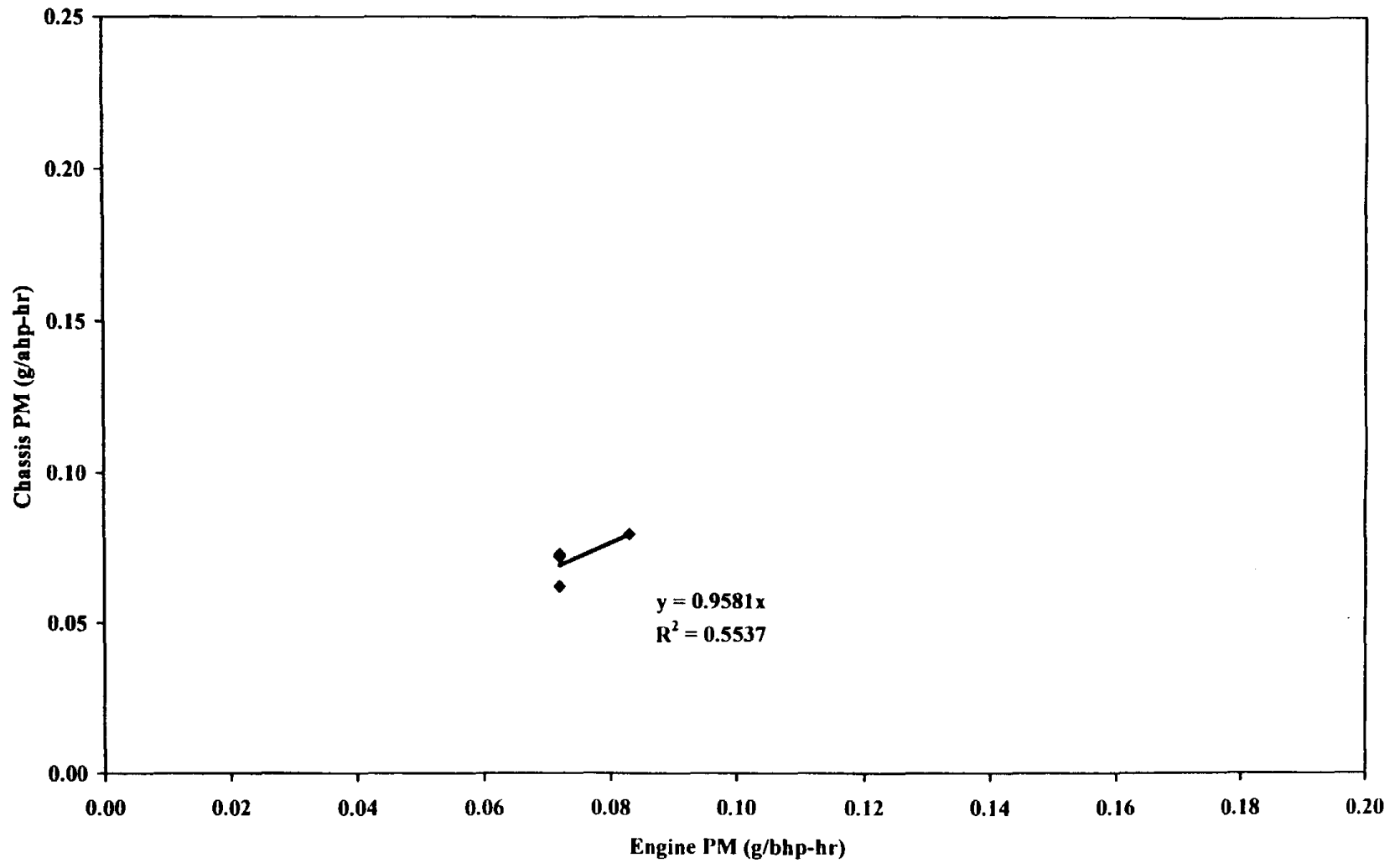


Figure 11.13 - Comparison of Cummins Engine and Chassis PM Mass/Work Emissions (Tandem Axle)

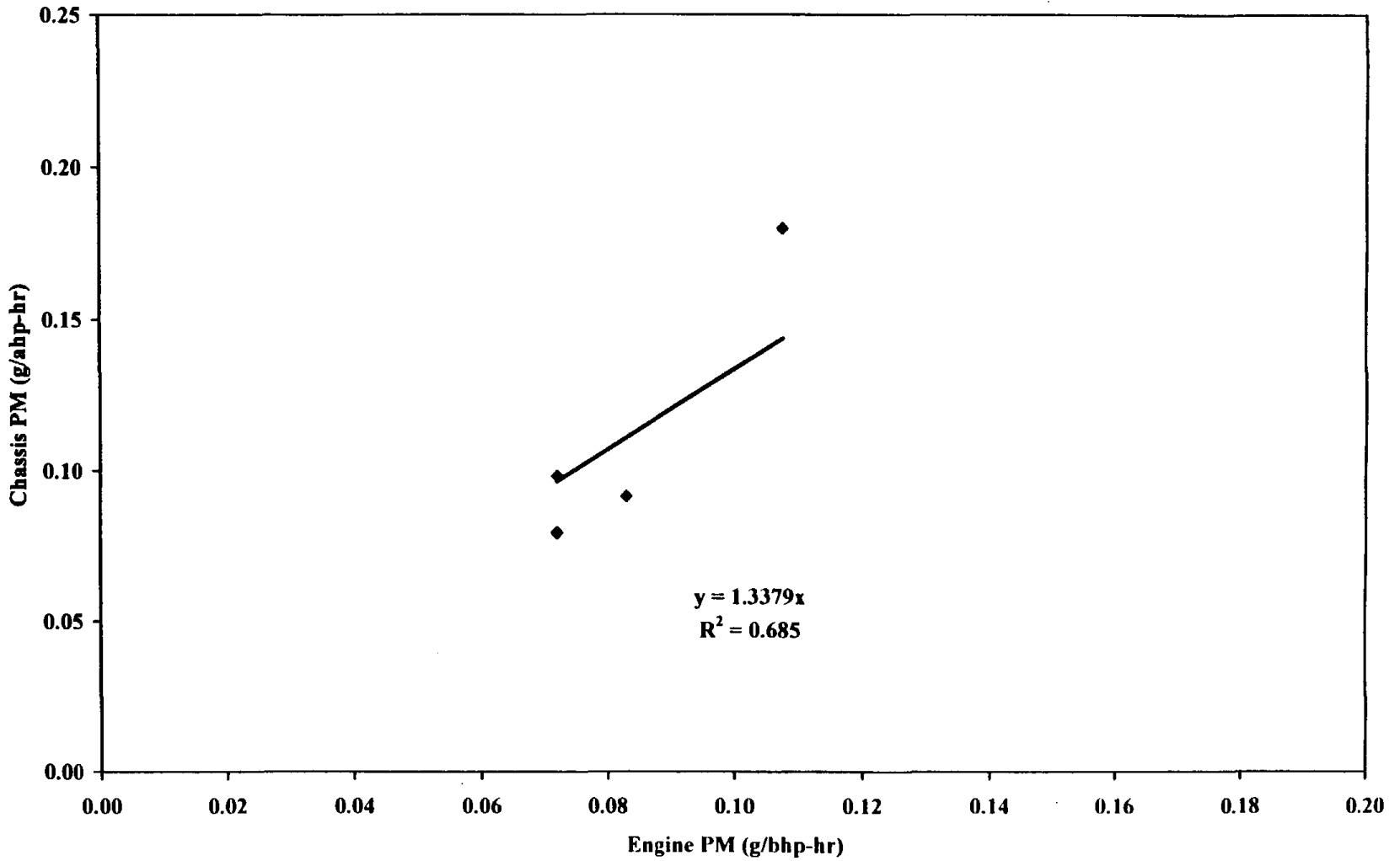


Figure 11.14 - Comparison of all Navistar and Cummins Engine and Chassis PM Mass/Work Emissions (Single and Tandem Axle)

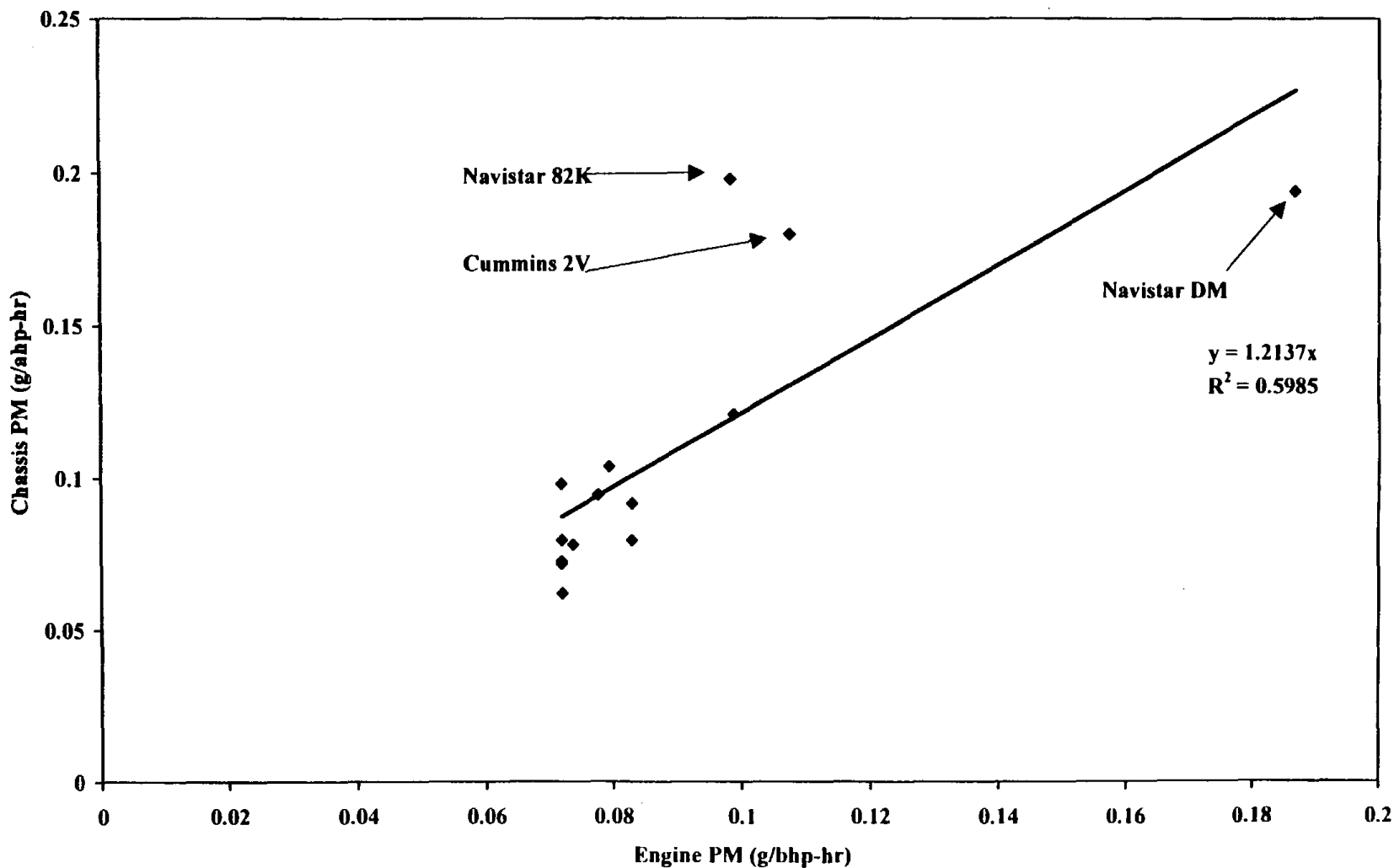


Figure 11.15 - Comparison of Navistar Engine and Chassis NO_x/CO₂ Ratios

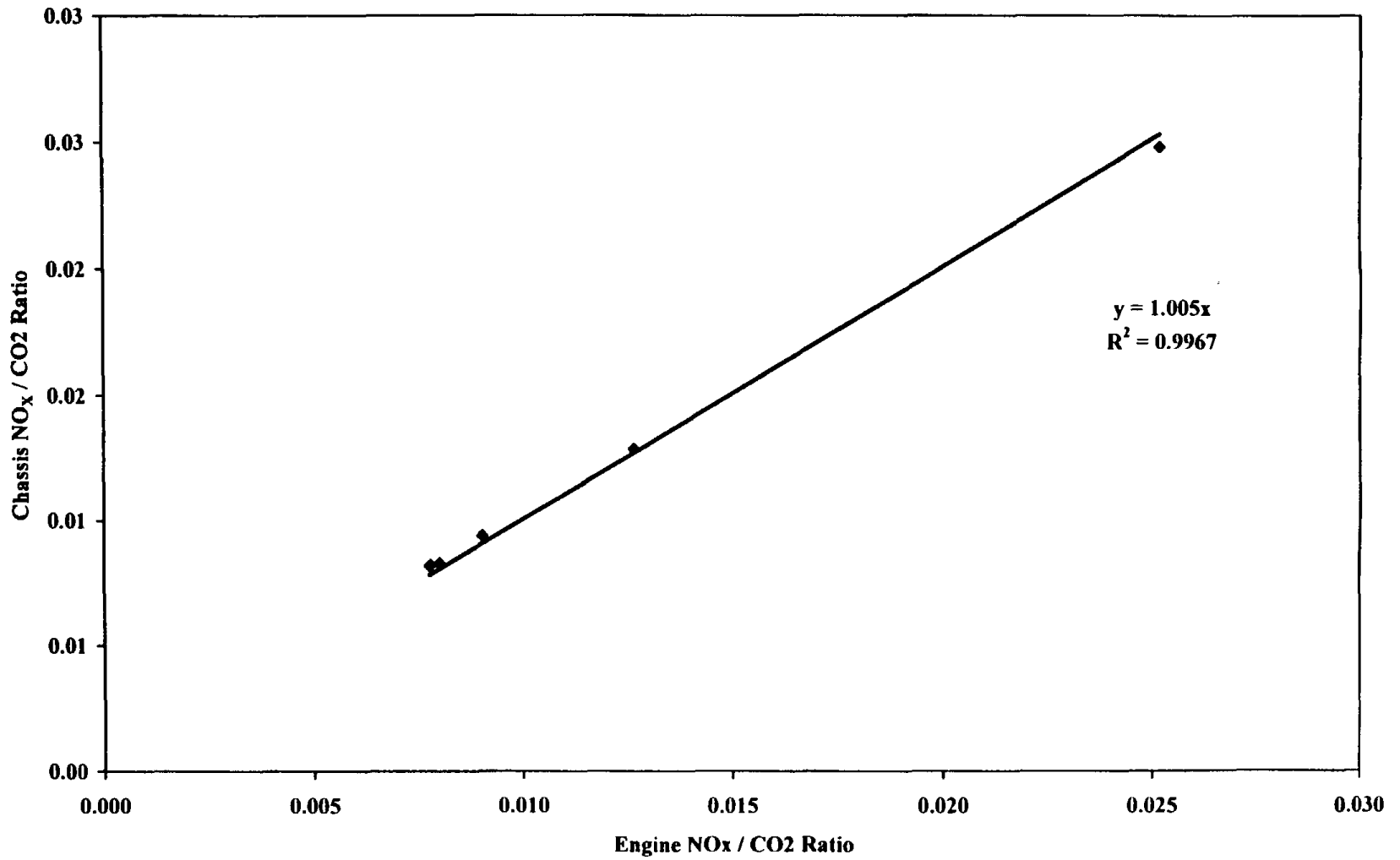


Figure 11.16 - Comparison of Cummins NOx/CO₂ Ratios (Single Axle)

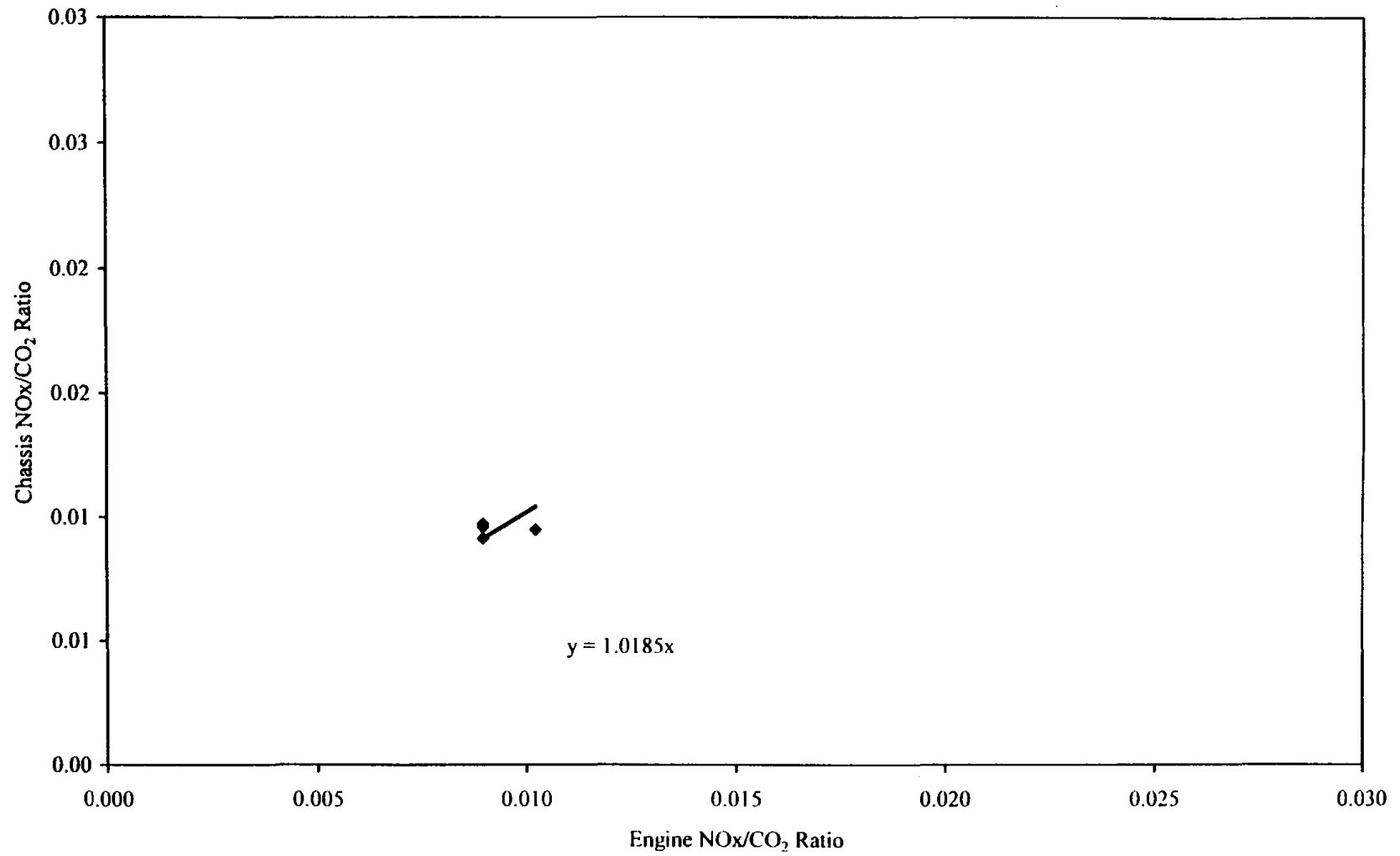


Figure 11.17 - Comparison of Cummins NO_x/CO₂ Ratios (Tandem Axle)

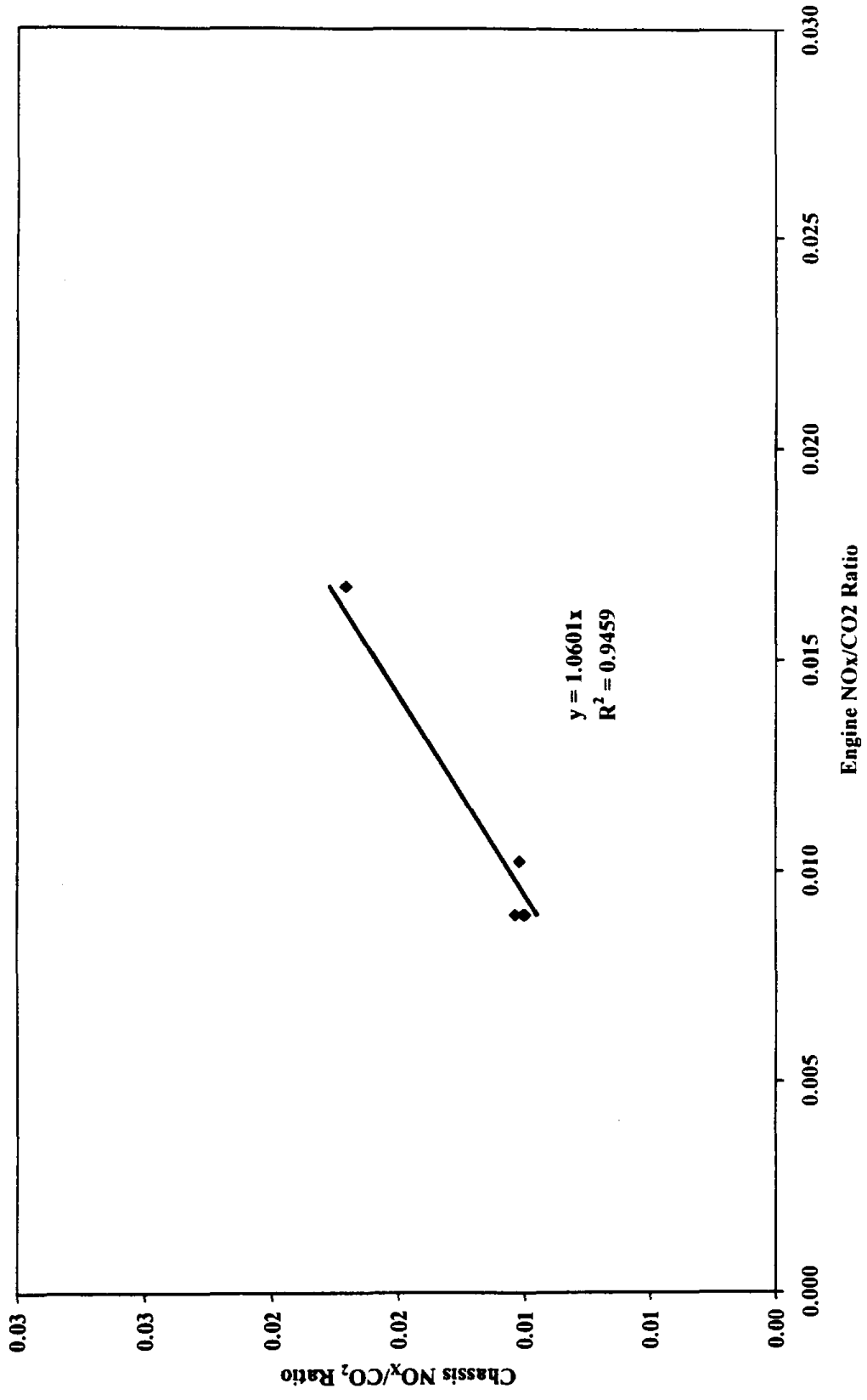


Figure 11.18 - Comparison of all Navistar and Cummins NOx/CO2 Ratios (Single and Tandem Axle)

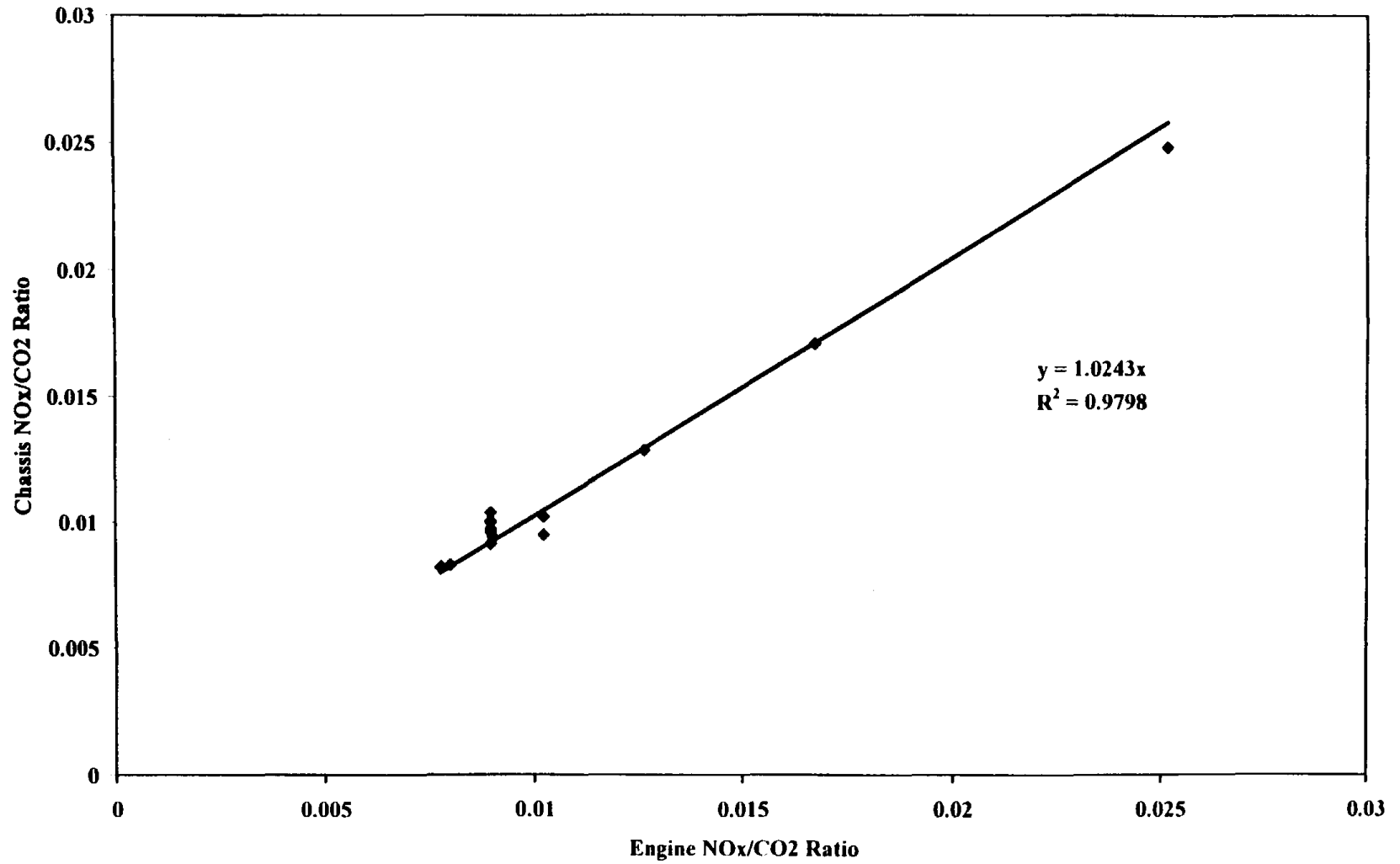


Figure 11.19 - Comparison of Navistar Engine and Chassis PM/CO2 Ratios

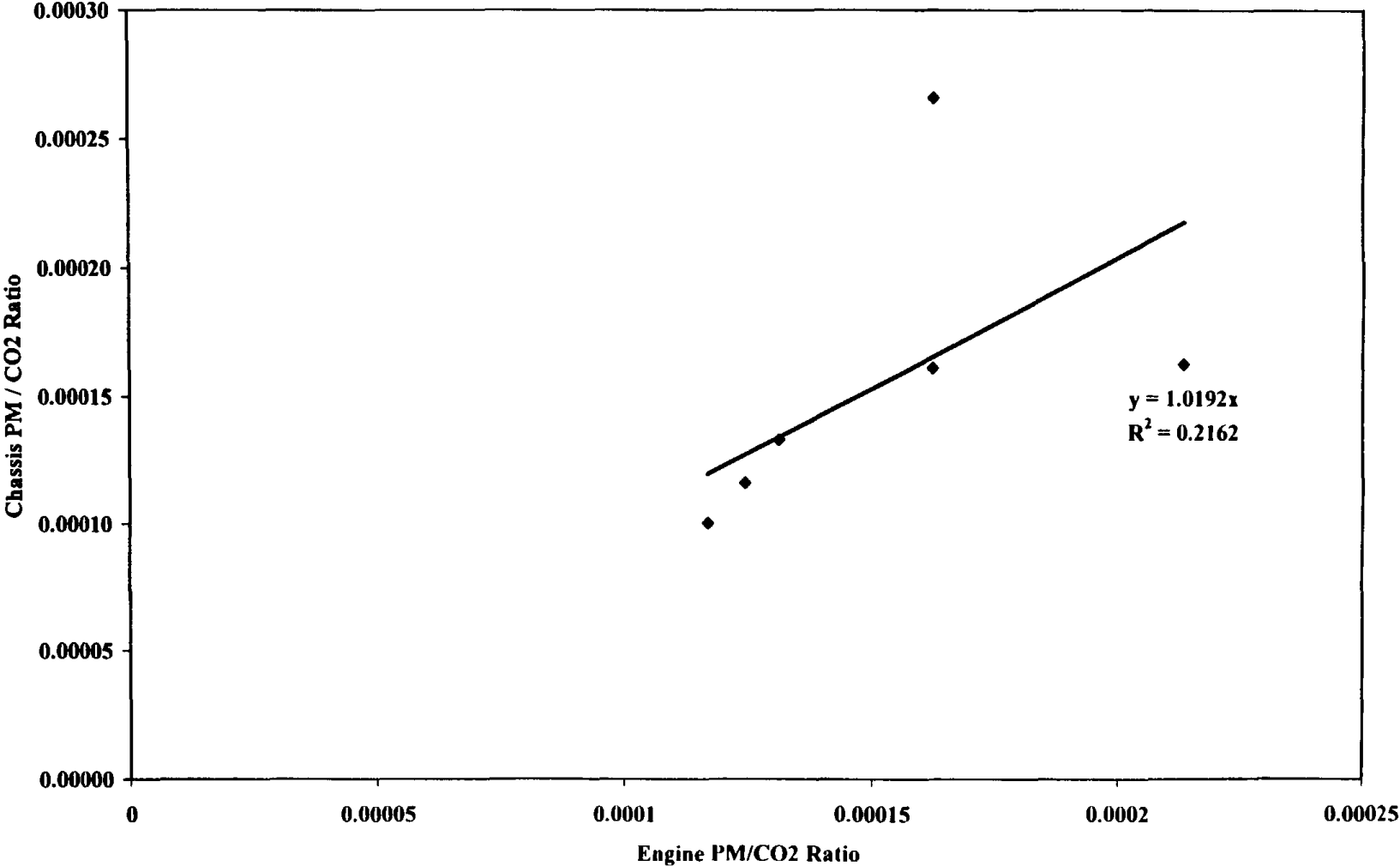


Figure 11.20 - Comparison of Cummins Engine and Chasis PM/CO2 Ratios (Single Axle)

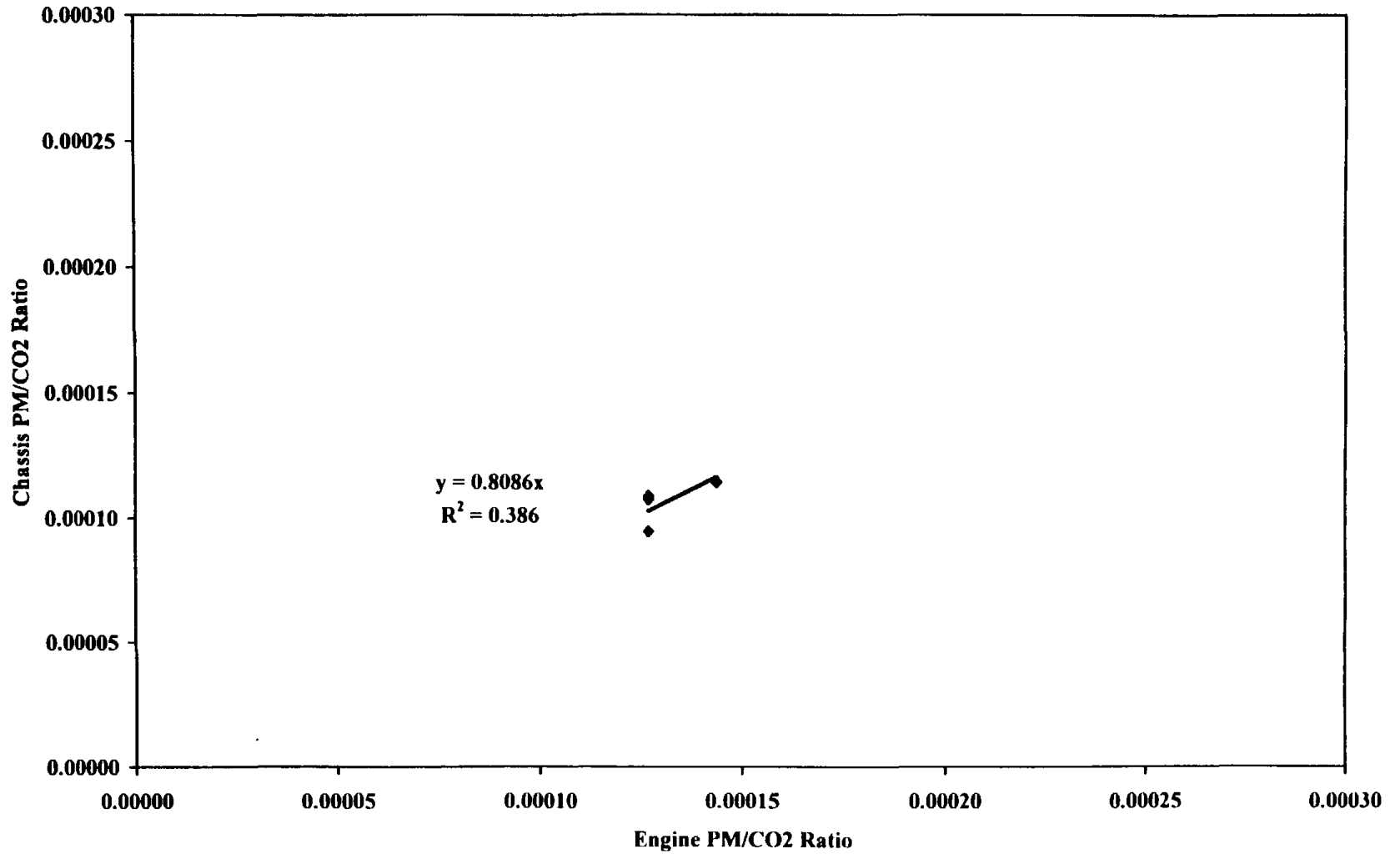


Figure 11.21 - Comparison of Cummins Engine and Chassis PM/CO2 Ratios (Tandem Axle)

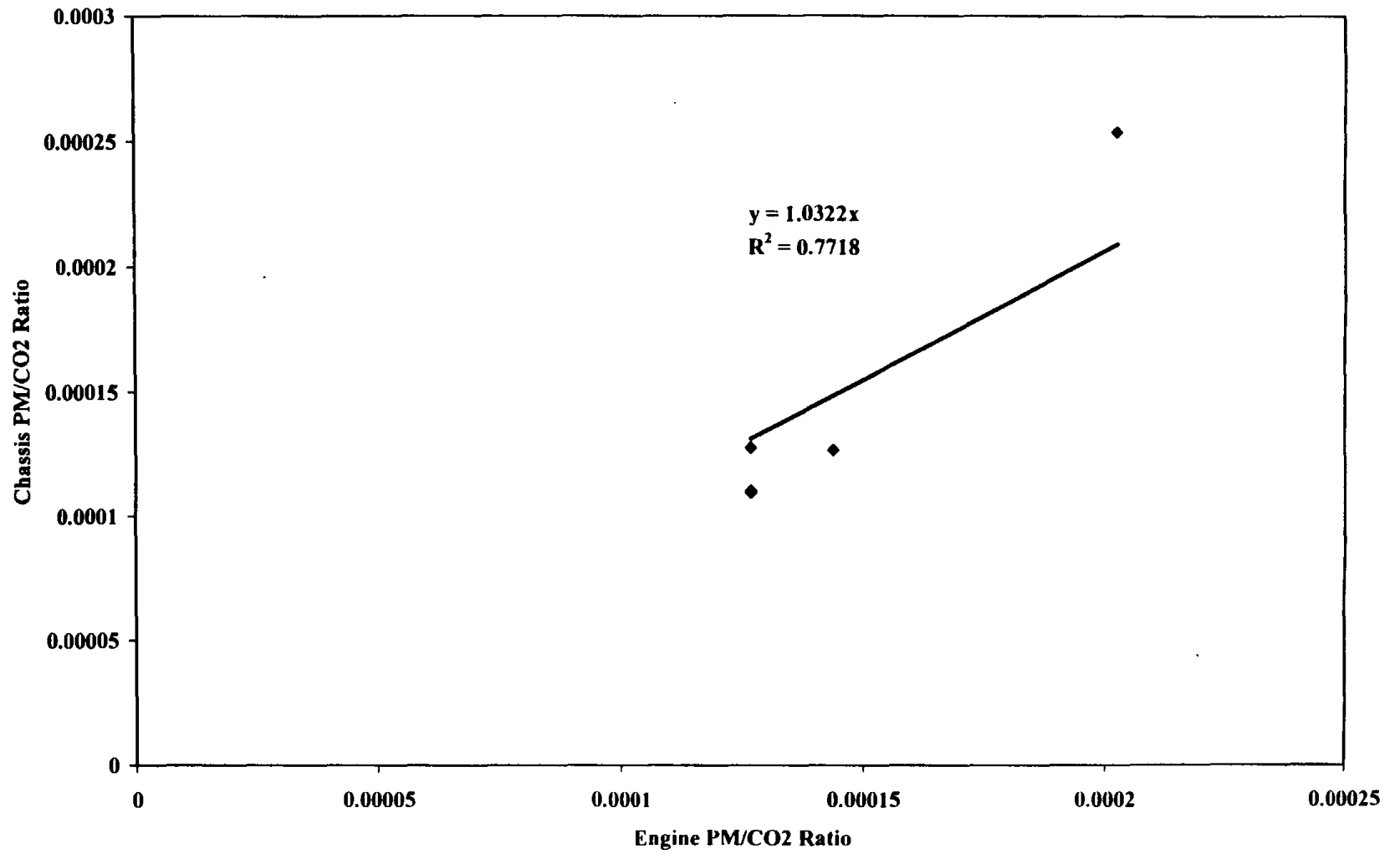


Figure 11.22 - Comparison of all Navistar and Cummins (Engine and Chassis) PM/CO2 Ratios

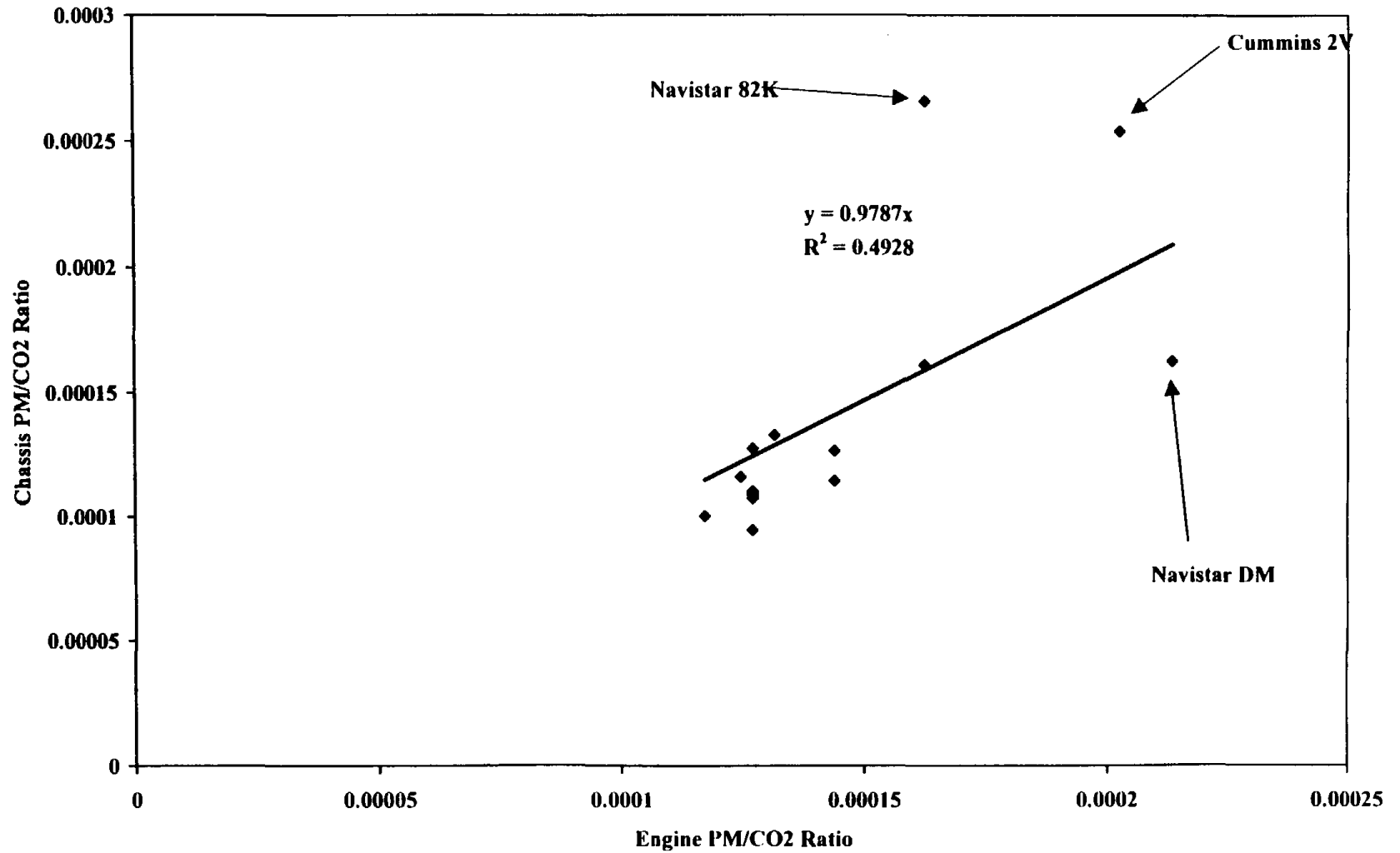


Figure 11.23 - Vehicle Pass/Fail Criteria for Navistar Chassis Testing

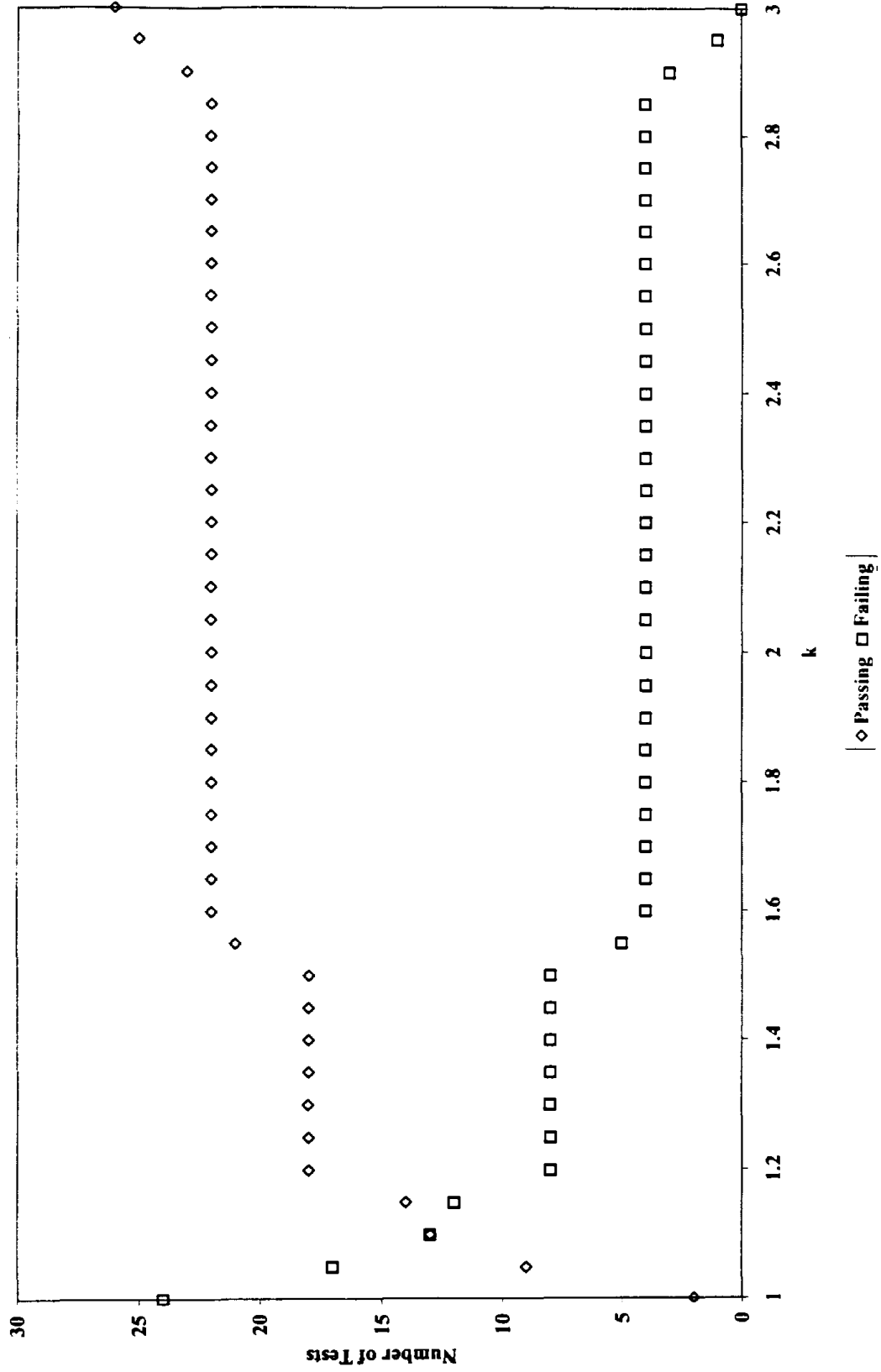


Figure 11.24 - Navistar Chassis Testing Failing and Passing Wrongly

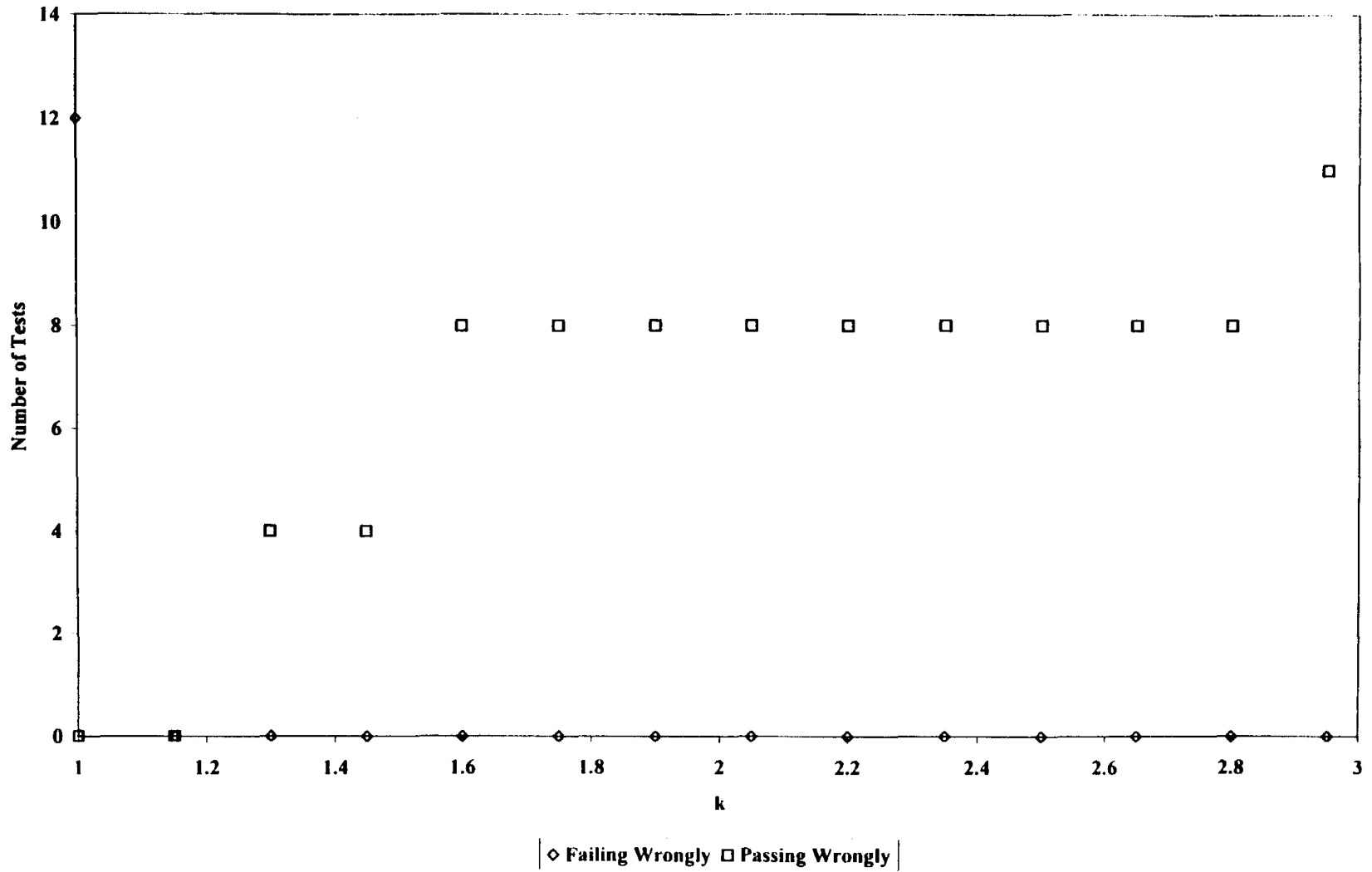


Figure 11.25 - Vehicle Pass/Fail Criteria for Cummins Chassis Testing

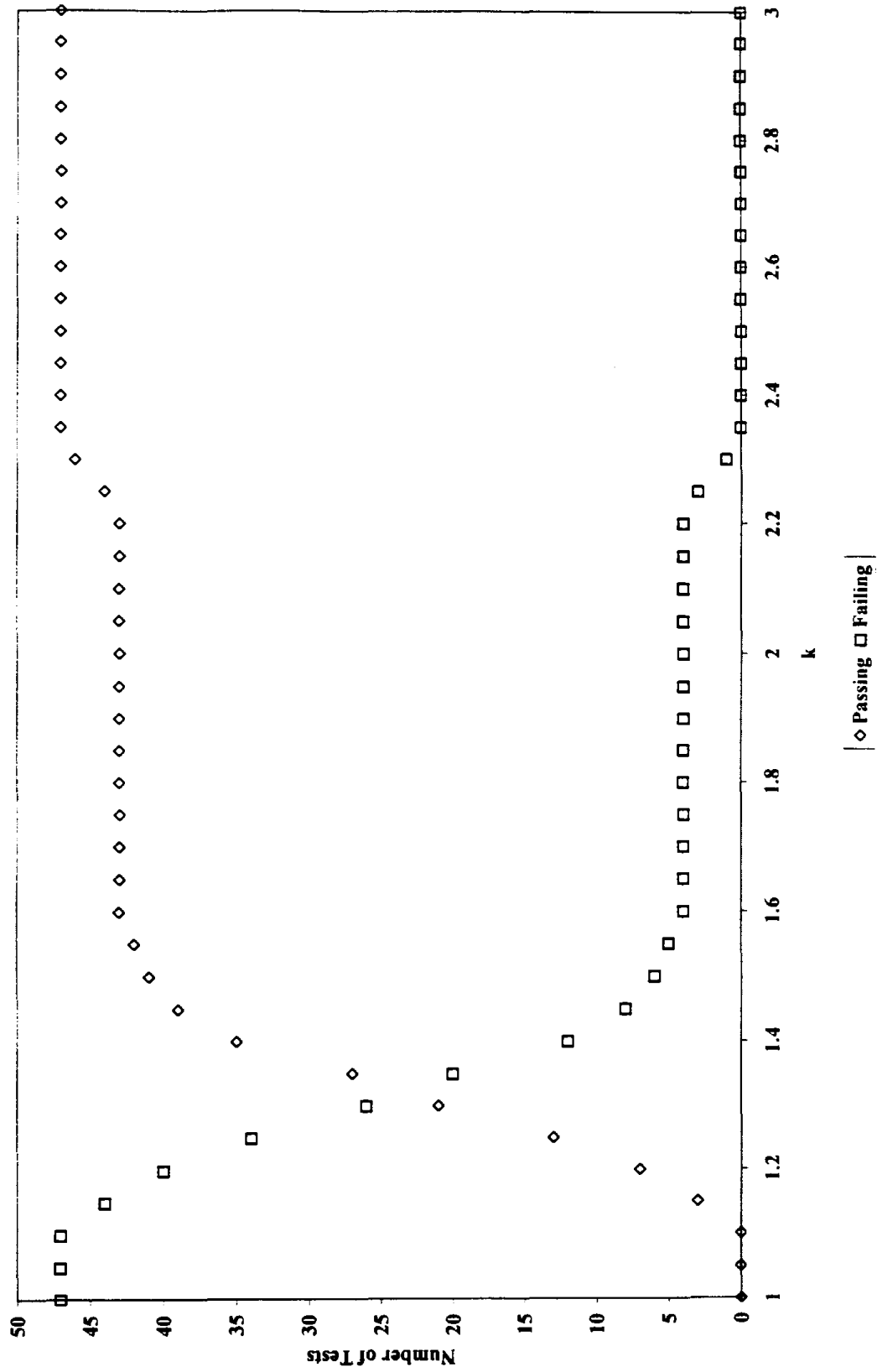


Figure 11.26 - Cummins Chassis Testing Failing and Passing Wrongly

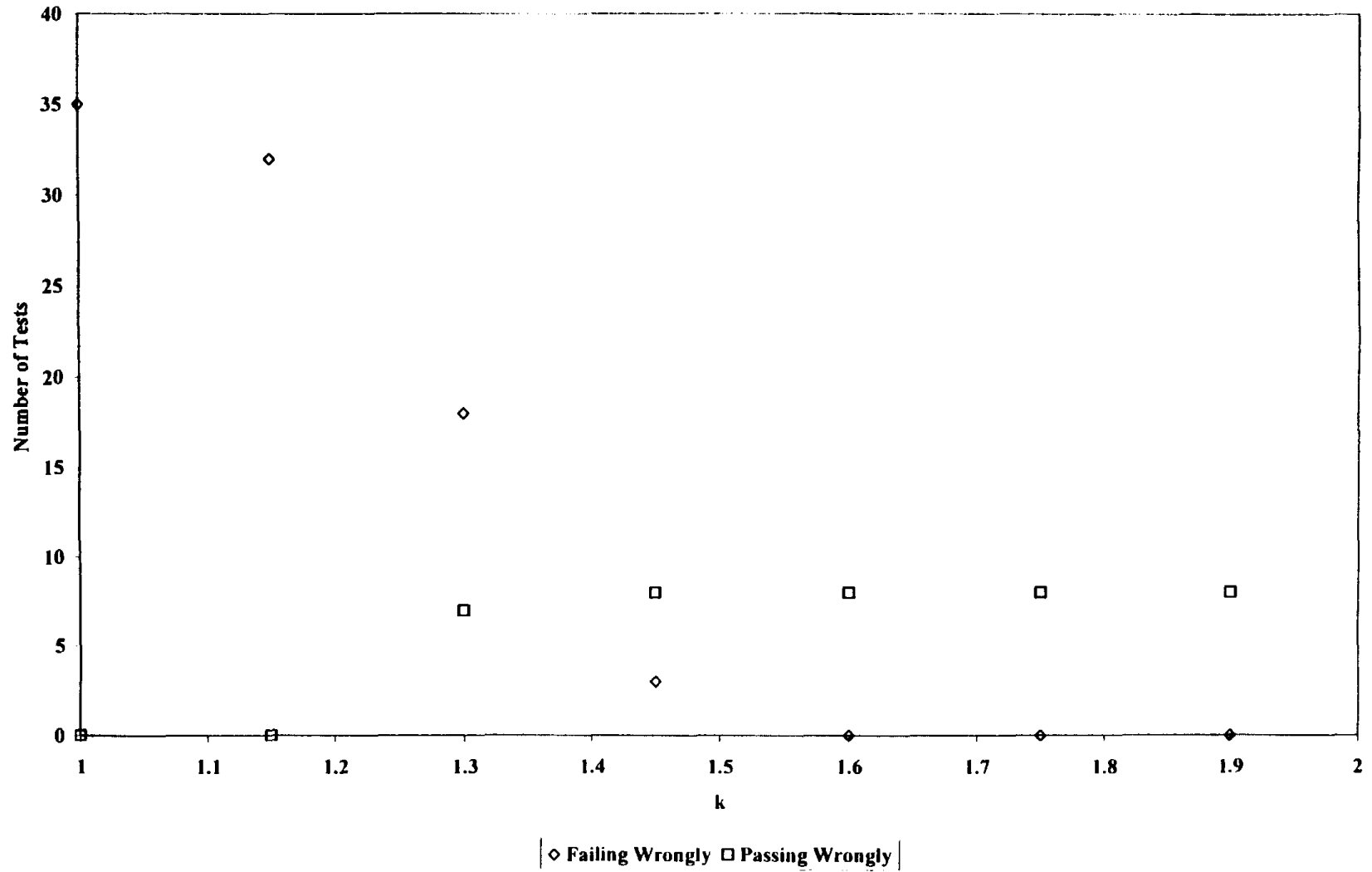


Figure 11.27 - Vehicle Pass/Fail Criteria for Navistar and Cummins Chassis Testing

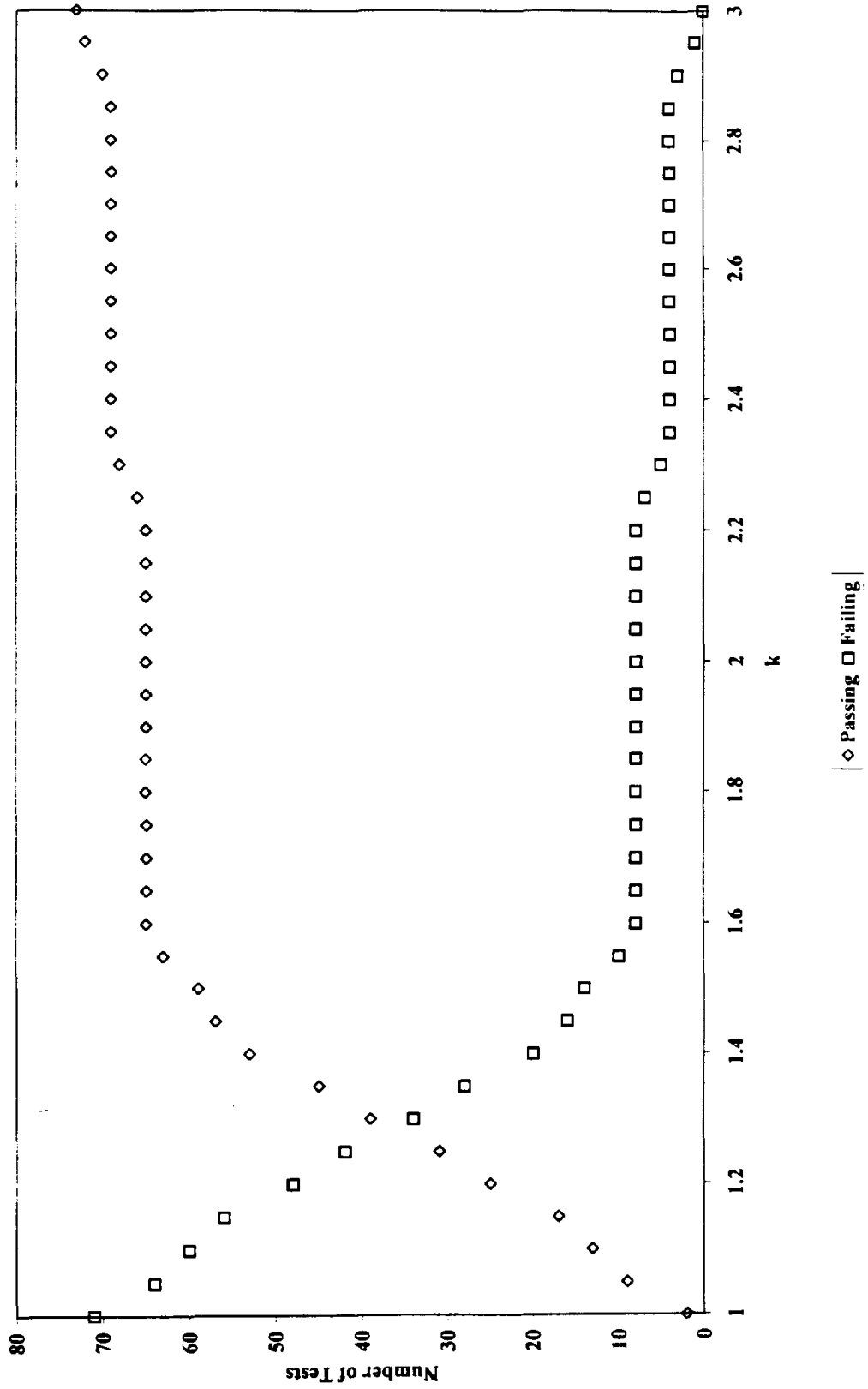
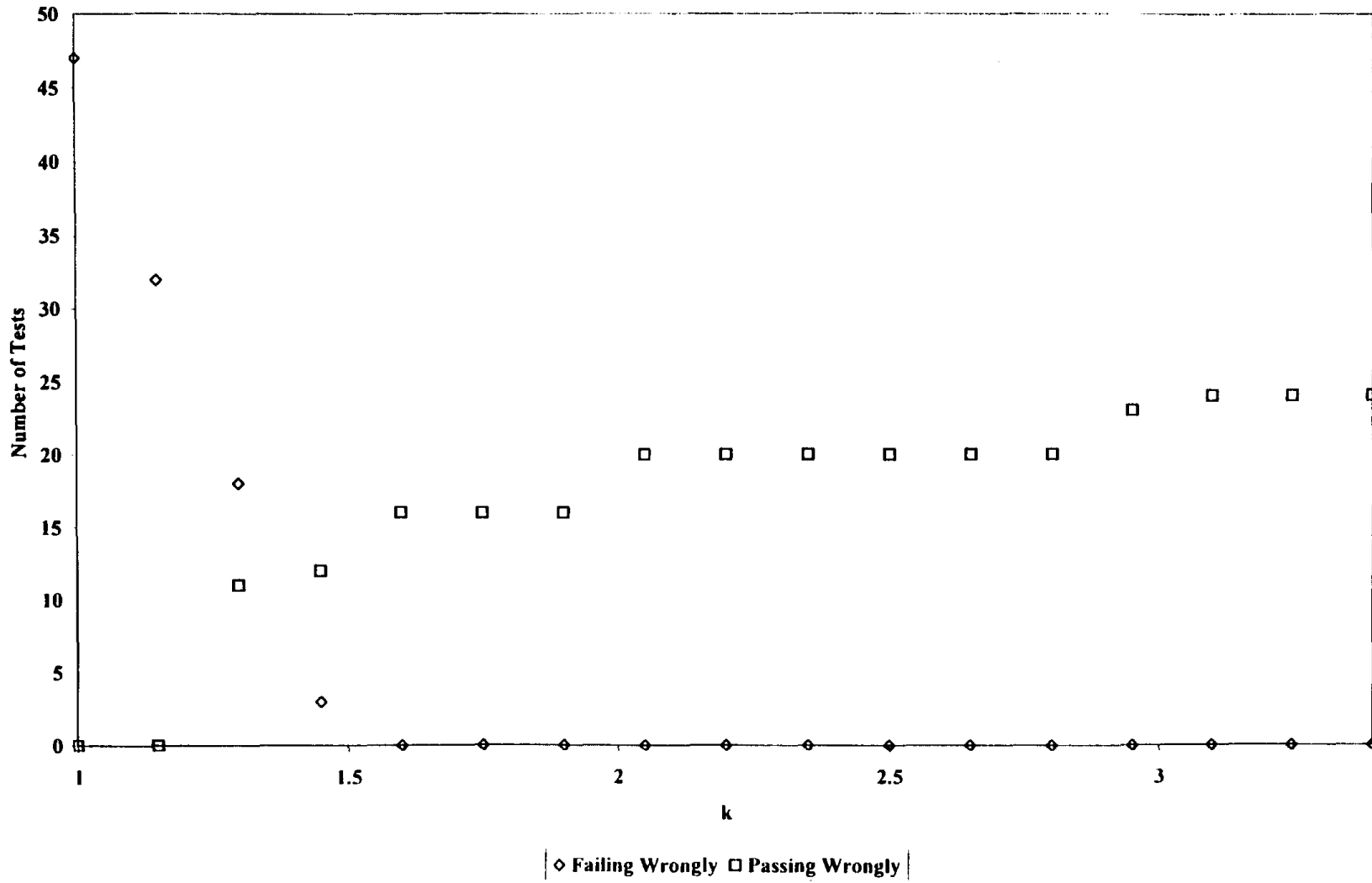


Figure 11.28 - Navistar and Cummins Chassis Testing Failing and Passing Wrongly



12. Conclusions

A program has been completed to create a chassis test cycle for heavy duty vehicles and to demonstrate the chassis test cycles efficiency as a screening test in inferring the emissions levels from engines present in the vehicles. The proposed cycle exercises the vehicle in a single gear and emulates as closely as possible the torques and speeds that the engine would encounter during an engine certification test. It has been shown that tampering with sensors can raise PM and NO_x emissions for the engine certification test and that the increased emissions can be identified by the chassis test.

The correlation between engine test NO_x and chassis test NO_x shows a strong trend and will permit NO_x screening with confidence. Scatter in PM data makes chassis screening less transferable, but gross PM emitters will be evident.

The following two correlations have arisen from this study.

$$\text{Engine NO}_x \text{ (g/bhp-hr)} = 0.775 \text{ Chassis NO}_x \text{ (g/ahp-hr)}$$

$$\text{Engine PM (g/bhp-hr)} = 0.826 \text{ Chassis PM (g/ahp-hr)}$$

Variation within and between laboratories, taking a conservative stance, suggests that one may assert with confidence that an engine emits above certification levels if the following criterion is met.

$$\text{Chassis NO}_x \text{ (g/ahp-hr)} > 1.6 \text{ Certification NO}_x \text{ (g/bhp-hr)}$$

It is suggested that additional data should be gathered to verify or refine these correlations and the cutpoints may be amended as in-use data are gathered.

This research as shown conclusively that a chassis screening test is practical to determine high NO_x emitters and gross PM emitters. This is, fortunately, in keeping with the fact that NO_x variations in diesel engines are usually modest, while PM emissions may escalate significantly due to tampering or malmaintenance.

Although this research was conducted specifically using the West Virginia University Engine and Emissions Research Laboratory, and the Transportable Heavy Duty Vehicle Emissions Testing Laboratory, the resulting approach is applicable to any engine and chassis dynamometer systems. The WVU chassis dynamometer removes power from the vehicle hubs, and not from the roller that carries the tire, but this is not seen to be a cause of significant variation between the laboratories. The vertical load (weight) placed upon the tires will influence the overall irreversible losses during chassis testing and protocols for constraining truck on the dynamometer must be formalized.

Appendix A – Emissions Modeling by Optimization, Inc.

Introduction

As part of the ARB study on transient chassis testing, an emissions model was developed to attempt to predict chassis emissions during a transient federal test from chassis speed and torque. The model was developed using speed, torque and emissions data from transient tests performed using the engine dynamometer testing laboratory and applied to the prediction of emissions from a whole vehicle under transient chassis test conditions.

Model Development

To develop an emissions model, one must first consider those engine parameters upon which the emission of concern is dependent and what engine parameters are measured during a test. From observation and analysis of engine and emissions data, it is known that carbon dioxide and oxides of nitrogen correlate well with instantaneous engine power, carbon monoxide correlates with power and acceleration, while hydrocarbons do not seem to correlate specifically with either engine speed or torque.

For a first approximation, emissions were modeled using the equation

$$E_t = C_1 + C_2(P_t) + C_3(P_t)^2$$

Where E_t is the emissions level at time t , P_t is the engine power in horsepower at time t , and C_1 , C_2 and C_3 are the constants for the model. C_1 provides compensation for the offset between power and emissions, C_2 accounts for the correlation between engine emissions and engine power and C_3 accounts for a second order of variation. While this model is appropriate for steady state operation, an additional term

$$C_4 d(\omega)/dt$$

where ω is engine speed in revolutions per minute was added to account for unsteady state operation and to account for turbocharger lag. This acceleration term was determined using the preceding three seconds of data.

To account for more efficient combustion at slower engine speeds, the term $C_5(\omega)$ was then added to make the complete model

$$E_t = C_1 + C_2(P_t) + C_3(P_t)^2 + C_4 d(\omega)/dt + C_5(\omega)$$

Since the emissions from the engine are measured not at the manifold but after they have traveled through exhaust system, into a dilution tunnel, and through a sampling system to the analyzers, two additional elements were added to the model. The first, C_6 , accounts for the lag time between when the emission was produced at the engine to when it is analyzed by the instrument. The second term, C_7 , is meant to account for axial diffusion as the sample flows through the

emissions measurement system. This portion of the model was applied iteratively C_6 times to the concentration at each second of the period of flow C_6 seconds long.

Model Application

Continuous engine speed, torque and NO_x emissions data were taken during FTP testing of a Cummins N-14 engine. Figure 1 shows the continuous schedule and actual engine speed from an FTP test with the engine in stock configuration. Continuous torque, both schedule and actual, is presented in Figure 2 under the same conditions. Actual NO_x emissions recorded during the test (Figures 1 and 2) are presented in Figure 3 along with predicted NO_x emissions. Predicted NO_x was obtained by applying the seven constant model using engine data in Figures 1 and 2 and actual NO_x data from Figure 3. It can be seen that the model performed adequately in predicting NO_x for the engine test. Additionally, the model was used to predict NO_x emissions (Figure 4) using engine speed and torque from a different stock test. This was done as an additional check of the model accuracy. Constants used in the model are listed in Table 1.

	C_1	C_2	C_3	C_4	C_5	C_6
NO_x	18.64089	1.07E-04	1.77E-11	-8.52E-04	4.97E-05	10.3776
CO	6.124813	-2.61E-05	3.37E-10	1.38E-03	-6.48E-04	13.46959
CO_2	52.532	1.40E-04	3.66E-11	-1.52E-02	0.051758	12.48738
HC	10.12668	-1.38E-06	1.21E-12	-2.03E-03	9.17E-04	6.578578

Table 1 – Model constants from regression on data from Stock FTP test on Cummins N-14 engine.

To apply the model to chassis test data, the engine torque must first be corrected for drivetrain efficiency. Using the drivetrain efficiency model developed in this study (Appendix D) for the Cummins engine in the International Chassis (single axle)

$$T_{\text{engine}} = (T_{\text{axle}} - 26.22 + 0.128\omega_{\text{engine}})/0.83$$

continuous axle torque from chassis tests were converted to engine torque. With this data, the emissions models developed from the engine tests could then be applied to the chassis data to predict engine emissions. Figure 5 shows continuous NO_x and predicted NO_x from a Cummins N-14 single axle chassis test.

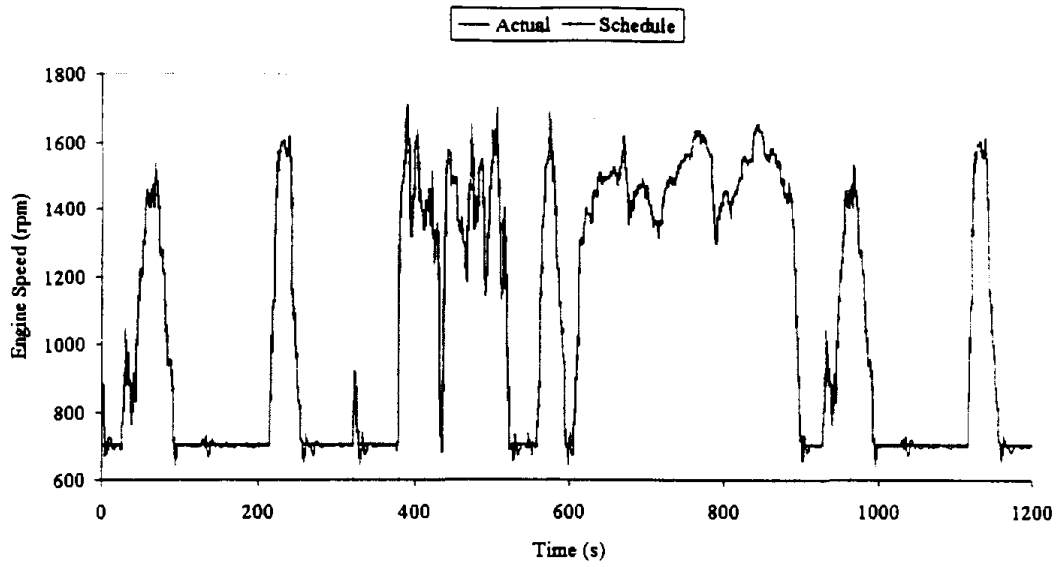


Figure 1 - Engine actual and schedule speed from the Cummins N-14 engine during a engine FTP tranient test.

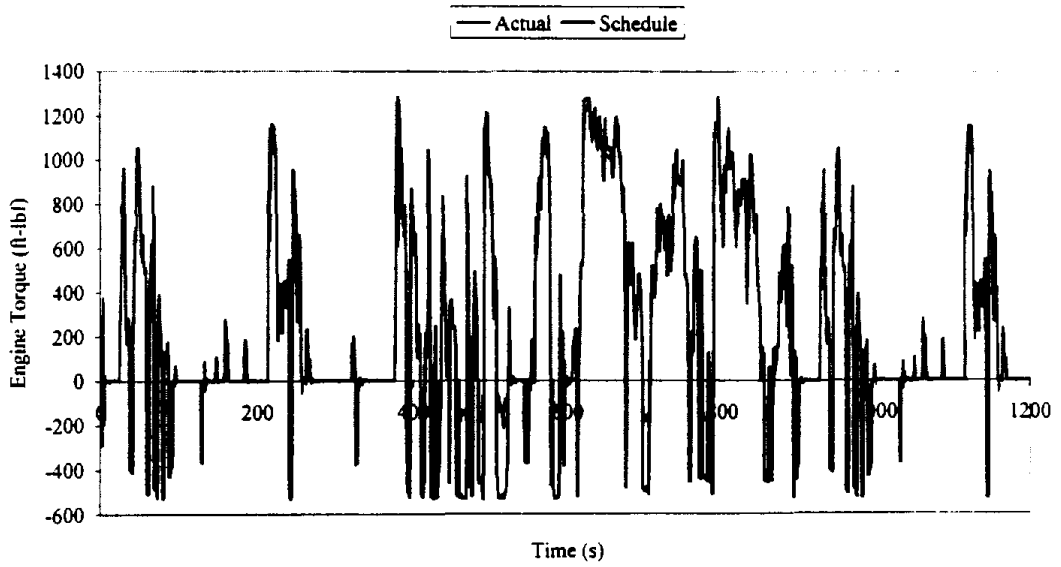


Figure 2 - Engine actual and schedule torque from the Cummins N-14 engine during a engine FTP tranient test.

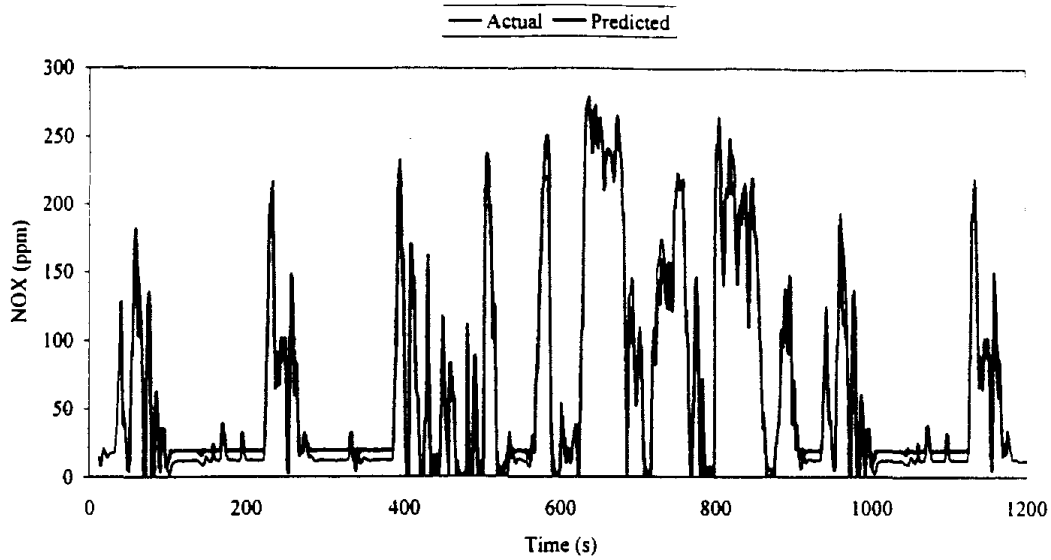


Figure 3 – Actual and predicted continuous NOX emissions from the Cummins N-14. Data is from the same test as Figures 1 and 2.

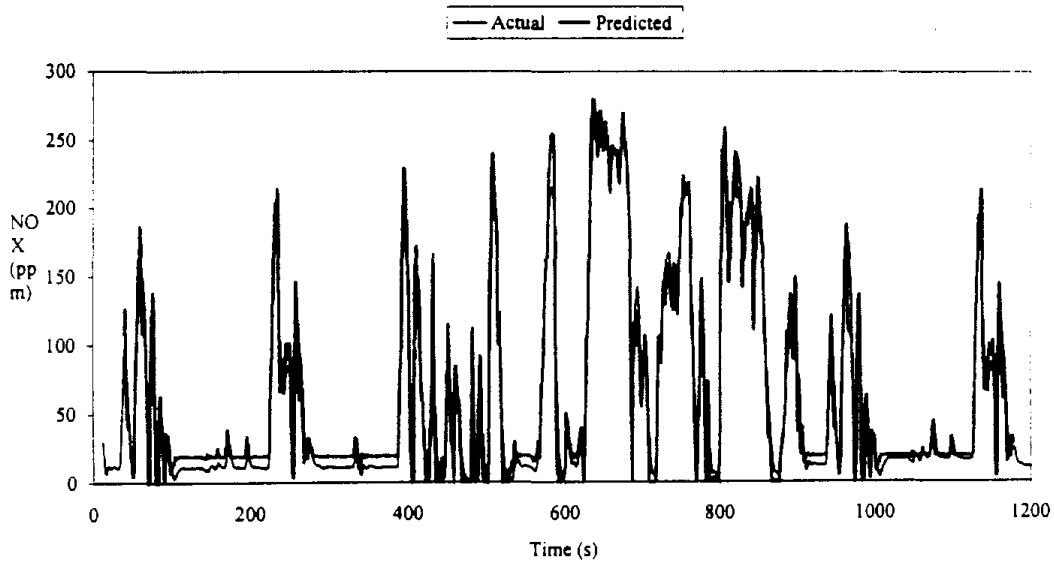


Figure 4 – Continuous actual and predicted NO_x emissions from the Cummins N-14 engine. The actual emissions are from a test performed on the same day and under the same conditions and the model used to obtain the predicted emissions was derived from data presented in Figures 1 – 3.

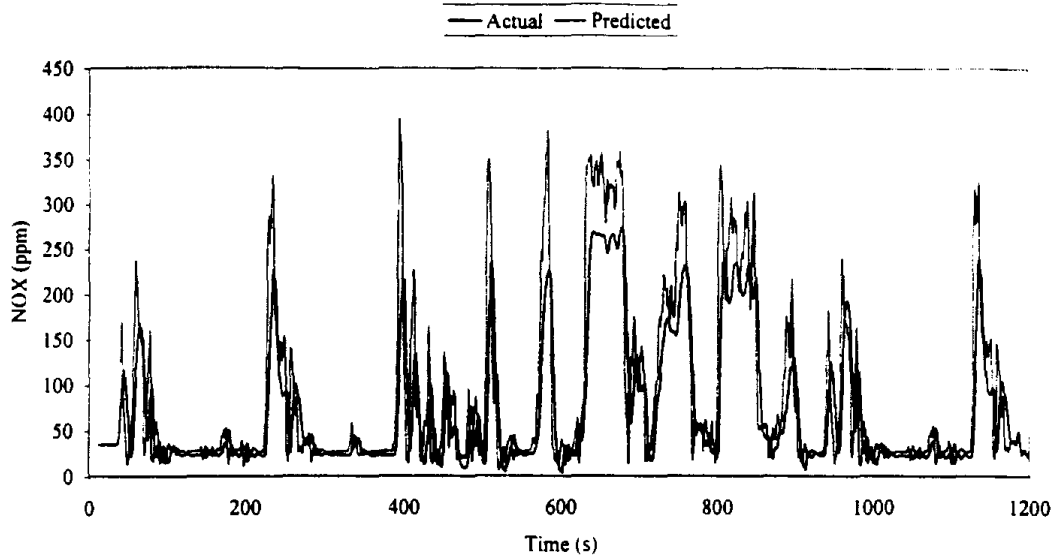


Figure 5 – Continuous actual and predicted NO_x from a transient chassis test of the Cummins N-14 engine. Prediction was done with the model developed for Figure 3. While the model is fairly accurate in predicting NO_x overall, accounting for differences in exhaust and emissions sampling line lengths in the emissions model would improve its accuracy and reduce overshoot of emission peaks.

Appendix B - Uncertainty Theory

Completely accurate measurements are impossible. There is undoubtedly some uncertainty associated with all measured values. Uncertainty, usually expressed as a range, is partially responsible for the random, unbiased, scatter found in measurement data. Errors also contribute to the biased difference between statistically derived mean values and true measured values [Figliola et al., 1991]. To lend credibility to measured data and the conclusions drawn from them, measurement uncertainty must be identified and reported. The process of estimating these combined measurement errors is called uncertainty or error analysis. Error analysis incorporates both statistical and engineering concepts, and to be accurately performed, requires thorough attention to the measurement process.

B.1 Error Types

Two types of error are regularly referred to, random error and bias error. Both of these error types contribute to the overall uncertainty of any given measurement.

B.1.1 Bias Errors

A bias error represents a fixed amount, by which the measured value varies from the true value for a set of repeat measurements. Bias errors result in the same offset value for all measurements and cannot be readily detected without some means of comparison. Errors that are estimated using non-statistical methods are classified as bias errors. Examples of bias errors would be manufacturer list errors and experimentally derived errors.

B.1.2 Random Errors

Random errors, also called precision errors, represent the variance in a data set from the mean. Random errors are defined by the repeatability of a measurement taken successively under identical conditions. These errors are typically statistically derived using the standard deviation of a data set. A large standard deviation indicates a large scatter in the measurements and subsequently a greater uncertainty. There are two concepts used to develop random errors, the distribution and population from which the sample was taken. It is assumed for all errors statistically calculated in this thesis, following statistical premises that the error distribution will be normal or Gaussian. The population is the infinite body from which a small amount of data is collected. This sample of data is in turn used to develop assumptions about the entire population with the aid of the student-t distribution [Beckwith et al., 1982]. A graphical depiction of bias and random errors for a specific measurement in a data set is shown in **Figure 6-1**.

B.1.2.1 Student-t distribution

The student-t statistic is used along with the standard deviation of a data set in order to extrapolate the results to the entire population. The student-t distribution ($t_{v,p}$) is obtained from a weighting function for finite data, in order to draw conclusions about an infinite population. It is the distribution of the mean divided by the standard deviation of a sample of normal distributed

values with unknown variance. The $t_{v,P}$ is a function of probability (P) and the degrees of freedom (v) in the standard deviation [Figliola et al., 1991].

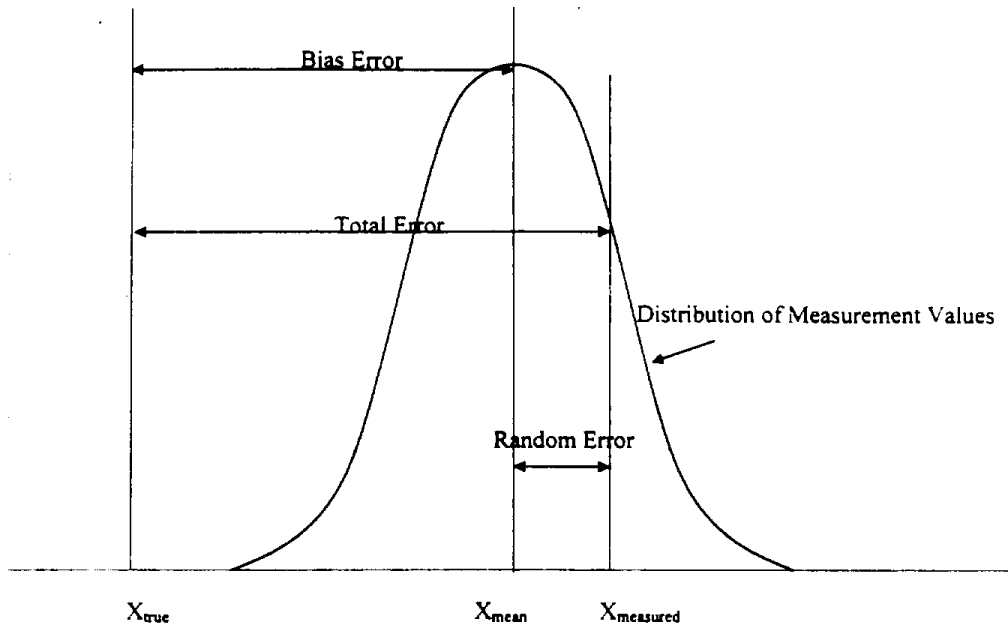


Figure B.1 Random, Bias and Total Errors for a specific measurement in a data set

Probability deals with the likelihood that an event will occur with some level of doubt. A probability of 95% will be assumed throughout this thesis. v refers to the number of data points used in analysis. The actual value of v is the number of data points used for analysis minus the number of restrictions placed on the data points by the statistical analysis. A restriction placed on almost all collected data is the mean value theorem, or the tendency for data to be scattered about the mean. The student-t statistic is used to assess the probability of the occurrence of random errors. It is used under the predication that the values from which the mean and variance are calculated are themselves normally distributed. **Table B.1** gives the student-t values, dependent on the degrees of freedom in the data set, at the 95% confidence level which were used for the uncertainty calculations in this report.

Student-t Distribution at 95% Confidence Interval	
t(3)	3.182
t(4)	2.77
t(5)	2.571
t(6)	2.447
t(7)	2.365
t(8)	2.306
t(9)	2.262
t(10)	2.228
t(11)	2.201
t(12)	2.179
t(13)	2.16

Table B-1 Student-t Distribution Table

B.2 Error Sources

There are three distinct areas where error can be introduced into the measurement process: calibration, data acquisition and data reduction. The random and bias errors must be identified at each of these stages and then combined for an overall uncertainty prediction for each measurement taken. Should any of these steps be omitted from the measurement process, they should also be omitted from the overall error calculation of the system.

B.2.1 Calibration Errors

Calibration is the process of feeding known input values into the measurement system and recording the output to use as a reference when reducing data. A calibration gas of known concentration, usually expressed in units of parts per million by volume (ppm), is routed through a gas divider, to the respective analyzer. A signal is sent to the signal conditioner, to the RTI board (i.e. analog to digital converter), then the resulting ADC code is stored in a data file for the channel in question. The gas divider is set to allow zero percent of the gas to flow through, then 10 percent and so on, in 10 percent increments, until a full 100 percent of the gas flows through the gas divider. The computer program reads the ADC output signal from the system at each step and forms a calibration file for the specified channel. The calibration file is a set of data which has an ADC code associated with eleven concentrations for each channel. Linear regression analysis is applied to the data in the calibration file and a mathematical model of gas concentration in ppm as a function of ADC code to be used for data reduction is developed.

The calibration process is important in that it reduces the amount of error incurred by the system relative to no calibration at all, but it does not eliminate it. Errors enter into the calibration process due to uncertainty in the input gas quality, gas divider, signal conditioning devices (e.g. sizing an electrical signal to a known range), analog to digital converters (e.g. conversion of the continuous electronic signal to a digital value), drift of the analyzers and conversion to engineering values (e.g. converting digital values to real engineering units).

B.2.2 Data Acquisition Errors

Data acquisition is the process of running tests and taking data. Errors enter data acquisition through the sensors, environmental conditions and data storage. Of course, random errors also occur through variation in the tested truck from run to run.

B.2.3 Data Reduction Errors

Data reduction is the process of taking the data acquired in the previous step and putting it into a form that can be readily applied to the real world. Errors enter data reduction from curve fitting to the equations derived from calibration files and truncation that occurs when storing data.

B.3 Error Propagation

The propagation of errors in the measurement process can be difficult to follow. The procedure outlined by Figiolo parallels the standards provided by the National Institute of Standards (NIST) [1991]:

- Identify the errors for the three source groups: calibration, data acquisition, and data reduction.
- Estimate the random and bias errors for each of the three sources.
- Estimate any propagation of error through to the result.

B.3.1 Error Identification

This step requires that every step and every instrument encountered in the preparation for and process of data collection is accounted for. For all instruments, the listed uncertainties in the manufacturer's manuals were used. And for all curve fit equations, the aforementioned statistical methods were used. Every possible influence was noted, although the least influential were eliminated due to lack of impact on the resulting overall uncertainty. The uncertainties are expressed as one standard deviation.

B.3.2 Methods of Uncertainty Propagation

After the measurement errors for each measurement are defined, the formulas used to combine these measurements and produce results must be identified. The propagation of errors through the system may then be characterized. When many measurements are used to produce results such as in engine and chassis testing, a sound method of combining the uncertainties encountered from each measurement must be developed. Two such methods are commonly used, absolute summation, which produces the maximum uncertainty to be expected and the Root Sum of Squares Method, which produces a more realistic value than absolute summation and is the method prescribed by the NIST to use for error propagation in a system.

B.3.2.1 Absolute Summation

Absolute summation uses a special application of Taylor's series, ignoring the higher-order terms, for analysis [Beckwith et al., 1982]. Each equation used in the formulation of results is identified. Then, the partial differential with respect to each measured variable (e.g. P) is multiplied by its individual uncertainty (ΔP), the absolute value of each product is taken and summed. The uncertainty of each value would be determined a priori either using statistical methods or the manufacturer list error. For example, if F were a function of a, b, and c. and a was a function of x and y then the absolute uncertainty would be defined

$$a = f(x, y)$$

$$\Delta a = \left| \frac{\partial a}{\partial x} * \Delta x \right| + \left| \frac{\partial a}{\partial y} * \Delta y \right| \quad \text{B.1}$$

$$F = f(a, b, c)$$

$$\Delta F = \left| \frac{\partial F}{\partial a} * \Delta a \right| + \left| \frac{\partial F}{\partial b} * \Delta b \right| + \left| \frac{\partial F}{\partial c} * \Delta c \right| \quad \text{B.2}$$

Δx , Δy , Δa , Δb , Δc and ΔF are the uncertainties associated with the respective variables

Absolute values are used, assuming that the uncertainties are expressed as equally probable plus and minus values. The above method describes the overall maximum uncertainty of the function, however it is not likely that this maximum value would be obtained and therefore the following RSS method is recommended [Beckwith et al., 1982].

B.3.2.2 Root Sum of Squares Method

The recommended method to use when combining these uncertainties is the root sum of squares method (RSS). The RSS is a Pythagorean summation that produces a more realistic uncertainty range. The partial differential with respect to each measured variable (P) in the equation is multiplied by its individual uncertainty (ΔP) and squared, these quantities are summed and then the square root is taken. The RSS procedure is used on each equation sequentially and then on each subset of equations as they follow in the reduction program, until the analysis is complete. Using the above example to determine the RSS uncertainty would give

$$a = f(x, y)$$

$$\Delta a = \sqrt{\left(\frac{\partial a}{\partial x} * \Delta x \right)^2 + \left(\frac{\partial a}{\partial y} * \Delta y \right)^2} \quad \text{B.3}$$

$$F = f(a, b, c)$$

$$\Delta F = \sqrt{\left(\frac{\partial F}{\partial a} * \Delta a\right)^2 + \left(\frac{\partial F}{\partial b} * \Delta b\right)^2 + \left(\frac{\partial F}{\partial c} * \Delta c\right)^2} \quad \text{B.4}$$

$\Delta x, \Delta y, \Delta a, \Delta b, \Delta c$ and ΔF are the uncertainties associated with the respective variables

RSS is the method used throughout this thesis to define the uncertainty ranges for WVU's stationary and transportable laboratories.

B.3.3 Example of Error Propagation

As an illustrative example, the equation used by the WVU Stationary Engine Laboratory as prescribed in the CFR to calculate the volumetric flowrate, V_{mix} , through the main dilution tunnel is [86.1319-90, 1996]:

$$V_{mix} = \frac{K * P}{\sqrt{T}} \quad \text{B.5}$$

- V_{mix} the volumetric flowrate of the dilute exhaust through tunnel
- K the venturi coefficient, a constant found by calibration
- P the pressure at the venturi throat
- T the absolute temperature at the venturi throat

Applying the RSS method, the formula for determining the uncertainty in the calculation of V_{mix} figuratively is:

$$\Delta V_{mix} = \sqrt{\left(\frac{\partial V_{mix}}{\partial K} \Delta K\right)^2 + \left(\frac{\partial V_{mix}}{\partial P} \Delta P\right)^2 + \left(\frac{\partial V_{mix}}{\partial T} \Delta T\right)^2} \quad \text{B.6}$$

and specifically:

$$\Delta V_{mix} = \sqrt{\left(\frac{P}{\sqrt{T}} \Delta K\right)^2 + \left(\frac{K}{\sqrt{T}} \Delta P\right)^2 + \left(-\frac{1}{2} \frac{KP}{(\sqrt{T})^3} \Delta T\right)^2} \quad \text{B.6a}$$

Variable	Instrument	Company & Model #	Uncertainty
Pressure (P)	Pressure Transducer	Viatran Corporation	± 0.15% fs output
Temperature (T)	RTD	Tayco Engineering	± 0.89 °F

Table B.2 Uncertainty Identification of Variables

Once the equations have been identified, the uncertainty range of each measurement variable needs to be quantified, see **Table B.2**, starting with the first variable, venturi pressure (P). Venturi pressure is measured using a pressure transducer from Viatran Corporation, Model #104. Viatran lists a ΔP of no greater than ± 0.15% full scale output (fs_{out}). The full scale output of this pressure transducer has been standardized by Viatran to be 2.5 mV/V (millivolt/volt). A 10 V excitation voltage is supplied to the pressure transducer for operation. Therefore the analog full scale output for this sensor is:

$$fs_{out} = 2.5 \frac{mV}{V} * 10V = 25mV$$

The West Virginia University Stationary Engine Laboratory uses a 12 bit, ±10 Volt data acquisition channel for this measurement. The channel has been calibrated linearly so that 0V corresponds to 0 ADC codes and 0 pounds per square feet (psf), +10 V corresponds to 2047 ADC codes and 2160 psf. Using the preceding information and interpolation, the full scale output of this pressure transducer in engineering units is:

$$fs_{out} = 25mV = 5.117ADC = 5.4psf$$

The error value then associated with any measured pressure (*P*) is then:

$$\Delta P = \pm 0.15\% * 5.4psf = \pm 0.0081psf$$

A resistance temperature detector (RTD), manufactured by Tayco Engineering Company, Model # 68-3839-10, measured the venturi temperature (*T*). The company reports a $\Delta T = \pm 0.89$ °F for the range that WVU takes data [Tayco, 1996].

The venturi coefficient, *K* is a constant in the reduction program, it varies depending on the dilution tunnel venturi selection. For this research, the 1000 scfm critical flow venturi was employed for all tests at the stationary laboratory. Venturi coefficients were determined using a subsonic venturi obtained from the Environmental Protection Agency (EPA). The subsonic venturi was connected in series with the WVU dilution tunnel, therefore characterizing the flowrate in the EPA and WVU venturis. This flowrate along with temperature and pressure measurements were subsequently used to calculate *K* for the WVU venturi. An extensive RSS analysis on the equations was performed using Mathcad Version 3.1 to calculate *K* and ΔK . The 1000 scfm venturi suggested that $K = 10.766$ and $\Delta K = \pm 0.05351$. This analysis which determined ΔK is contained in Appendix C.

Using **Equations B.5 and B.6a**, for *V_{mix}* and ΔV_{mix} , when *T* = 82 °F, *P* = 2053 psf and *K* = 10.766 ; the values *V_{mix}* = 908 scfm and $\Delta V_{mix} = \pm 4.59$ scfm were calculated. Recognizing that during a test, recorded *T* values can range 60 - 300 °F and *P* values from 2045 - 2065 psf, ΔV_{mix} and *V_{mix}* was found for all possible scenarios and found that the % error ($\Delta V_{mix} \div V_{mix} * 100$), does not vary significantly from ±0.50%.

Therefore, for all future calculations $\Delta V_{mix} = \pm 0.50\% * V_{mix}$. ±0.50% is also the listed tolerance for *V_{mix}* in the CFR [86.1319-90, 1996].

Appendix C - Uncertainty Analysis

A program was prepared to find the uncertainty range of emissions values obtained from standard chassis and engine dynamometer tests. The following results from the reduced data file of each test were read into the program: the dilution factor, the volume of mixing air, brake (axle) horsepower hour, background gas values, in ppm and the average continuous gas values, in ppm. The program then calculated each of the source errors: calibration, data acquisition, data reduction, and combined them using the RSS method. These values were then used by the program to calculate the overall uncertainty in the reported results. Similar programs were used to analyze the data from each laboratory and minor alterations were necessary due to the different methods used by each laboratory for data storage.

C.1 Specific Laboratory Errors

C.1.1 Calibration Error

As discussed in Appendix B, error from gas analyzer calibration is associated with uncertainties in the reported calibration gas concentration, the gas divider, the signal conditioner, the RTI board and the conversion of ADC codes to engineering unit values. Calibration gases are required by the CFR to be accurate to within 1% of NIST standards and are therefore considered to have an uncertainty of $\pm 1\%$ for this thesis [86.1314-84, 1996]. **Table C.1** lists the uncertainty contributions given by the manufacturers in the instrument manuals. These uncertainties, representing one standard deviation, were combined using the RSS method and the overall uncertainties for each instrument are depicted in **Table C.2**. Accuracy refers to how close the measured value is to the true value and reproducibility denotes how close repeat measurement values are to each other.

Manufacturer Listed Uncertainty Contributions		
Calibration Gas	Accuracy $\pm 1.0\%$	
Gas Divider	Accuracy $\pm 0.5\%$ fs	Reproducibility $< 0.2\%$ fs
Signal Conditioner	Accuracy $\pm 0.1\%$	
RTI Board	Accuracy $\pm 0.02\%$ fs	

Table C-1 Manufacturer List Errors

Source	Manufacturer	Model Number	Applied Error % of full scale
Calibration Gas	Scott Specialty Gases	N/A	$\pm 1.0\%$
SGD Gas Divider	Stec Inc.	SGD-710-C	$\pm 0.54\%$
Signal Conditioner	Analog Devices Inc.	3B Series	$\pm 0.1\%$
RTI Board	Analog Devices Inc.	RTI-815F	$\pm 0.02\%$

Table C-2 Calibration Error Sources

The overall calibration error for the four gases is then

$$R_{cal} = \sqrt{1.0^2 + 0.54^2 + 0.1^2 + 0.02^2} = \pm 1.14\% \text{ of full scale}$$

C.1.2 Data Acquisition Error

Uncertainty enters during data acquisition through the instruments, environment and data storage. The companies that manufacture the instruments publish uncertainty contributions for them, at one standard deviation, they are listed in **Table C-3**. These uncertainties were combined as before and the values used for the calculation of data acquisition uncertainty are shown in **Table C-4**. The overall uncertainty percentage for each gas analyzer is multiplied by the full scale calibration value in ppm to give an uncertainty in ppm to be used as the analyzer error in formulas. Any errors due to environmental changes are assumed to be included with the listed precision errors due to the pains taken to assure uniformity in the laboratory environment.

Analyzer Manufacturer Listed Uncertainty Contributions		
CO & CO ₂	Repeatability 1% fs	Noise 1% fs
NO _x	Linearity ±1% fs	Precision ±0.5% fs
HC	Stability ±1% fs/24hrs	Reproducibility ±1% fs

Table C.3 Analyzer Manufacturer Listed Error Sources

Gas	HC	CO	CO ₂	NO _x
Analyzer Error % of full scale	± 1.41%	± 1.41%	± 1.41%	± 1.12%

Table C.4 Overall Analyzer Errors Used in Analysis

These uncertainties given as percent of full scale calibration of the instrument are found to be quite conservative due to the nature of transient testing. The CFR states that the analyzers must be operated between 15 and 100 percent of full-scale chart deflection during the measurement of the emissions for each mode. There are several exceptions to this stipulation listed in the CFR. The analyzer's response may be less than 15 percent of full scale if: automatic range change circuitry is used and the limits of range changes are within 15 and 100 percent of full scale, a 16 point gas divider is used for calibration, the full scale range value is 155 ppm or less, emissions from the engine are erratic and the integrated chart deflection value for the cycle is greater than 15 percent of full scale, the contribution of all data read below the 15 percent level is less than 10 percent by mass of the final test results, during the engine start-up. Another allowable fault is that the HC analyzer is allowed to "spike" off-scale for a maximum of 5 seconds [CFR, 86.1338-84, 1996].

C.1.3 Data Reduction Error

Uncertainty introduced in the data reduction process is from the goodness of fit of the models used, also from truncation and rounding of values for data storage.

C.1.3.1 Goodness of Fit

Goodness of fit is particular for each calibration performed, even when calibrating the same instrument. This value must, therefore be calculated for each instrument every time a calibration is performed. The goodness of fit error is defined as the accuracy of the curve fit to the calibration data at the 95% confidence level. It is calculated using the standard deviation of the curve fit equation, from the 10 pairs of calibration data, and multiplying by the t-distribution at the respective degrees of freedom. Degrees of freedom represent the number of points in the data set minus the number of parameters estimated using that data set.

$$curvefit_{error} = \sqrt{\frac{\sum (y_{real} - y_{curvefit})^2}{\nu}} * t_{\nu,95} \quad C.1$$

$\nu = n - p + 1$

n number of data points summed
 p order of the fit equation

C.1.3.2 Truncation and Rounding Errors

Truncation and rounding errors are dependent on the resolution of the RTI board, the smallest increments it is capable of reading. WVU uses 12 bit resolution RTI boards with an input voltage range from 0-10V. Due to a finite resolution, “quantization” error is introduced since the actual analog voltage will lie somewhere in between the available bit levels. An estimate of quantization uncertainty is given by the following equation [Beckwith et al., 1982]:

$$quantization_{error} = \frac{\Delta V_{fs}}{(2)2^n} (95\%) \quad C.2$$

ΔV_{fs} the full scale input voltage range
 n number of bits used in the RTI board

WVU uses only 11 bits for data processing and an input voltage range of 10V, the quantization error for this system is then, $\pm 2.45\text{mV}$. For example, the quantization uncertainty of temperature measurements in the range of 0 to 600 °C then gives an uncertainty due to quantization of ± 0.2 °C.

Another type of error introduced in data storage is conversion error due to slight nonlinearity of the RTI boards. This nonlinearity error is listed in the manufacturer manual as $\pm \frac{1}{2}$ LSB. The LSB for the systems at WVU is $\frac{1}{2}$ a bit, therefore the nonlinearity uncertainty is ($\pm \frac{1}{4}$ bit * 4.90mV/bit) or $\pm 1.22\text{mV}$. For the temperature example, this corresponds to an uncertainty of ± 0.066 °C.

Using the RSS method to combine these two error sources gives an uncertainty due to truncation and rounding of ± 0.21 °C for the temperature example. The error contribution is typically very small and therefore is neglected in this uncertainty analysis with minimal effect on the reported results.

C.1.4 Uncertainty Calculation Example

In the reduction programs at the dynamometer laboratories, the recorded concentrations, in ppm are first converted to grams. This value is then divided by the total power produced by the engine or distance traveled by the vehicle to give the final results. To convert ppm concentration to grams, **Equation C.3** is used, with HC as the representative gas [CFR, 86.1342-90, 1996]. **Equation C.4** is the error calculation for HC_{mass} .

$$HC_{mass} = HC_{ppm} * V_{mix} * \rho_{HC} * 0.000001 - HC_{back} * \left(1 - \frac{1}{DF}\right) * V_{mix} * \rho_{HC} * 0.00001 \quad \text{C.3}$$

$$\Delta HC_{mass} = \sqrt{\left(\frac{\partial HC_{mass}}{\partial HC_{ppm}} * \Delta HC_{ppm}\right)^2 + \left(\frac{\partial HC_{mass}}{\partial V_{mix}} * \Delta V_{mix}\right)^2 + \left(\frac{\partial HC_{mass}}{\partial HC_{back}} * \Delta HC_{back}\right)^2 + \left(\frac{\partial HC_{mass}}{\partial DF} * \Delta DF\right)^2} \quad \text{C.4}$$

ΔHC_{mass}	the error associated with HC_{mass} in grams
HC_{ppm}	the continuous HC in ppm
ΔHC_{ppm}	the error associated with HC_{ppm} in ppm
V_{mix}	the volumetric flow rate through primary dilution tunnel (scfm)
ΔV_{mix}	the error associated with V_{mix} in scfm
ρ_{HC}	the density of HC kg/m ³
HC_{back}	the background bag concentration of HC in ppm
ΔHC_{back}	the error associated with HC_{back} in ppm
DF	the dilution factor
ΔDF	the error associated with DF

HC_{ppm} and HC_{back} are values read from the results and their uncertainties, ΔHC_{ppm} and ΔHC_{back} are calculated in the uncertainty reduction program and are the same since they are evaluated using the same analyzer. The density, ρ_{HC} , is a constant, and is considered to have no contribution to the resulting uncertainty. The technique used to calculate V_{mix} and ΔV_{mix} were addressed in section 6.3.3 of this thesis. **Equations C.5** and **C.6** were used to calculate the dilution factor (DF) and its uncertainty (ΔDF). **Equation C.5** is prescribed in the CFR [86.1342-90, 1996] but is valid for petroleum based fuels only and although it is used, is not an accurate representation for diesel fuels.

$$DF = \frac{13.4}{(CO_{2,ppm} + CO_{ppm} + HC_{ppm}) * .001} \quad \text{C.5}$$

$$\Delta DF = \sqrt{\left(\frac{\partial DF}{\partial CO_{2,ppm}} * \Delta CO_{2,ppm}\right)^2 + \left(\frac{\partial DF}{\partial CO_{ppm}} * \Delta CO_{ppm}\right)^2 + \left(\frac{\partial DF}{\partial HC_{ppm}} * \Delta HC_{ppm}\right)^2} \quad \text{C.6}$$

Considering all variables and their uncertainties, and using the methodology described in section 6, the uncertainty reduction program produced the results shown in **Table C.5**.

7stock	Units	Value	uncertainty	Analyzer error	calibration error	Curvefit error
dilution factor	ppm-l	14.240	1.675			
Vmix	scfm	31,466.000	157.330			
Energy	ahp-hr	19.580	1.566			
HC	ppm	21.140	2.725	2.111	1.706	.245
HC background	ppm	8.180	2.725	2.111	1.706	.245
HC mass	grams	6.934	1.905			
HC results	g/ahp-hr	.354	0.101			
CO	ppm	26.230	18.722	14.114	11.411	4.594
CO background	ppm	3.740	18.722	14.114	11.411	4.594
CO mass	grams	23.609	26.506			
CO results	g/ahp-hr	1.206	1.357			
CO ₂	ppm	9,362.850	1095.677	846.000	684.000	130.136
CO ₂ background	ppm	824.540	1095.677	846.000	684.000	130.136
CO ₂ mass	grams	14,015.620	2438.598			
CO ₂ results	g/ahp-hr	715.813	137.080			
NO _x	ppm	83.300	18.381	14.227	11.502	1.774
NO _x background	ppm	3.590	18.381	14.227	11.502	1.774
NO _x mass	grams	136.279	42.753			
NO _x results	g/ahp-hr	6.960	2.253			

Table C.5 Example Calculation of Uncertainty

An explanation of **Table C.5** follows. This is the data for a chassis test, named *7stock* in the reduction program, run on the Cummins N-14 engine operated in 7th gear, stock operation, with a dual axle configuration. The name column lists the name of the variable being described. The first variables dilution factor, volumetric flowrate, and axle horsepower-hour are the values obtained for the entire test and used in calculation of each of the four gases results. For the four gases, HC, CO, CO₂, and NO_x, each have four values represented: (1) the value for overall concentration of gas contained in the exhaust, in ppm, (2) the overall value, in ppm, of gas contained in the background sample, (3) the calculated values of mass, in grams and (4) the calculated results, in g/ahp-hr. The value column is the value obtained in engineering units, read from the test results file, calculated in the case of mass and g/ahp-hr values. The uncertainty column gives the derived uncertainty contribution for each variable of this test in engineering units of the associated variable. The last three columns are present only for the gas concentration and background bag concentration, both in ppm. These columns represent the uncertainty contributions, in ppm, to the overall listed uncertainty for the exhaust and background samples from analyzer error, calibration error and curve fit error, respectively. For the uncertainty reduction program, the values in the last three columns were combined to give one representative value, **Equation C.7**. Note that due to the conservative nature of the uncertainty analysis that the uncertainty of the background values for all gases, excluding HC, is greater than the background reading itself. Experience with the laboratories assures us that these are not inaccurate measurements, they are just in the lower end of the calibration range of our instruments.

$$\Delta HC_{ppm} = \sqrt{\text{analyzererror}^2 + \text{calibrationerror}^2 + \text{curvefiterror}^2} \quad \text{C.7}$$

The importance of each of these uncertainty values in the final results is accounted for by the weighting principles of the RSS method.

C.2 Particulate Matter Error

The method of collecting particulate matter in the exhaust from a vehicle was outlined in section 4, Laboratory Description, and follows the strict guidelines outlined in the CFR [86.1339-90, 1996]. Briefly, climatized, pre-weighed primary and secondary filters collect PM from an exhaust sample, drawn through the secondary dilution tunnel by a mass flow controller. After a test run, these filters are placed in covered petri dishes (to prevent dust contamination) but unsealed (to promote humidity exchange), are climatized to 70 °F and 50% relative humidity in the environmental chamber for at least 8 hours then weighed again. The pre-weights are subtracted from the post-weights to give the amount of particulate matter in grams (P_e). The following formula is used to calculate the volumetrically corrected particulate matter mass (PM_{mass}) [CFR, 86.1343-88, 1996].

$$PM_{mass} = (V_{mix} + V_{sam}) * \left[\frac{P_e}{V_{sam}} - \left(\frac{P_{back}}{V_{back}} * \left[1 - \frac{1}{DF} \right] \right) \right] \quad \text{C.8}$$

$$V_{sam} = V_{vf} - V_{pf} \quad \text{C.9}$$

V_{sam}	Volume of sample exhaust removed from primary dilution tunnel
V_{vf}	Actual Volume of secondary sample which passes PM filters
V_{pf}	Actual volume of dilution air added to the secondary tunnel
P_e	Particulate mass in grams from gravimetric analysis on test filters
P_{back}	Net weight of Particulate in grams on background filters
V_{back}	Volume of background flow across background filters

Errors in the particulate matter measurements are primarily from the calibration and reading of the microbalance and mass flow controller, although climatization may also introduce some error. However, the filters are carefully equilibrated to the same temperature and relative humidity before and after testing. Also, the CFR [86.1312-88, 1996] requires that two unused reference filters remain in the environmental chamber at all times and that they are weighed within four hours of the sample filters. Should the weight of the reference filters change by ± 5 percent or more between sample filter weighings, then the sample filters should be thrown out and the emissions tests repeated. These precautions assure that climatization would not be an issue in particulate matter measurements.

Gautam et al. [1996] investigated the uncertainty associated with PM measurements at the transportable laboratory and found the uncertainty in PM_{mass} to be just less than $\pm 2\%$. Therefore, an uncertainty of $\pm 2\%$ was assigned to PM_{mass} results obtained by the WVU laboratories for this thesis.

C.3 Power or Energy Error

The emissions gathered at the stationary laboratory are reported in grams per brake horsepower hour (g/bhp-hr). This value is arrived at by dividing the total mass, in grams, of a selected gas produced by the engine during a test cycle by the amount of energy, in brake horsepower hour which is the brake horsepower integrated over time, that the engine created during the test cycle. Brake horsepower is the power produced by the engine and can be directly measured when performing engine tests. This value cannot be directly measured during chassis testing, since torque is measured at the rear axle. For this project, chassis dynamometer data is reported in grams/axle horsepower-hour as opposed to the traditional grams/cycle or grams/mile. Brake horsepower hour is calculated along CFR guidelines in the WVU Stationary Laboratory reduction program using the following equation:

$$bhp - hr = (torque + acceleration * (coef)) * rpm * \frac{2\pi}{550 * 60} \quad C.9$$

torque the torque measure at the engine output shaft
acceleration differentiation of the velocity signal
coef reported inertia of the dynamometer
rpm the engine output shaft speed

Due to the nature of an acceleration in that it must be conserved throughout the cycle, any uncertainties in acceleration and it's torque conversion coefficient may be neglected.

Therefore, the equation that determines the error in this calculation using RSS is then:

$$\Delta bhp - hr = \sqrt{\left(\frac{\partial bhp - hr}{\partial torque} * \Delta torque\right)^2 + \left(\frac{\partial bhp - hr}{\partial rpm} * \Delta rpm\right)^2} \quad C.10$$

$\Delta torque$ the error associated with torque measurements
 Δrpm the error associated with speed measurements

At the stationary laboratory, the engine speed is measured using an AN Digital Tachometer, model GEH-5358, that was factory installed in the GE Dynamometer. Since the tachometer is digital, it is highly accurate and therefore there is no error contribution due to the instrument itself, all of the uncertainty associated with the speed measurement is attributed to calibration, signal conditioning and storage. Torque at the stationary laboratory is measured with a Lebow Tension and Compression Load Cell, model 3132. Force applied to the load cell is translated to an electrical signal by means of changes in electrical resistance of strain gages in a Wheatstone bridge configuration bonded to the interior of the load cell. This strain gage lists a repeatability of 0.05% of full scale. Using the average torque and speed produced during the test, and the RSS method to define the uncertainty in the torque and speed measurements, the average uncertainty in bhp-hr was found to be approximately 3% for tests run on the stationary laboratory. The value varies of course, from test to test, the calculated value for each test is used in the analysis.

Mobile Laboratory #1 uses Lebow Strain Gage Shaft Torque Sensors, model 1241, to measure hub torque on both sides of the dynamometer. These torque sensors were calibrated by Eaton to a rated capacity of 200,000 in-lb_f (16,667 ft-lb_f), this gave a very high error when considering full scale uncertainty since the average torque values produced by the vehicles would be as much as 90% lower. In order to give an accurate value of torque uncertainty, the torque sensors were observed when the vehicle was resting on the test bed, no wheels were turning. The reading should be 0 ft-lb_f, therefore any deviation from this point could be considered hysteresis, or a bias uncertainty in the lower range of torque. The maximum deviations observed by mobile laboratory operators were ± 20 ft-lb_f. This value was used as the error in torque measurements at Mobile Laboratory #1. The uncertainty in torque, $\pm 8\%$, is much greater than the uncertainty in measured rpm, $\pm 0.05\%$ and is the predominant source of error in the energy, axle horsepower hour.

C.4 Final Analysis

The emissions are reported in g/bhp-hr or g/ahp-hr, depending on the laboratory; the total grams produced are divided by the amount of energy produced. A corresponding uncertainty range was calculated and assigned to the emissions produced by the mobile and stationary laboratories. **Figures C.1 to C.4** show sample results, one for each test scenario, in bar graph form for the four gases, CO, CO₂, HC and NO_x, taken at Mobile Laboratory #1. Also shown are the average concentration and the uncertainty associated with them for each engine. **Table C.6** explains the test scenario for these graphs.

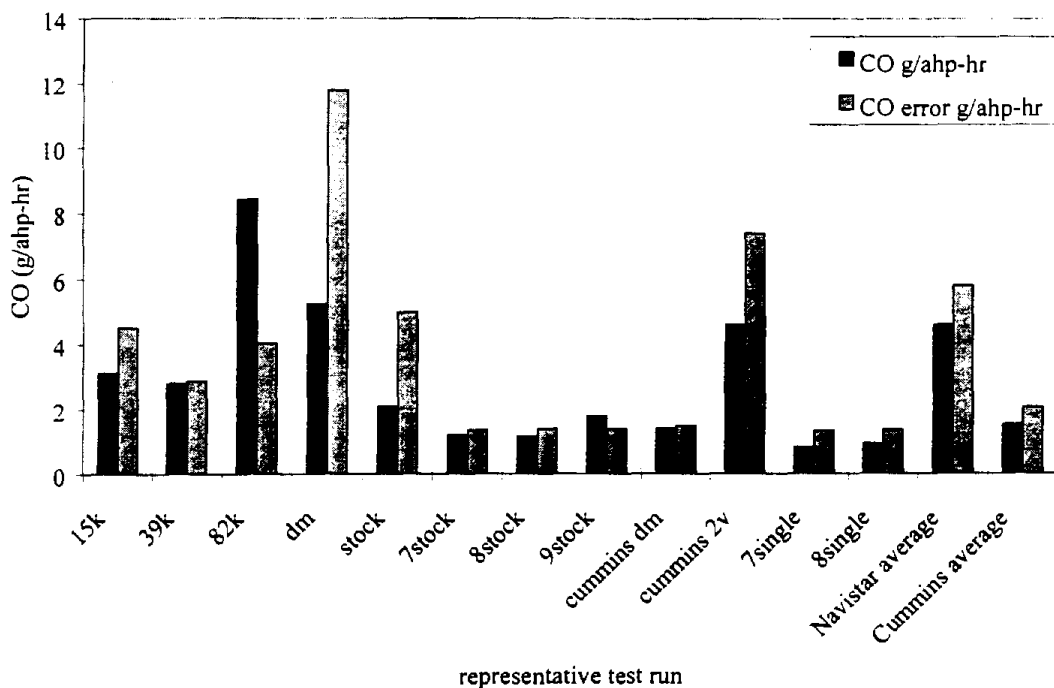


Figure C.1 CO Emissions and Uncertainties for Transportable Laboratory #1

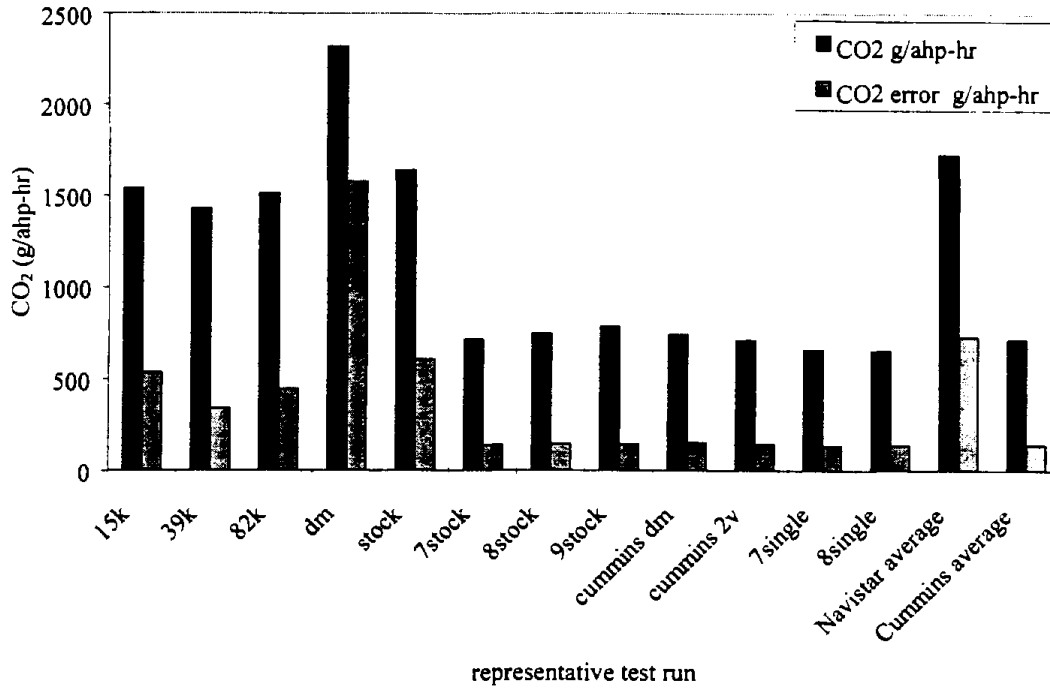


Figure C.2 CO₂ Emissions and Uncertainties for Transportable Laboratory #1

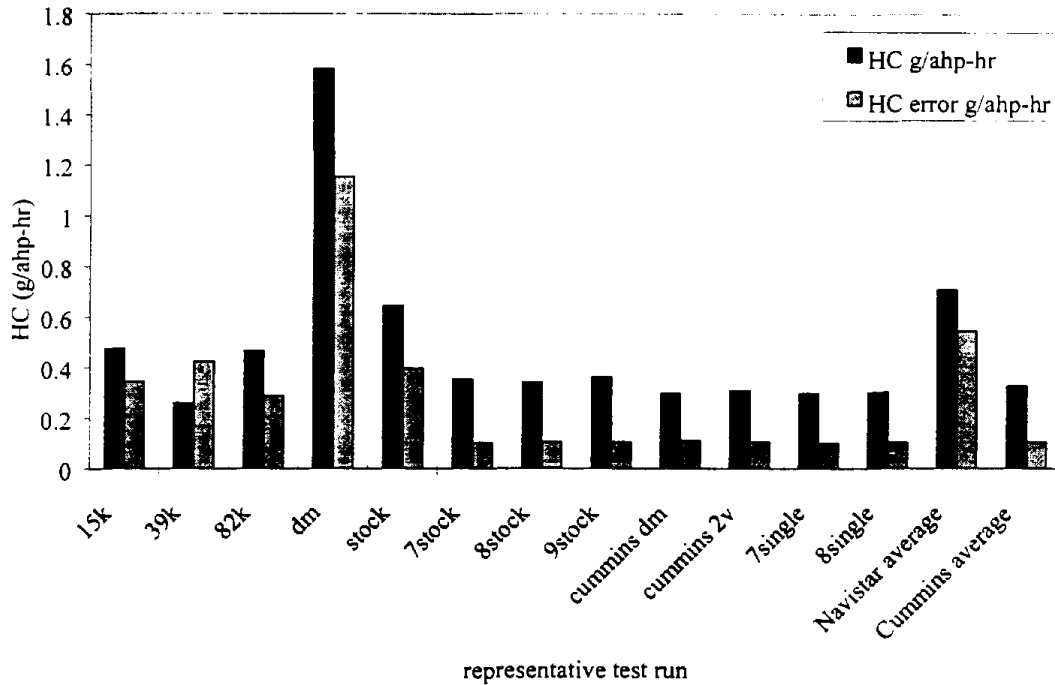


Figure C.3 HC Emissions and Uncertainties for Transportable Laboratory #1

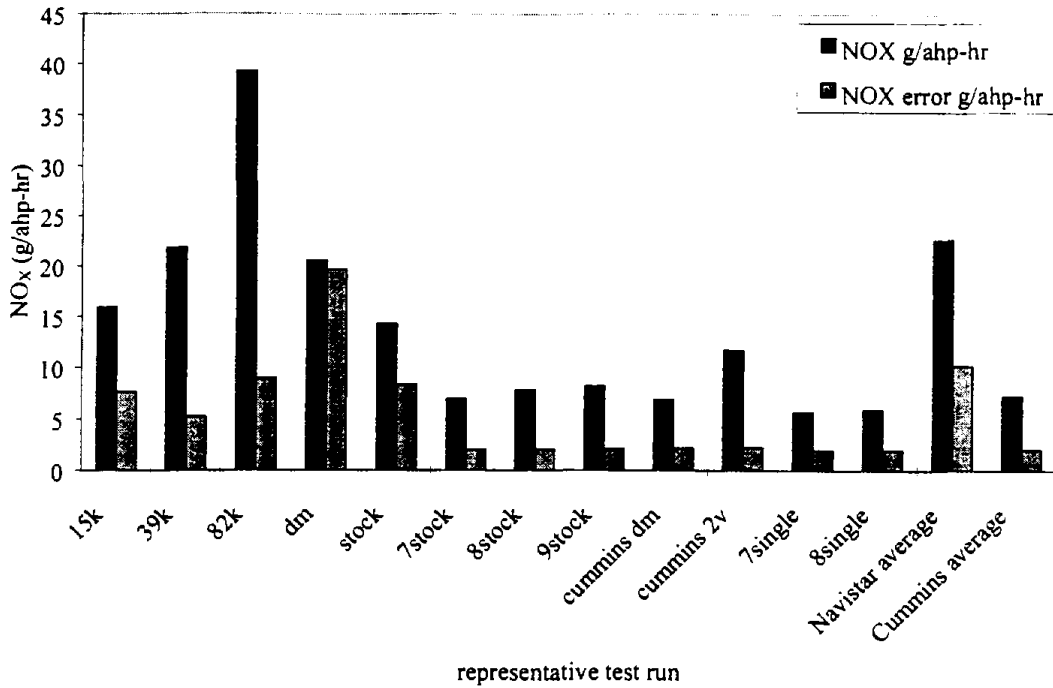


Figure C.4 NO_x Emissions and Uncertainties for Transportable Laboratory #1

Test Name & # of tests	Engine / Chassis	Chassis and Engine Configurations
15k--(3)	Navistar T 444E/ Navistar 4700 Single-axle trailer	Temperature Sensors Replaced with 15kΩ Resistors
39k--(4)		Temperature Sensors Replaced with 39kΩ Resistors
82k--(4)		Temperature Sensors Replaced with 82kΩ Resistors
Dm--(4)		Disconnected Manifold Air Pressure (MAP) Sensor
Stock--(4)		Stock engine
Alt. Stock--(4)		Engine control module replaced with truck's
7stock--(6)	Cummins N-14 / International Cabover Class 8	7 th gear, stock, dual axle
8stock-- (11)		8 th gear, stock, dual axle
9stock--(4)		9 th gear, stock, dual axle
Cummins dm--(4)	Dual-axle tractor	8 th gear, disconnected MAP, dual axle
Cummins 2v--(4)		8 th gear, MAP replaced with 2Volt signal, dual axle
7single--(4)		7 th gear, stock, single axle
8single--(3)		8 th gear, stock, single axle

Table C.6 Definition of Test Scenarios for Chassis Tests

Likewise, **Figures C.5 to C.8** show similar results for the stationary laboratory. For each of these eight figures, the darker, larger bars represent the reported results in g/bhp-hr, and the lighter, smaller bars, the error associated with each in g/bhp-hr. **Table C.7** gives the description of test scenarios.

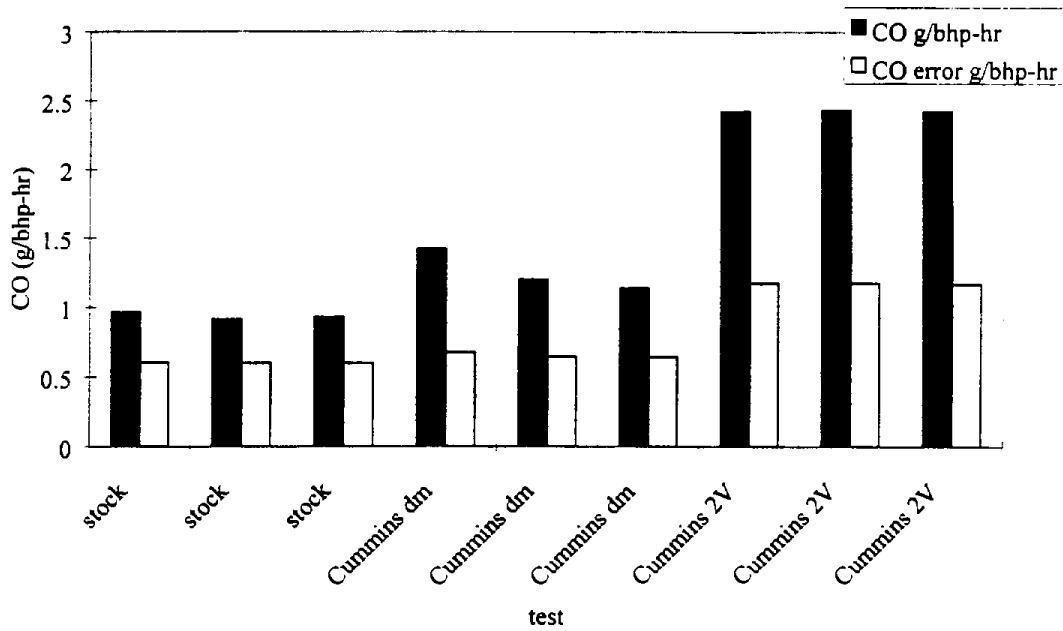


Figure C.5 CO Emissions and Uncertainties for Stationary Laboratory

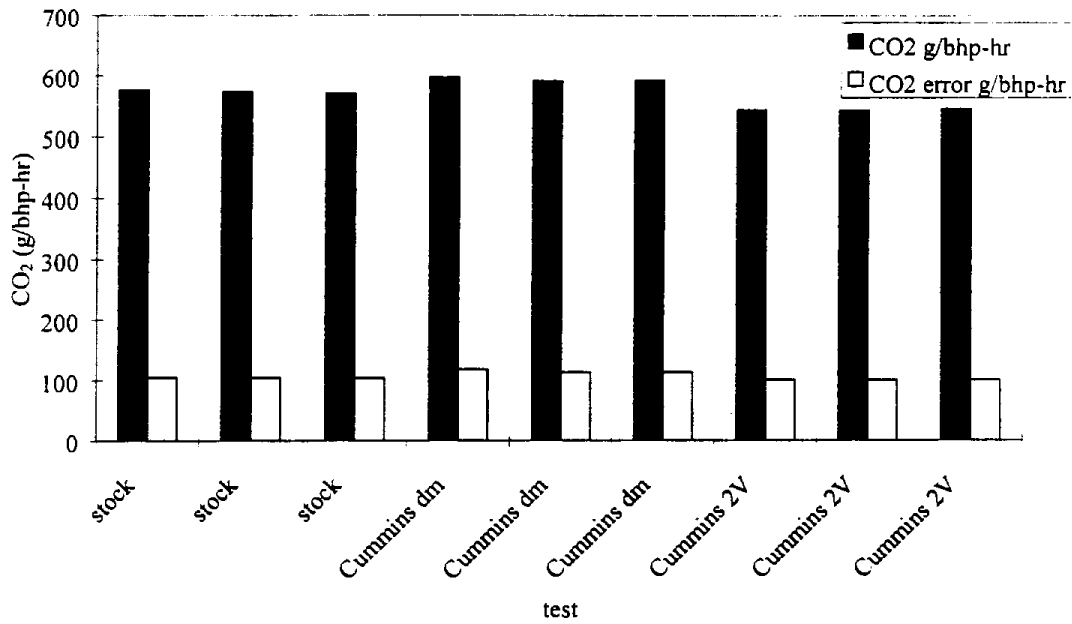


Figure C.6 CO₂ Emissions and Uncertainties for Stationary Laboratory

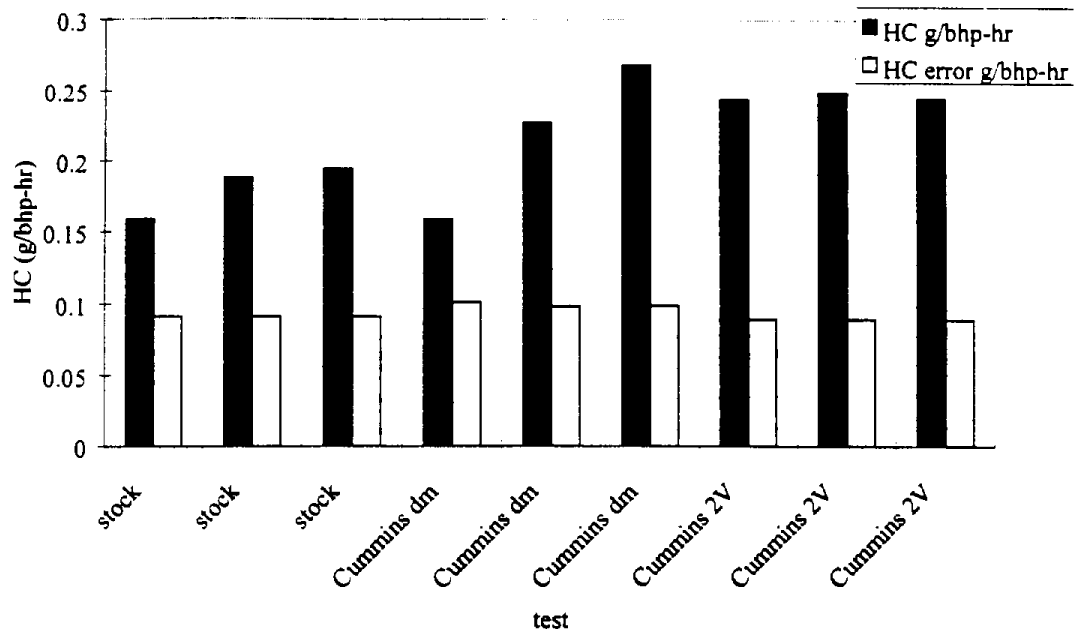


Figure C.7 HC Emissions and Uncertainties for Stationary Laboratory

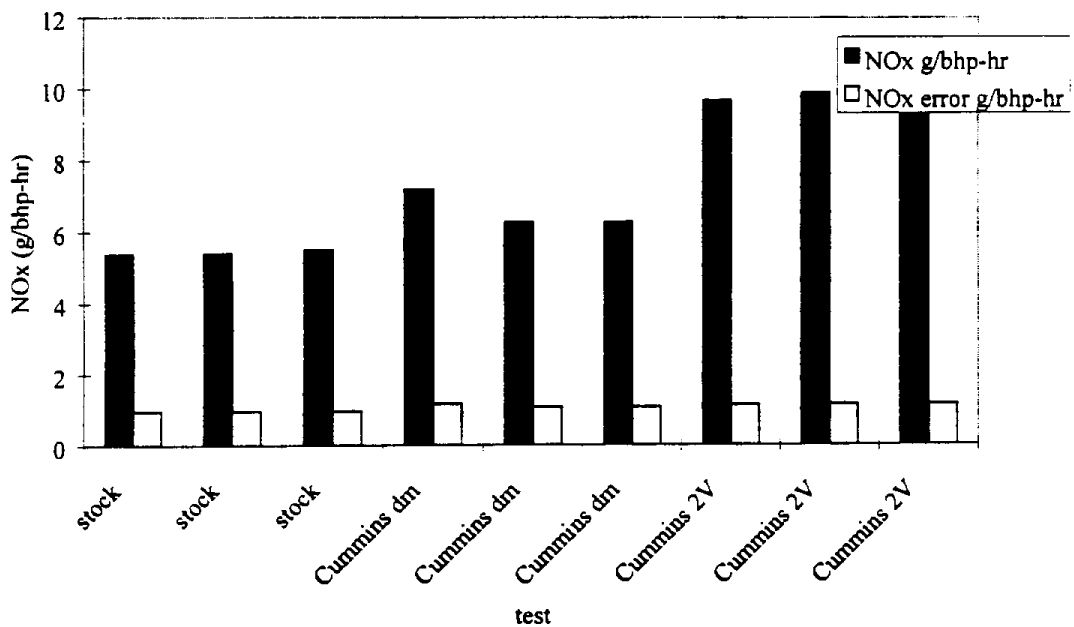


Figure C.8 NO_x Emissions and Uncertainties for Stationary Laboratory

Test Name and # of tests	Engine	Configuration
Stock	Cummins N-14	Stock operation
Cummins dm		Disconnected MAP
Cummins 2V		MAP replaced with 2Volt signal

Table C.7 Engine test configurations

The reported uncertainty for each test was then depicted as a percentage and an average percentage error was generated for each laboratory for each of the gases analyzed. The average percentage errors are shown in **Table C.8**.

<i>Average Theoretical Uncertainty ±%</i>		
Gas	Mobile Laboratory #1	Stationary Laboratory
CO	133.59	54.91
CO ₂	26.58	18.67
NO _x	51.05	15.39
HC	36.52	44.95

Table C.8 Theoretical Uncertainty Percentages

In order to quantify the uncertainties encountered by the laboratories, coefficients of variance (CV%) for the stationary and mobile #1 laboratories were calculated using the emissions database at WVU. CV% compares the run to run variation in tests run sequentially on the same vehicle and averages them to develop a representative CV% for each facility. The representative values can be seen in **Table C.9**. This CV% represents 67% of the uncertainty for each engine and vehicle being tested as well as laboratory variations between consecutive tests, in reported data. Therefore, it is realized that the CV% values listed in **Table C.9** include engine and vehicle variations between tests as well as laboratory variations. The CV% values are not solely representing the laboratory, they also include variations in the engine and vehicle and in no way represent bias errors that may occur due to poor testing practices.

<i>Average Laboratory Variation CV%</i>		
Gas	Mobile Laboratory #1	Stationary Laboratory
CO	4.69	3.98
CO ₂	0.81	0.63
NO _x	2.15	1.78
HC	4.18	10.36

Table C.9 Laboratory Variations Represented by CV%

C.5 Uncertainty Results and Discussion

The values of theoretical uncertainty given in **Table C.8** are high, ranging 134% to 15%. This can be explained by the extremely conservative method used to determine the theoretical uncertainties. The method requires that errors be defined as % of full scale for the analyzers and other measurement devices. Transients are a major concern of testing, these transients requires that the analyzers be calibrated to much greater values than the final integrated values that

represent the tests. Experience has shown that the laboratories at WVU are not in error, as the numbers suggest. Considering that both of the laboratories use the same techniques, instruments and formulas to obtain exhaust emissions results, the values in **Table C.8** should be similar for both laboratories. The variation in torque calculation, approximately $\pm 2\%$ uncertainty for the engine laboratory and $\pm 8\%$ for the chassis laboratory, and greater error contribution due to % of full scale calibration gases causes the mobile laboratory to have a significantly higher theoretical uncertainty. Some of this discrepancy can be explained by the curve fit uncertainty since that value is the one that is unique between facilities. **Figure C.9** shows the scatter that occurs when using the data from the CO analyzer calibration files at Mobile Laboratory #1, **Figure C.10** shows the same plot for the stationary laboratory.

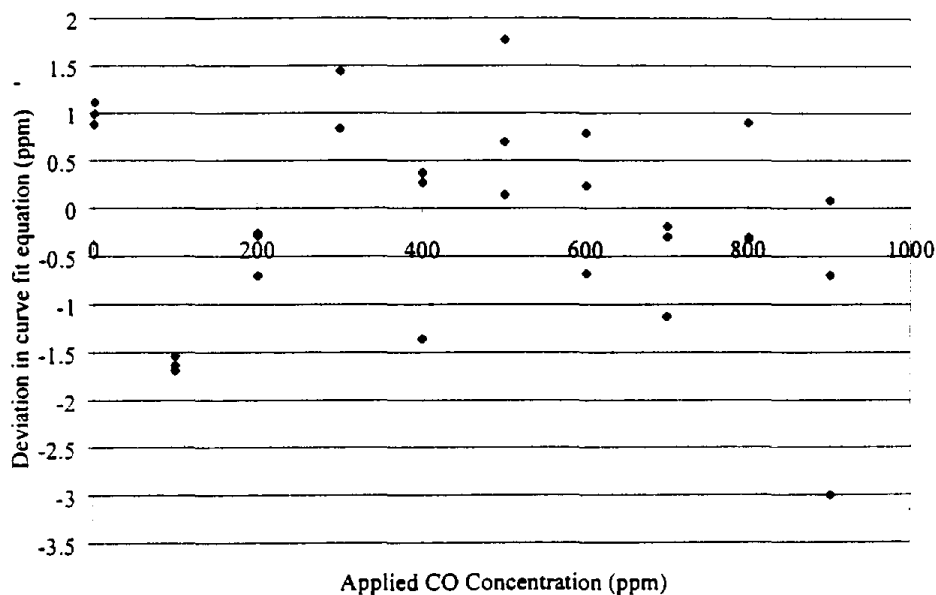


Figure C.9 Scatter in curve fit calibration equation for CO at Transportable Laboratory #1

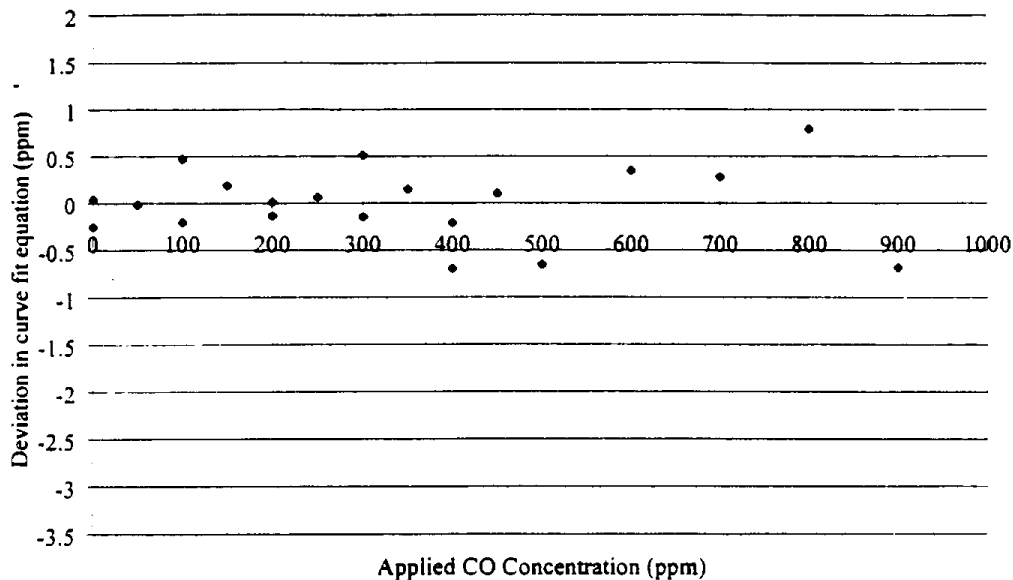


Figure C.10 Scatter in curve fit calibration equation for CO at the Stationary Laboratory

Each of these plots represents the calibration curve data derived from calibration of the CO analyzers and is plotted using the same axis scale. A calibration gas of concentration 1001 ppm was used for Mobile Laboratory #1, whereas the stationary laboratory used a calibration gas of 900 ppm. The horizontal zero line represents where the true values would lie, the scatter represents how far off, in ppm, the values obtained using the curve fit equation are. As can be seen in these plots, the scatter for Mobile Laboratory #1 is much greater than that of the Stationary Laboratory, with a maximum value of 3 ppm away from the true value for the Mobile Laboratory and only 0.81 ppm askew for the stationary facility. This discrepancy will give a much greater standard deviation between the curve fit value and the true value, therefore contributing to a curve fit error and overall uncertainty of greater proportion for Mobile Laboratory CO values. The same sort of discrepancy is observed for the NO_x curve fit equation, with Mobile Laboratory #1 having a maximum scatter of 3.8 ppm for an overall concentration of 1012 ppm and the stationary laboratory with a maximum of only 0.48 ppm in a concentration of 447.3 ppm.

One possible explanation for the large curve fit discrepancy between facilities could be that the mobile laboratory is subject to greater vibration and noise since the instruments are mounted in a movable trailer as opposed to the solid block foundation of the engine test laboratory.

The real concern here is that the prescribed method of error analysis is so conservative that unrealistic values of uncertainty are reported. The analyzers list uncertainty as \pm percentage of full scale, and due to the nature of transients and the restrictions listed in the CFR, the facilities are required to calibrate the analyzers using gas concentrations over 50% greater than the values obtained from integrating the results over the entire test. WVU has been testing engines and

vehicles for years. Their results are comparative with other similar engine and chassis test facilities when using the same engines and vehicles. Experience, as well as common sense tell us that the theoretical uncertainty values listed in this thesis are unrealistic and are not truly representative of the facilities at WVU.

Appendix D - Drivetrain and Transmission Efficiency

The issue of transmission and driveline efficiency is central to this study, since it is the link between testing on an engine dynamometer and the chassis dynamometer. Literature searches have revealed that little quantitative knowledge exists to describe energy losses in a transmission, although the inertias of internal transmission components are well documented by manufacturers. Information which does exist is anecdotal, but usually ascribes a value of between 80 and 90% to the efficiency of power transmission between the flywheel and the drivewheels. Conversation with Robert G. Joyner of Spicer Driveshaft Division [1997], suggested that the majority of the losses, approximately 10%, occur in the transmission due to the amount of heat generated there. Joyner stated that experiments using dynamometers at Spicer revealed loss of less than 1% in rear differentials. In speaking with Chad Hatch of the Volvo Driveline Division [1997], Hatch revealed that for their analysis, Volvo assumes a 10% loss in the transmission and a 5% loss in the rear differential. Therefore, the assumption of 80 to 90% efficiency of power transference from the engine to the rear tires may be accepted as accurate.

In considering total driveline efficiency one must acknowledge losses in:

- (a) the transmission.
- (b) the driveshaft universal joints and, where fitted, center bearing.
- (c) the final drive units, customarily consisting of a power divider and two rear axle assemblies on a tandem vehicle and one axle assembly on a single axle vehicle. This includes losses in the wheel bearings.
- (d) the tires.

D.1 Tire Losses

Tire losses were addressed empirically in the following fashion, but it is acknowledged that this information, separately, cannot be used directly in an efficiency model. The Navistar test vehicle was held down on the dynamometer rollers with varying downward loads. At each load, the torque required to start the tire turning was measured, in a fashion akin to assessing static friction between surfaces. A torque wrench was used for this purpose and the operator simply read the torque required from the wrench. Figure D.1 shows the data that arose. Scatter in the points arose from error in reading the torque, but may also be ascribed to any "out of roundness" of the tire or inhomogeneities in the structure of the tire as different points on the circumference were in contact with the rollers.

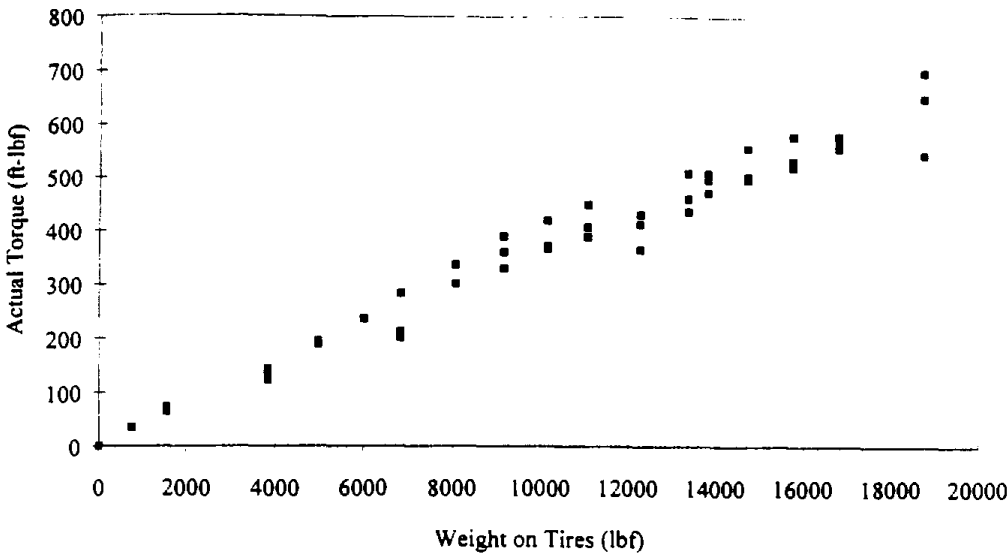


Figure D.2 Torque Required for Tire Turning at Varying Loads [Boyce, 1996]

It is evident that the curve in Figure D.1 is not linear, which is reasonable since tire deflection is not geometrically similar as load increases. Also, Figure D.1 takes no account of the effect of wheel speed on tire losses, nor can this be assessed without sophisticated instrumentation. It does, however, demonstrate that recommended tire loss formulae which assume that loss (as torque) is proportional to load (as does the Code of Federal Regulations) are at best an approximation.

D.2 Navistar Driveline Loss Analysis

In order to assess total driveline losses, the following plan was prepared and executed. The Navistar engine was a governed engine with the "throttle command" delivered to the engine as a voltage. In theory, it should be possible to set the engine to a reproducible setpoint by prescribing the throttle voltage and the engine speed precisely. In this program, throttle voltage was interpreted as computer counts, so that prescribed values of speed and computer counts should specify the engine operating condition, provided that parameters such as engine temperature were held constant. The objective was to hold the engine at the same set of conditions while it was (a) in the truck (on the chassis dynamometer) and (b) directly coupled to the engine dynamometer. A matrix of twelve speed and load (computer count) combinations was set up on the chassis dynamometer and the torque output to the chassis dynamometer was measured using torque cells at the vehicle hubs. However, it was found that flywheel torque values obtained when essentially the same speed and computer count combinations were used, were not coherent with the chassis data in any sense.

D.2.1 Navistar T 444E Governor Response

This incongruence was caused by the high response of the governor installed in the Navistar engine, a fabricated model of which is shown schematically in Figure D.2. The governor droop characteristic can be such that the slope of the operating curve (see Figure D.2) at the operating point (T_{set} , S_{set}) is so steep that very small variations in engine speed or throttle voltage (computer counts) can lead to significant deviations in produced torque. Figures D.3, D.4 and D.5 show three operating curves with three different fixed values of throttle voltage held on the engine. These figures were obtained using the Navistar engine on the engine dynamometer, and sweeping the speed slowly upward, at a rate of 8 rpm per second. The three maximum slopes found on the "crossover" portion of Figures D.3, D.4 and D.5 were 0.4095, 0.4064 and 0.4091 ft-lb_f/rpm respectively. In other words, for the throttle setpoint in Figure D.5, a deviation in speed of only 10 rpm could cause the torque to change by 4.091 ft-lb_f. With a governor this "tight", reproducing set conditions on the chassis and engine dynamometers is impossible without instrumentation beyond the scope of this program.

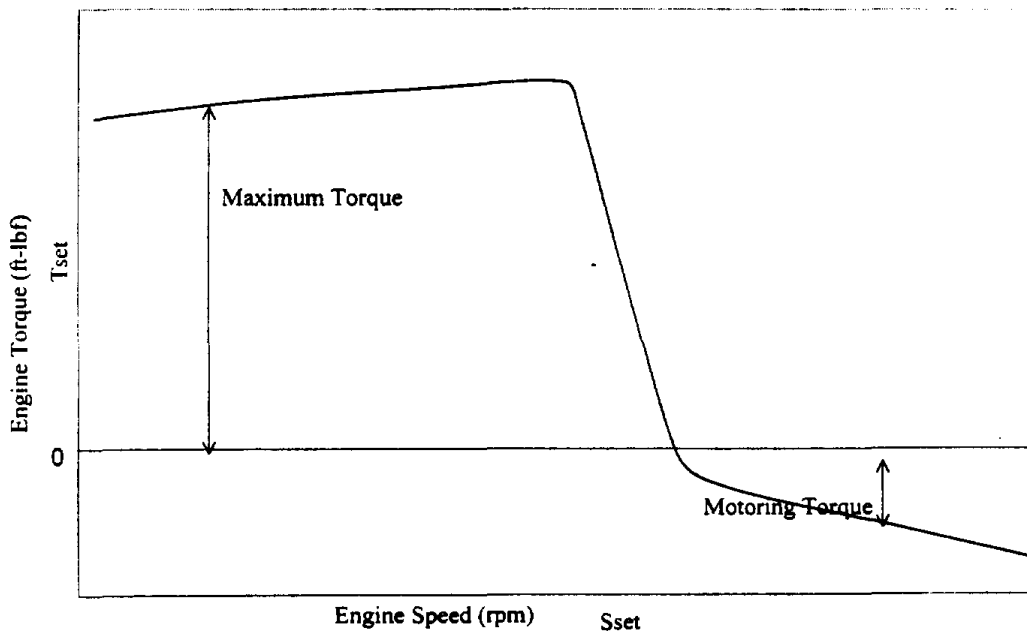


Figure D.3 Schematic of Governor Response

Response of engine torque to speed when throttle voltage is set to a torque T_{set} at a speed S_{set} . The slope of the operating curve at (T_{set} , S_{set}) is crucial.

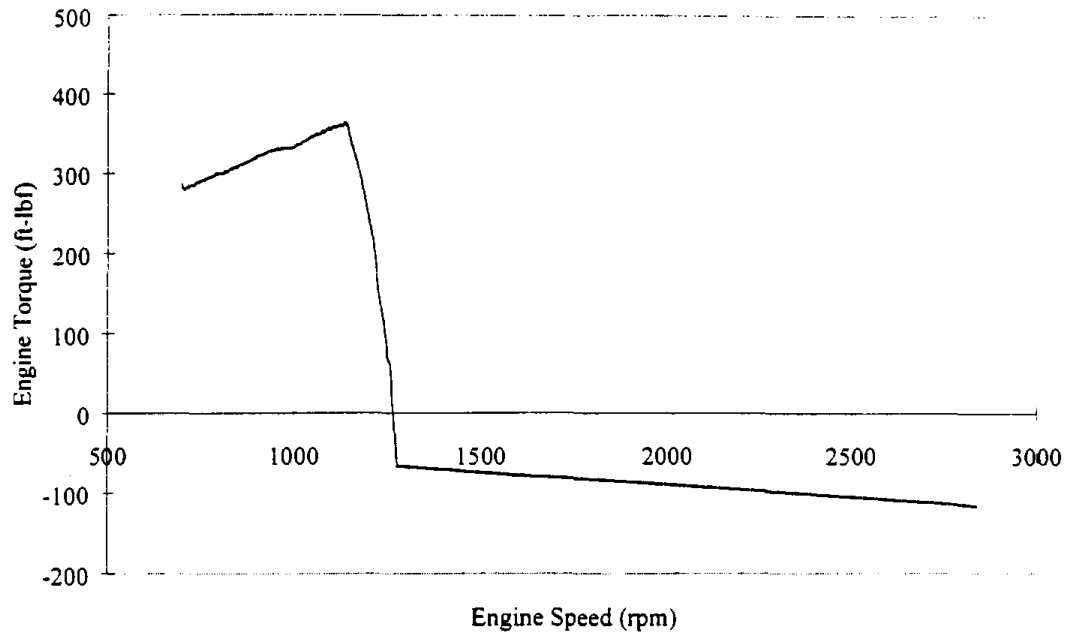


Figure D.4 Operating Curve for Navistar T 444E Engine at 25% Throttle Voltage, with sweep of increasing speed

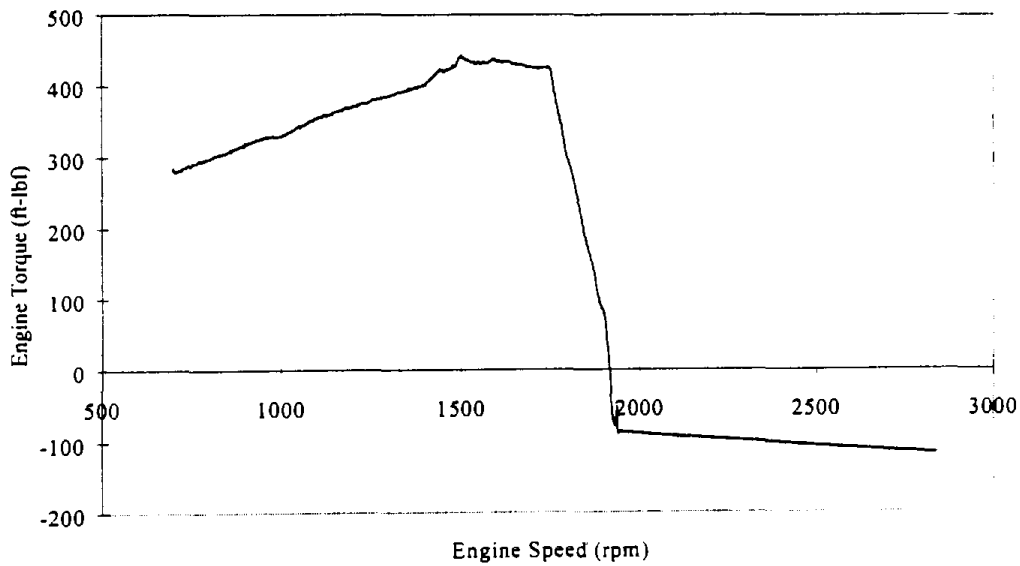


Figure D.5 Operating Curve for Navistar T 444E Engine at 50% Throttle Voltage, with sweep of increasing speed

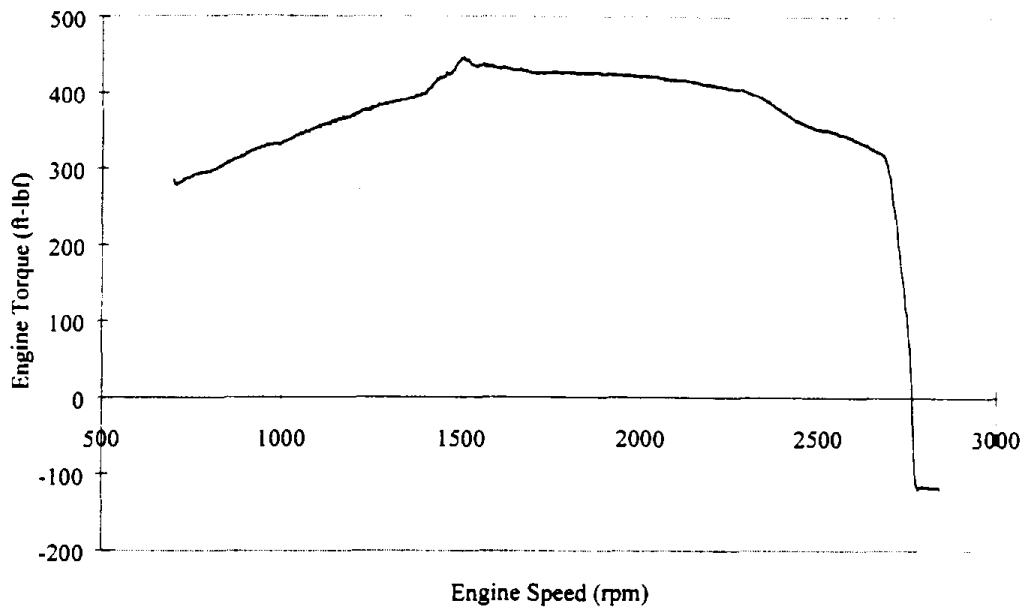


Figure D.6 Operating Curve for Navistar T 444E Engine at 75% Throttle Voltage, with sweep of increasing speed

D.2.2 Navistar Tampering

In order to obtain a full range of data, the Navistar engine was subjected to several tampering scenarios. First, the coolant, intake air and oil temperature sensors were removed from the engine and tested to determine their resistance to change in response to changes in temperature. The relationship between temperature and resistance for these sensors is shown in Figure D.6 and modeled by Equation D.1.

$$k\Omega = 7 \times 10^{-7} * T^4 - 0.0004 * T^3 + 0.0686 * T^2 - 6.1809 * T + 237.85 \quad \text{D.1}$$

$k\Omega$ Resistance in $k\Omega$
 T Temperature Sensor Reading in $^{\circ}\text{F}$

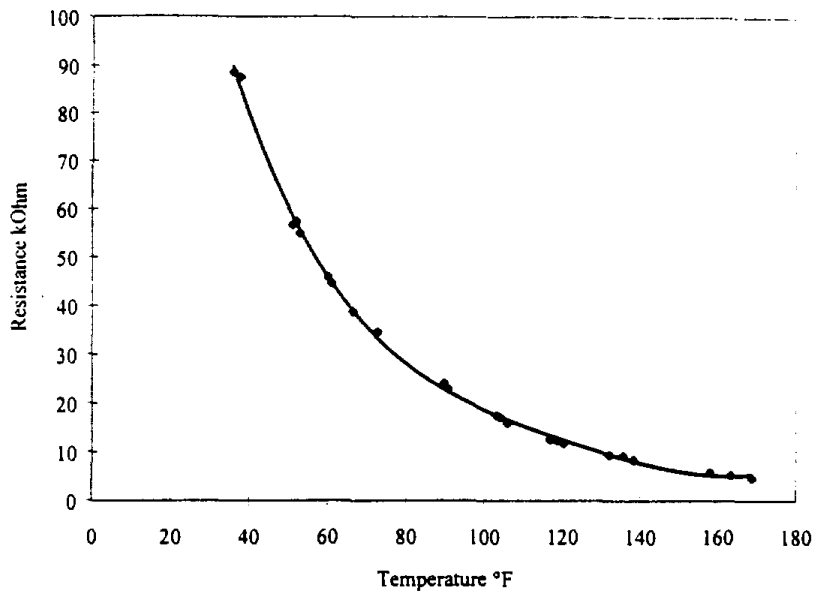


Figure D.6 Navistar T 444E Engine Temperature Sensors Resistance Plot

The Navistar engine was tested in three different temperature simulation modes of 110°F (15kΩ, 43°C), 66°F (39kΩ, 19°C) and 40°F (82kΩ, 4°C). It was expected that PM, CO and NO_x emissions as well as torque output would increase as engine temperature decreased. Also, the engine torque requirements would increase as temperature dipped. The MAP sensor was disconnected to give a scenario of decreased engine power output.

D.2.3 Navistar Engine and Chassis Test Comparisons

Fortunately, some reliable setpoint data could be obtained using “full throttle” operation on the engine and chassis dynamometers, because the throttle voltage is such that small changes in speed affect the torque little under these conditions for the Navistar engine. Also, since the engine had undergone a full tampering study, a range of full throttle engine maps was available, each with a unique torque curve. Figures D.7, D.8, D.9, D.10, and D.11 provide examples of the data available.

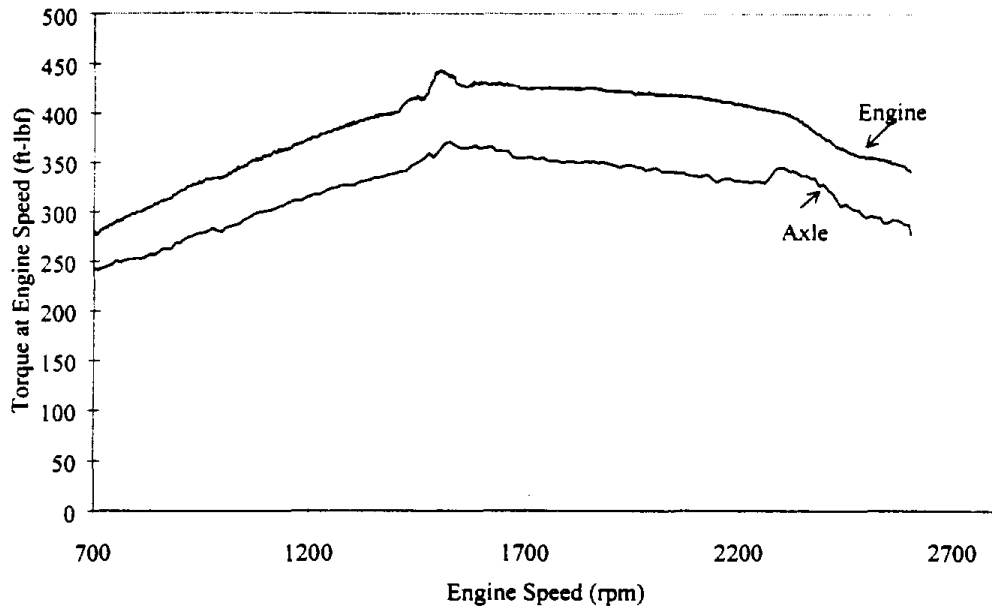


Figure D.7 Engine and Axle Torque for Stock Operation

Figure D.7 shows the engine map from the engine dynamometer for stock operation, and on the same set of axes is plotted the map for stock operation for the engine installed on the chassis dynamometer, with hub (i.e. axle) torques translated to reflect axle torque at engine speed. For this testing, performed in 4th gear, a ratio of 2.04:1, on a chassis with a rear end ratio of 4.11:1, the overall ratio of 8.38:1 (2.04×4.11) was used to translate the speed values. Figures D.8, D.9 and D.10 are similar plots for high torque tampering scenarios, temperature sensors replaced with 15, 39 and 82 k Ω resistors, respectively. Figure D.11 is a similar plot for the low torque tampering scenario, with the MAP sensor disconnected.

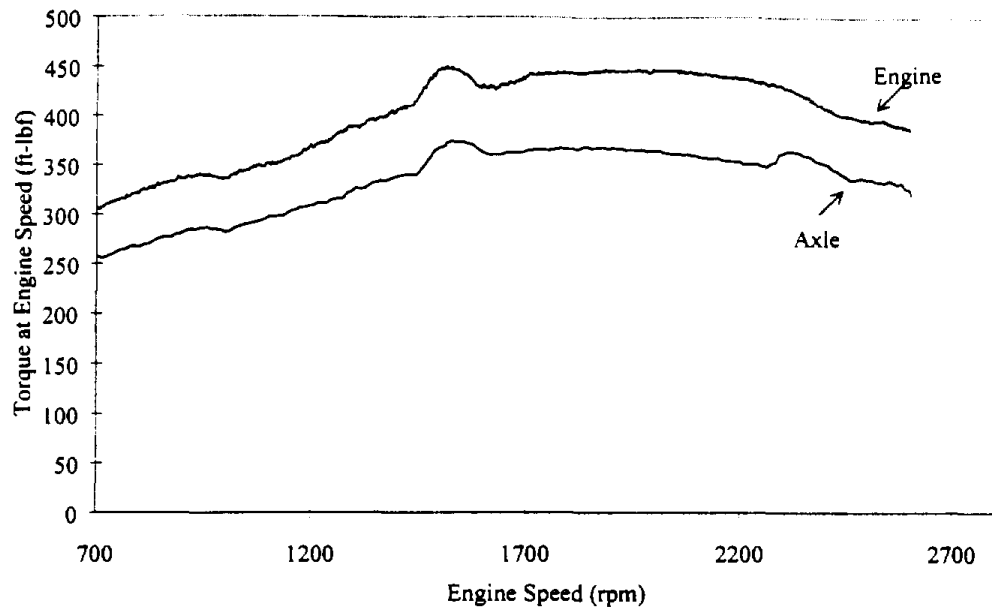


Figure D.8 Engine & Axle Torque for Temperature Sensors Replaced with 15kΩ Resistors

It should be noted, that the “axle torque” values depicted in Figures D.7 to D.11 have been altered slightly from the values taken at the West Virginia University Transportable Heavy-Duty Vehicle Emissions Testing Laboratory. The axle torque and axle speed was recorded separately for each side of the vehicle, at the rear hubs. The hub torques were then combined to represent a single torque. The combined axle torque at axle speed was then translated to axle torque at engine speed through the ratio in the driveline. Due to the nature of chassis testing and the inertia of the drivetrain system, the

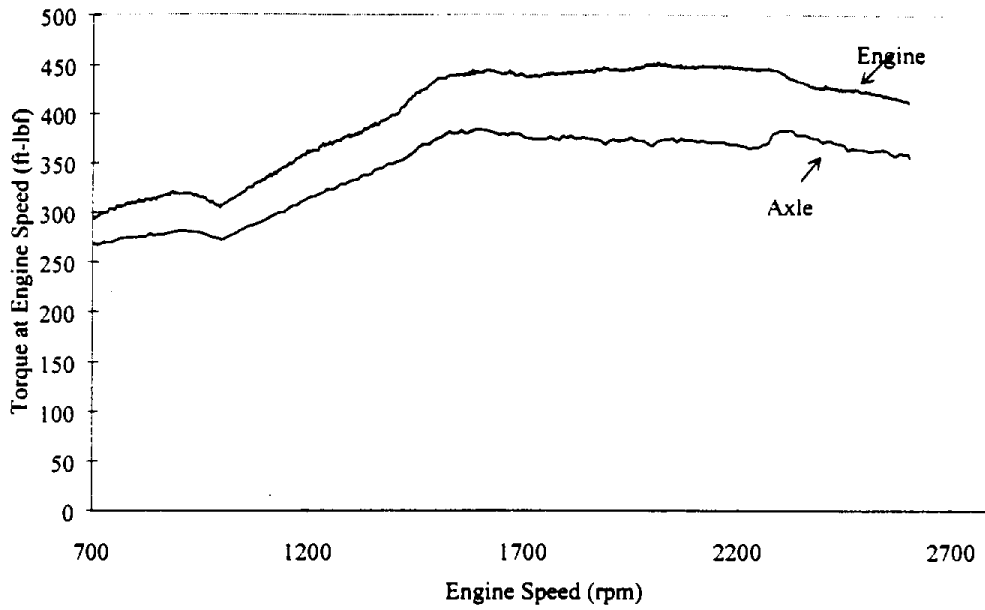


Figure D.9 Engine & Axle Torque for Temperature Sensors Replaced with 39kOhm Resistors

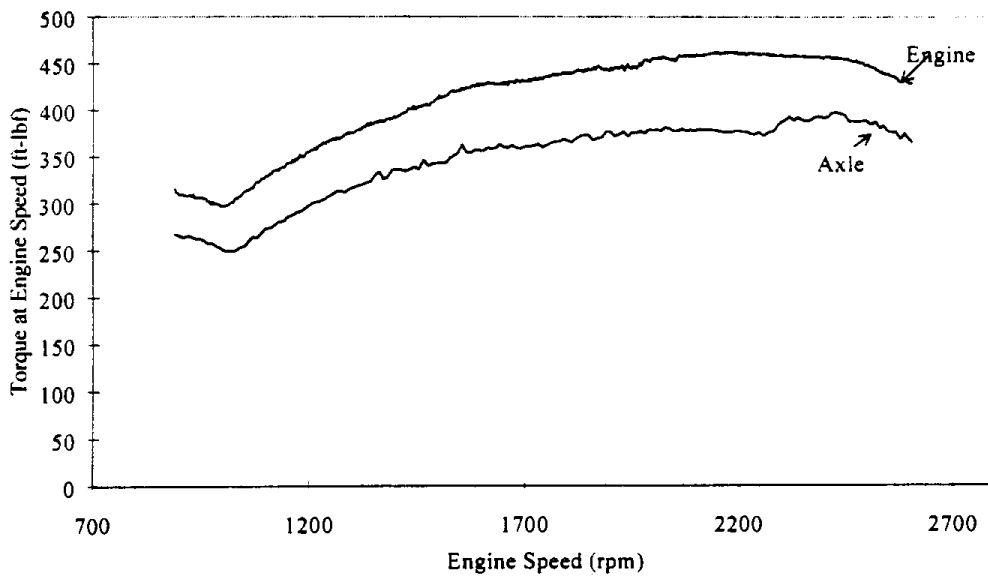


Figure D.10 Engine & Axle Torque for Temperature Sensors Replaced with 82kOhm Resistors

NOTE: Idle speed increased at this apparent temperature.

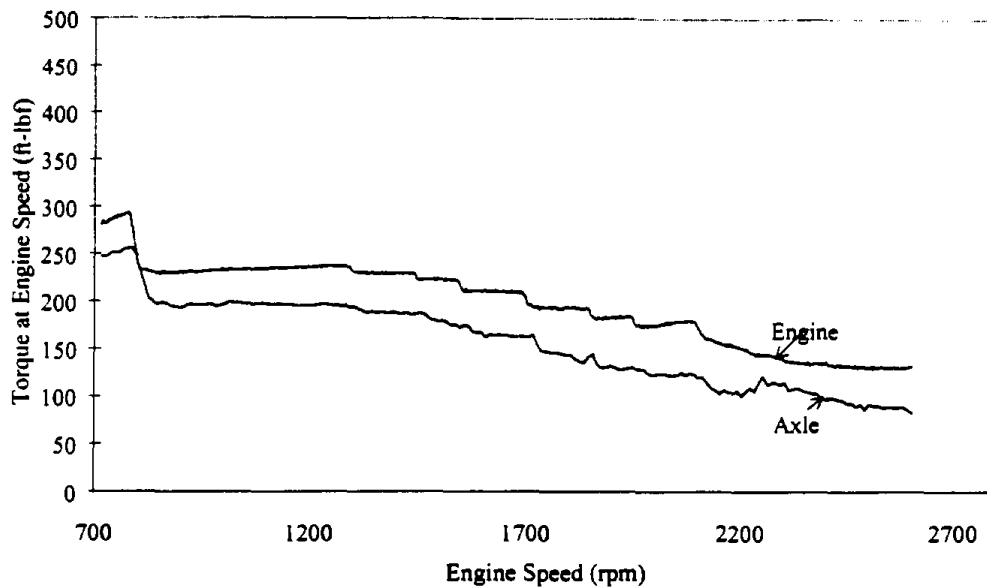


Figure D.11 Engine and Axle Torque for Disconnected MAP

speed was not implicitly controlled and did not step sequentially through a speed schedule identical to that used in the engine tests. Also, the engine speed range in which chassis data was taken varied slightly from the engine tests. In order to perform an accurate regression analysis, any repeat measurements were eliminated and interpolation was performed to fill in blanks in the chassis data.

One way of interpreting driveline efficiency is to look at the ratio of axle torque, at engine speed, measured on the chassis dynamometer, to engine torque, measured on the engine dynamometer. The information in Figures D.7 to D.11 were used to create Figure D.12, which shows the driveline efficiencies for all scenarios, except the disabled MAP, ranging from 80 to 90%, as expected.

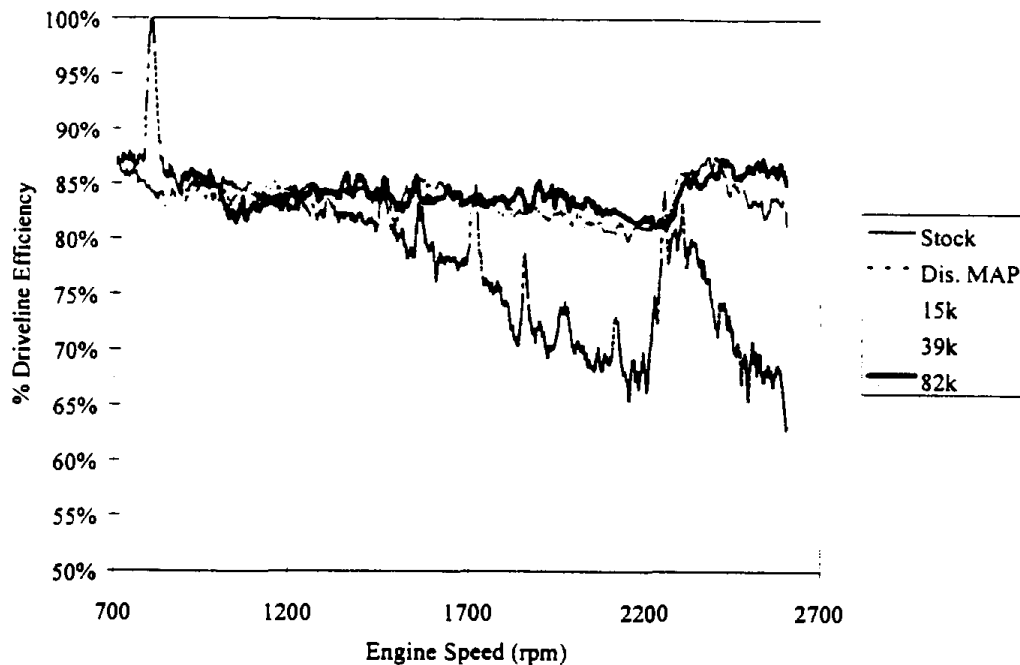


Figure D.12 Navistar Percentage Efficiency of Axle Torque (at engine speed) to Engine Torque

In Figure D.11, there is evidently a lag in torque response between the engine and chassis laboratories, this lag is most likely present in all plots, just not as evident. The disconnected MAP would cause a decrease in power once the engine moves away from idle conditions since the MAP is not able to tell the engine to produce boost. The lag is due to the drivetrain of the vehicle since axle torque is measured at the rear hubs of the vehicle and the transfer of torque would not be immediate. This is clear in Figure D.12 which shows an efficiency of greater than 100% at approximately 800 rpm.

D.3 Modeling of Drivetrain Losses

D.3.1 Multiple Regression Analysis

In order to translate data of the type shown in Figures D.7 to D.11 into a usable model, a functional form for drivetrain losses was developed and is presented below. Consider a drivetrain to include a transmission, driveshaft, rear axle assembly and tires. The following types of energy losses can be expected.

(a) Rubbing Frictional Losses

These would correspond to losses not associated with fully lubricated surfaces. The torque loss associated with such friction could be proposed to be independent of speed, and may be argued to be either dependent on torque throughput, or independent of torque throughput, depending on whether the frictional forces are influenced by the transmission of torque. These losses (as loss of torque between the engine and wheels) may be modeled as

$$C_1 + C_2 T_{engine} \quad \text{D.2}$$

Where C_1 and C_2 are constants and T_{engine} is the engine input torque into the drivetrain.

(b) Losses at Lubricated Surfaces

Where sliding surfaces are lubricated, or where squeeze-action on lubricant is present, losses will depend on lubricant viscous shear or viscous flow. Viscous lubricant stirring might be included in this classification. Where the geometry of the surfaces in relative motion is free of load considerations, the torque loss should be proportional to the speed of component movement, since it is the shear rate of the oil that is causing the loss. When the surfaces under consideration are under load, such that they are caused to move closer together as a result of torque throughput, then the torque loss must be dependent on both the speed and torque throughput. Making linear assumptions, it is proposed that the torque loss has the form

$$C_3 S_{engine} + C_4 S_{engine} T_{engine} \quad \text{D.3}$$

(c) Stirring of Lubricant

Where any inertial lubricant flows may occur, such as in pumping or stirring in the transmission, the losses will not be dependent solely on the viscous behavior of the oil. Using the simple turbulent loss argument, these torque losses would be given by

$$C_5 S_{engine}^2 \quad \text{D.4}$$

on the assumption that such losses are not load independent.

(d) Tire losses

Tire losses have already been shown not to vary linearly with the weight that they carry, but for a fixed weight upon the tires, without knowledge of influence of speed, tire losses can be lumped into the value of C_1 in Equation D.2 above.

The whole model for torque loss in the drivetrain therefore becomes:

$$T_{engine} - T_{axle} = C_1 + C_2 T_{engine} + C_3 S_{engine} + C_4 S_{engine} T_{engine} + C_5 S_{engine}^2 \quad \text{D.5}$$

Note that the "percentage efficiency" models in Figure D.12 took only the constant C_2 into account (the 2nd term), neglecting the other four terms.

Values for C_1 through C_5 in Equation D.5 may be found through regression on the map data such as those shown in Figures D.7 to D.11. These maps provide the full range of speeds and, in addition to the natural variation in torque over the map speed range, also provide several levels of torque through the tampering study.

Optimization Inc. performed as a subcontractor on the CARB program. They executed multiple linear regression analysis in order to find values for the constants in the torque loss model depicted above, Equation D.5. The values of the regression coefficients, C_1 through C_5 , for each of the five cases using the Navistar engine and chassis tests are shown in Table D.1 below. CV% represents the standard deviation divided by the mean, of the difference in the predicted model to the real data. Optimization also developed an overall five constant model that encompasses all five tampering scenarios; these regression coefficients are also shown in Table D.1.

Engine Condition	Stock	Disconnected MAP	15kΩ	39kΩ	82kΩ	Overall Model
C_1	4.241	15.26	69.35	3.326	11.99	-46.95
C_2	0.0051	-0.0023	-0.0236	0.0326	-0.203	0.177
C_3	0.0434	-0.0575	-0.0711	-0.0043	0.0966	0.0638
C_4	6.12×10^{-5}	2.89×10^{-4}	1.96×10^{-4}	1.22×10^{-4}	1.38×10^{-4}	-3.35×10^{-5}
C_5	-1.80×10^{-5}	1.22×10^{-5}	-2.66×10^{-6}	-1.23×10^{-5}	-4.04×10^{-5}	-1.40×10^{-5}
CV%	8.37	14.14	6.219	8.907	6.928	12.24

Table D.1 Regression coefficients for each scenario using the original model

Naturally, the usefulness of the information obtained through regression analysis is dependent on the accuracy of the model selected. In order to test the validity of the overall model developed by Optimization, each loss term was calculated for four extreme conditions: high speed/low torque, high speed/high torque, low speed/high torque and low speed/low torque. This data revealed that the most significant terms were the second and third, engine torque and engine speed. Negative values calculated for the first, fourth and fifth terms indicated a breakdown in the model due to the limited data available, therefore, a new model was developed.

The reduced model containing only engine torque and speed was

$$T_{engine} - T_{idle} = K_1 T_{engine} + K_2 S_{engine} \quad \text{D.6}$$

Optimization Inc. again performed regression analysis on Equation D.6 and developed an overall model with values for K_1 and K_2 . The resulting coefficients are seen in Table D.2.

Regression Coefficients	Overall Model
K_1	0.1348
K_2	6.494×10^{-3}
CV%	14.23

Table D.2 Regression Coefficients for reduced model

Further analysis of the Equation D.6 regression coefficients revealed a breakdown in the model at idle conditions. The data used to create these models provided a full range of speed, yet due to the nature of engines, there was less data for torque therefore; the model breaks down at very low

torque. This occurred since there was no information available on torque output at idle from the engine while installed in the vehicle.

D.3.2 Comparison of Engine and Chassis CO₂ Emissions

In order to establish idle engine torque produced in chassis, the following tests were performed using the Navistar T 444E engine. It is known that CO₂ emissions are proportional to fuel consumption in diesel engines and it is assumable that for each speed/fuel combination that torque is reproducible. Therefore, CO₂ emissions at idle from chassis FTP tests could be compared with those from idle engine dynamometer tests to yield the idle engine torque, in chassis. The governor slope was an issue since all tests were conducted at idle conditions. The Navistar engine was run on the engine stand, at idle speed (700 rpm), with loads of 5 ft-lb_f applied every 30 seconds, from 0 to 100 ft-lb_f. CO₂ data was collected in mg/second and multiple regression analysis was used to develop a polynomial mathematical model of engine torque output, at idle speed (700 rpm), as a function of CO₂ concentration in mg/second. Equation D.7.

$$T_{engine} = -7 \times 10^{-7} * CO_2^2 + 0.0585 * CO_2 - 67.5 \quad \text{D.7}$$

Subsequently, the CO₂ data collected from similar chassis dynamometer tests, along with Equation D.7 for engine idle torque, theoretically could be used to accurately predict engine torque output at idle conditions on the chassis dynamometer. Knowing the engine torque at idle would enable Optimization Inc. to develop a more accurate model, capable of predicting the drivetrain losses for all engine operating conditions at idle.

Using Equation D.7 and data obtained from the stock condition tests, it was found that engine torque was approximately 61.8 ft-lb_f at idle conditions (700 rpm), a believable value, on the chassis dynamometer. This value of 61.8 ft-lb_f represents the running losses experienced in the drivetrain, or the minimum torque required to turn the wheels of the vehicle at idle conditions.

D.4 Cummins Drivetrain Losses

D.4.1 Equal Engine Speed and Loading via Voltage Signals

To obtain a better understanding of driveline losses, data was also collected using the Cummins test engine and vehicle in the following manner. Since the governor slope of the Cummins engine was far less steep than that of the Navistar, the loading voltage signals of the engine could be used to apply the same loads while in chassis, given that similar engine speeds at the given load applications were maintained. While installed on the engine dynamometer, sixteen steady state, speed and load combinations were applied to the engine and the throttle voltage at each of the sixteen operating conditions was recorded. The engine was then installed in the Cummins cabover tractor, which was mounted on the chassis dynamometer. The same engine speeds and throttle voltages were applied via computer while axle torque was recorded, for the sixteen scenarios. Two sets of chassis tests, in 8th gear, were run, one with tandem-axles connected and the other in single-axle configuration. The data collected can be seen in Table D.3. *Applied engine torque*, refers to the torque applied to the engine during the engine tests. *Engine torque*,

refers to the engine torque output measured during the engine tests. *Single-axle torque*, refers to the torque at the rear hubs during chassis tests, with vehicle in single-axle mode. *Tandem-axle torque* refers to the torque at the rear hubs during chassis tests, with vehicle in tandem-axle mode.

Theoretically, the engine would receive the same loading signals in the vehicle as it did alone, as long as the engine speeds were the same, the engine torque in chassis could then be predicted. Simple plots of engine torque versus axle torque were prepared for both single and dual axle scenarios, Figure D.13 and Figure D.14. Simple linear regression on these plots revealed the trend lines in Equations D.8 and D.9, which are in the same form as Equation D.2.

$$T_{axle} = -142.83 + 0.8344 * T_{engine} \quad \text{for single-axle} \quad \text{D.8}$$

$$T_{axle} = -160.94 + 0.8038 * T_{engine} \quad \text{for tandem-axle} \quad \text{D.9}$$

As can be seen from Equations D.8 and D.9 the slopes of these curves, remarkably, reveal efficiencies of 83% and 80%, respectively.

Speed	Applied Engine Torque	Engine Torque	Single-Axle Torque	Tandem-Axle Torque
rpm	ft-lb _f	ft-lb _f	ft-lb _f	ft-lb _f
1000	290	280	189	152
1000	579	572	377	321
1000	869	850	629	544
1000	1158	1126	810	767
1200	330	310	90	73
1200	657	653	358	313
1200	984	960	622	567
1200	1313	1275	989	931
1400	317	308	83	82
1400	634	618	373	323
1400	951	928	599	554
1400	1268	1247	898	870
1600	275	264	85	82
1600	550	539	245	205
1600	825	799	520	470
1600	1100	1076	698	660

Table D.3 Sixteen Point Engine and Chassis Torque Results

To better fit the data in Figures D.13 and D.14, a more extensive multiple regression analysis was performed on this data to develop single and tandem-axle models which incorporated both engine speed as well as engine torque, much like Equation D.6. Equations D.10 and D.11, reveal similar torque influences to Equations D.8 and D.9. However, higher speeds cause more torque

to be removed from the powertrain. Figures D.15 and D.16 gives a plot of these equations against engine torque.

$$T_{axle} = 26.22 - 0.128 * S_{engine} + 0.830 * T_{engine} \text{ for single-axle} \quad \text{D.10}$$

$$T_{axle} = -42.29 - 0.090 * S_{engine} + 0.8011 * T_{engine} \text{ for tandem-axle} \quad \text{D.11}$$

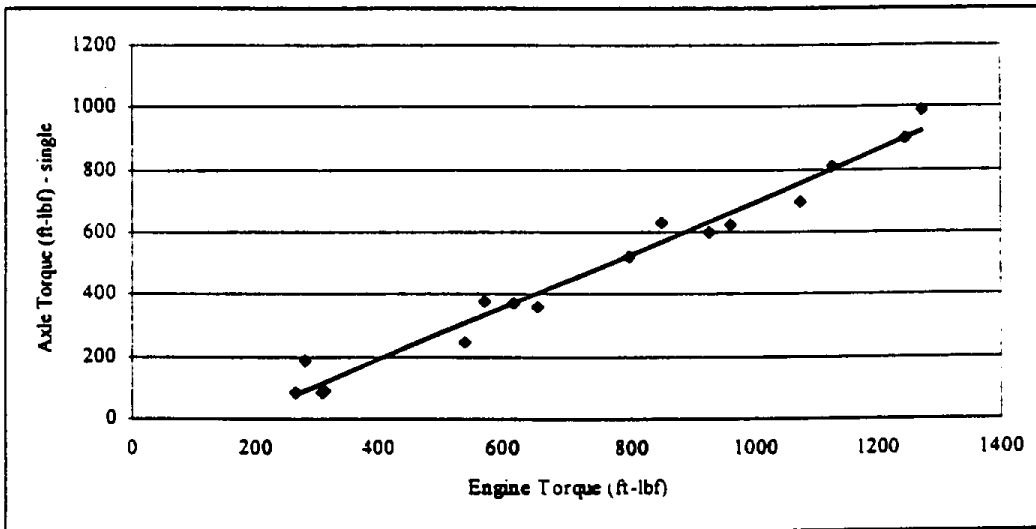


Figure D.13 Engine vs Single-Axle Torque for Cummins N-14

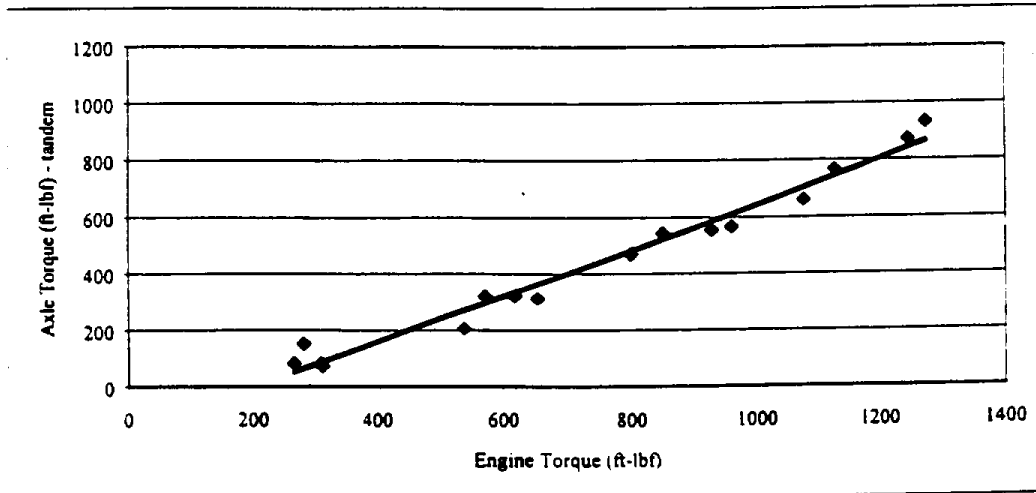


Figure D.14 Engine vs Tandem-Axle Torque for Cummins N-14

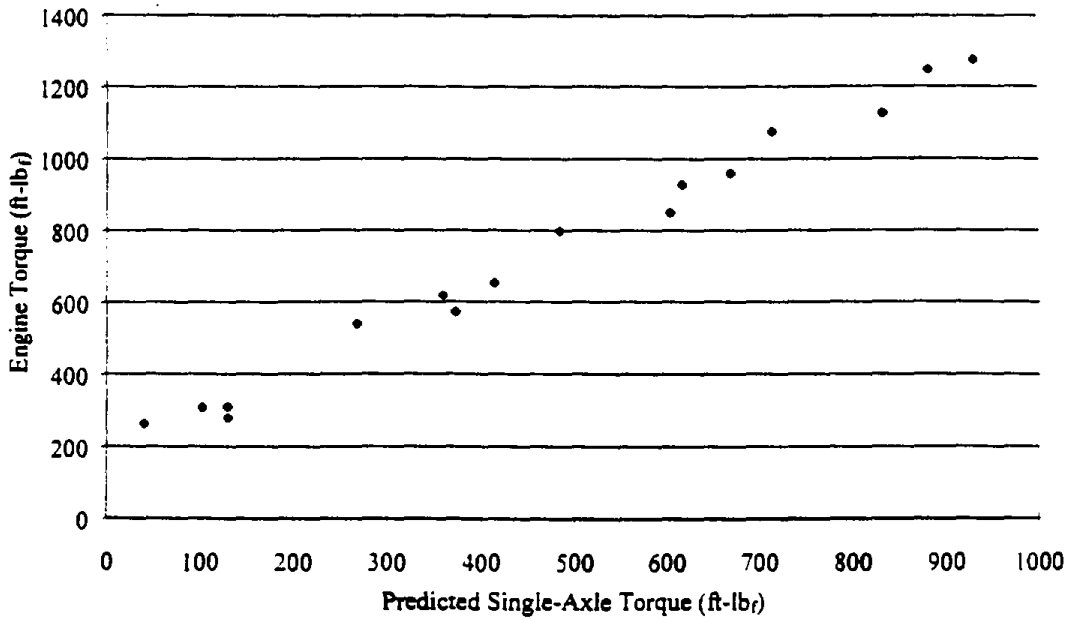


Figure D.15 Predicted Single-Axle Torque vs Engine Torque for Cummins N-14

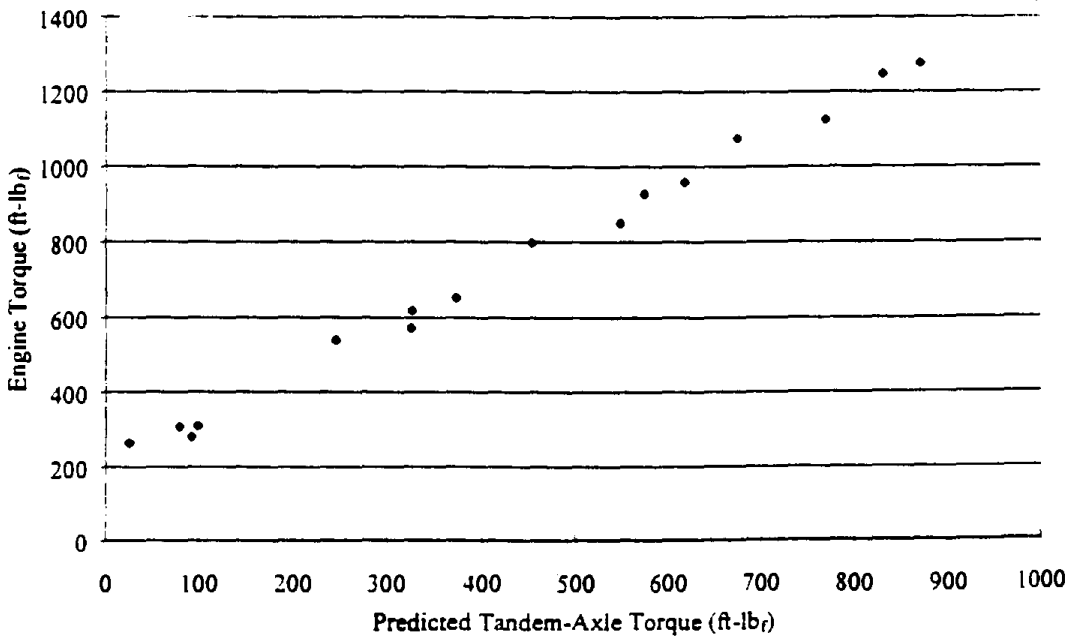


Figure D.16 Predicted Tandem-Axle Torque vs Engine Torque for Cummins N-14

D.5 NO_x and Power Relationship

Emissions of NO_x, gathered from the Cummins and Navistar tests showed a strong correlation between chassis and engine data. This supports the sound relationship between diesel NO_x and power, and is fortunate since NO_x is the gaseous emission of major concern in the heavy-duty community. Figure D.15 discloses the correlation of this data, also expressed in Equation D.12.

$$\text{Engine NO}_x \text{ (g/bhp-hr)} = 0.775 * \text{Chassis NO}_x \text{ (g/ahp-hr)} \quad \text{D.12}$$

Equation D.12 implies a drivetrain efficiency of 77.5%, just lower than expected for a heavy-duty truck if NO_x emissions are assumed to be linear with power. This can be attributed to the fact that the chassis test produces slightly more than 1 ahp-hr of energy during the idle periods whereas the idle sections in the engine test result in no energy flywheel energy production. Little NO_x is produced during the chassis idle periods. The implication of Figure D.15 is that the chassis test offers a clear method for screening vehicles in order to identify non-compliance of NO_x levels emitted from their engines [McKain et al., 1997].

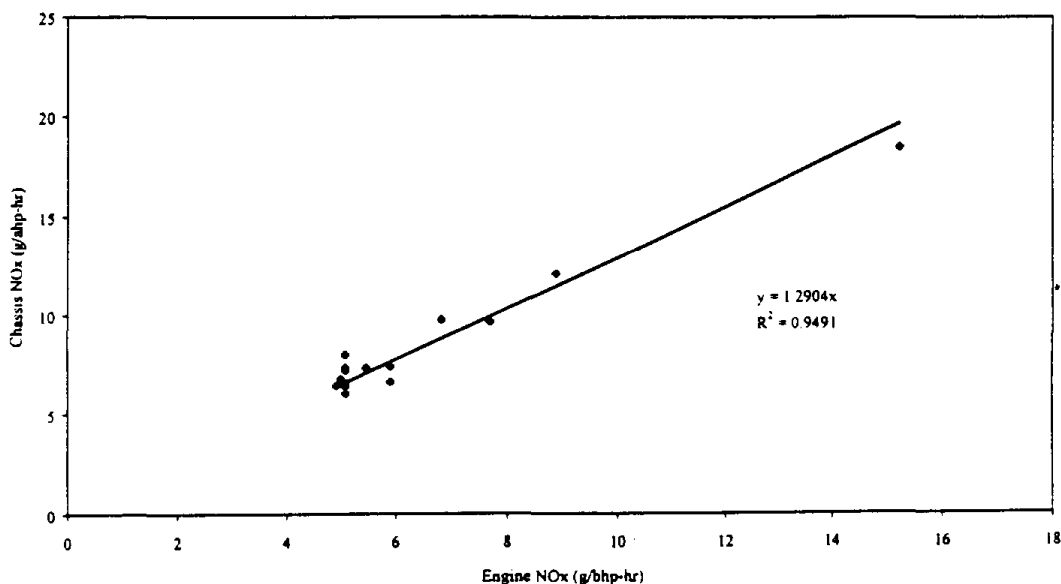


Figure D.17 Comparison of engine and chassis FTP NO_x emissions [McKain et al., 1997]

D.6 Results of Driveline Efficiency Analysis

Several methods were used to analyze the losses in the driveline. Tire losses were studied at the mobile laboratory and although the data was crude, it showed that loss was not proportional to load, as the in-use tire loss formulae indicate. Since the engines were operated in “drive by wire” mode, throttle voltages could be used to set reproducible torques on the engine, in and out of chassis, at exact engine speeds. This procedure was accomplishable by the Cummins engine only, because the governor of the Navistar engine was so steep that minor changes in speed created gross variations in torque, unacceptable for an accurate investigation. Simple analysis of the

Cummins data, based solely on torque ratios (axle:engine), disclosed an efficiency of 83% for single-axle operation and 80% for tandem-axle. When incorporating speed, similar results were found. The Navistar engine performed engine maps under high and low torque scenarios. again using only torque ratios, efficiencies ranged 80 to 90%. From multiple regression analysis on the Cummins and Navistar data, it was found that the most influential variables on driveline efficiency were engine speed and engine torque, predominantly engine torque. One of the most difficult tasks of the analysis was identifying idle engine torque while the engine was installed in the chassis. An experiment was devised using CO₂ emissions that modeled engine torque as a function of CO₂, in mg/second. This revealed an idle engine torque in chassis of approximately 61.8 ft-lb_f. This information was combined with previous regression information to give a drivetrain efficiency model for the Navistar vehicle. NO_x emissions from the Cummins apparatus had a high correlation between engine and chassis data due to the relationship between power produced and NO_x production in diesel engines. Direct comparison of NO_x emissions from chassis and engine tests showed an efficiency of 78.84%. This drivetrain efficiency was slightly lower than expected and may be attributed to the idle sections of the FTP which produce zero energy on the engine dynamometer and approximately 1 axle-horsepower hour on the chassis dynamometer. Although the results from each method varied, an average efficiency of greater than 80% was reported. The various results corresponded to the values ranging 80 to 90 % efficiency given by the driveline manufacturers.